AWARD NUMBER: W81XWH-13-1-0119

TITLE: Therapeutic Targeting of Lipid Droplets as Disease Markers in Ovarian Cancer

PRINCIPAL INVESTIGATOR: Vijayalakshmi Shridhar, Ph.D.

CONTRACTING ORGANIZATION: Mayo Clinic
Rochester, MN 55905

REPORT DATE: March 2016

TYPE OF REPORT: Final

PREPARED FOR: U.S. Army Medical Research and Materiel Command
Fort Detrick, Maryland 21702-5012

DISTRIBUTION STATEMENT: Approved for Public Release;
Distribution Unlimited

The views, opinions and/or findings contained in this report are those of the author(s) and should not be construed as an official Department of the Army position, policy or decision unless so designated by other documentation.

REPORT DOCUMENTATION PAGE

Form Approved
OMB No. 0704-0188

The public reporting burden for this collection of information is estimated to average 1 hour per response, including the time for reviewing instructions, searching existing data sources, gathering and maintaining the data needed, and completing and reviewing the collection of information. Send comments regarding this burden estimate or any other aspect of this collection of information, including suggestions for reducing the burden, to Department of Defense, Washington Headquarters Services, Directorate for Information Operations and Reports (0704-0188), 1215 Jefferson Davis Highway, Suite 1204, Arlington, VA 22202-4302. Respondents should be aware that notwithstanding any other provision of law, no person shall be subject to any penalty for failing to comply with a collection of information if it does not display a currently valid OMB control number.

PLEASE DO NOT RETURN YOUR FORM TO THE ABOVE ADDRESS.

1. REPORT DATE *(DD-MM-YYYY)*	2. REPORT TYPE	3. DATES COVERED *(From - To)*
March 2016	Final	15Jun2013 - 14Dec2015

4. TITLE AND SUBTITLE

Therapeutic targeting of lipid droplets as disease markers in ovarian cancer

5a. CONTRACT NUMBER

5b. GRANT NUMBER

W81XWH-13-1-0119

5c. PROGRAM ELEMENT NUMBER

6. AUTHOR(S)

Vijayalakshmi Shridhar, Ph.D.

E-Mail: Shridhar.Vijayalakshmi@mayo.edu

5d. PROJECT NUMBER

5e. TASK NUMBER

5f. WORK UNIT NUMBER

7. PERFORMING ORGANIZATION NAME(S) AND ADDRESS(ES)

Mayo Clinic
200 First Street SW
Rochester, MN 55905

8. PERFORMING ORGANIZATION REPORT NUMBER

9. SPONSORING/MONITORING AGENCY NAME(S) AND ADDRESS(ES)

U.S. Army Medical Research and Materiel Command
Fort Detrick, Maryland 21702-5012

10. SPONSOR/MONITOR'S ACRONYM(S)

11. SPONSOR/MONITOR'S REPORT NUMBER(S)

12. DISTRIBUTION/AVAILABILITY STATEMENT

Approved for Public Release; Distribution Unlimited

13. SUPPLEMENTARY NOTES

14. ABSTRACT

It is increasingly being recognized that altered lipid metabolism is an early event in carcinogenesis and a central hallmark of many cancers. Under nutrient deprived conditions, excess free fatty acids are stored as triglycerides in lipid droplets (LD) to be used for energy. Microarray and Metabolomics profiling identified the lipid pathway as one the major pathways modulated by loss of HSulf-1 in ovarian cancer. HSulf-1 deficient cells (OV202 Sh1/sh2, OV2223 and Sulf-1 KO MEFs) possess high levels of lipid droplets (LD) that are absent in the HSulf-1 proficient isogenic cells (TOV21G and SKOV3). More importantly, TEM analysis showed that all HSulf-1 deficient cells displayed increased number of LDs compared to isogenic HSulf-1 proficient cells. Increased accumulation of LDs in HSulf-1 depleted cells was associated with increased ERK mediated cPLA2S505 phosphorylation, a well-known marker for lipid biogenesis. Pharmacological inhibition and ShRNA downregulation of cPLA2 activity, a protein involved in LD biogenesis resulted in decreasing the # of LDs. Using mouse model of OV202 Sh1 derived xenograft, we show that AACOCF3 effectively attenuated tumor growth, LD biogenesis and reduced tumorigenesis in vivo

15. SUBJECT TERMS

Nothing listed

16. SECURITY CLASSIFICATION OF:			17. LIMITATION OF ABSTRACT	18. NUMBER OF PAGES	19a. NAME OF RESPONSIBLE PERSON
a. REPORT	b. ABSTRACT	c. THIS PAGE			USAMRMC
Unclassified	Unclassified	Unclassified	Unclassified	85	19b. TELEPHONE NUMBER *(Include area code)*

Reset

Standard Form 298 (Rev. 8/98)
Prescribed by ANSI Std. Z39.18

TABLE OF CONTENTS

1. **INTRODUCTION:** We had proposed to evaluate lipid droplets (LDs) as a disease marker and therapeutically target them in ovarian cancer. Our preliminary results showed that stable downregulation of HSulf-1 in OV202 (Sh1/2) and OV2223 lead to increased LDs as evidenced by BODIPY staining and transmission electron microscopy (TEM) analysis compared to non-targeted control (NTC) cells. Conversely, enhanced expression of HSulf-1 in TOV21G and SKOV3 cells also resulted in reducing the number of LDs in these cells compared to vector transfected controls. Additionally, our microarray analysis identified $cPLA_{2\alpha}$, a protein involved in LD biogenesis as one of the genes that was significantly upregulated OV202 Sh1 and Sh2 cells compared to NTC cells .Based on this finding and work done by others we hypothesized that the activation of extracellular signal–regulated kinase 1/2 (ERK1/2) by increased growth factor signaling leads to the activation of cytosolic phospholipase A2 alpha (cPLA2α), which culminated in a higher accumulation of LDs in ovarian cancer cells. We further hypothesized that tumors with activated cPLA2α can most likely be treated with targeted therapy against LDs in addition to standard chemotherapy. We also proposed to elucidate the role of cPLA2α in LD formation. The role of LDs in chemoresistance and metastasis will be examined using *in vitro* and *in vivo* models. Lastly, we proposed to determine the expression of phospho-cPLA2α (p-cPLA2α) in primary ovarian tumors and correlate it with clinical outcome.

2. **KEYWORDS:** Ovarian Cancer, TEM-Transmission Electron Micrographs, Lipid droplets, c-PLA2 (PLA2G4A)-cytosolic phospholipase A2, iPLA2- Ca++-independent phospholipase A2, Arachidonic Acid, AACCOF3- arachidonyl trifluoromethyl ketone, MAFP- methyl arachidonyl fluorophosphonate, BODIPY- Boron-dipyrromethene, BEL, Biomol- Bromoenol lactone, DEDA- 7,7- dimethyl-5,8-eicosadienoic acid, FFA-Free Fatty Acids, TMA- Tissue microarray, TTR-Time to Recurrence, PFS-Progression Free Survival, OS-Overall Survival

3. **OVERALL PROJECT SUMMARY:**

Milestone 1: Animal Use Approval-Prepare IACUC protocol for animal related studies.
The IACUC protocol #A69212-Therapeutic targeting of lipid droplets as a disease marker in ovarian cancer is approved by the Animal Care Committee at Mayo Clinic.

Aim1: *Elucidate the role of cPLA2α in LD formation.*

We previously reported that stable genetic downregulation of HSulf-1 in OV202 cells achieved by two different shRNAs targeting HSulf-1 (OV202Sh1 and Sh2 cells) displayed increased LDs compared to non-targeted control transduced cells (NTC)(*1*). We further confirmed these findings using OV202Sh1 to OV202Sh1 Clone C17 cells (generated by re-expression of CMV driven HSulf-1 construct in Sh1 cells.) HSulf-1 levels were verified in these clones by western blot analysis as shown in Fig 1A. Subsequently, lipid droplets were monitored by Bodipy staining in these cells. Rescue of HSulf-1 in OV202Sh1Cl7 cells reduced the number of LDs compared to OV202Sh1 and Sh2 cells (Fig.1B, Insets). Mean fluorescence intensity of Bodipy staining in these cells is shown in Fig.1C. We further performed quantification of the changes in the LDs by Transmission Electron Microscopy (TEM). Data showed significantly higher numbers of LDs in OV202Sh1 and Sh2 cells compared to NTC cells (Figs. 1D and E). Please note that in our previous (Year 2 short report) we had indicated that increased lipid droplets in cells with loss of HSulf-1 are associated with inhibition of autophagy. We pursued this angle since loss of LDs by lipophagy is a very novel concept not tested before in ovarian cancer and therefore we had indicated that we will focus on the mechanistic aspects of the connection between lipid droplets and autophagy in ovarian cancer.

The increased lipid droplets indicate the nutrient rich or energy proficient state of the cells and therefore we hypothesized that cells will not activate catabolic process such as autophagy. Therefore, to verify, we determined the extent of autophagy via TEM analysis in these cells and observed that HSulf-1 depleted OV202Sh1 and Sh2 cells exhibit less autophagic vesicles (AV) when compared to OV202NTC cells. Also, rescue of HSulf-1 in Sh1Cl7 cells resulted in increased AV compared OV202Sh1 cells. To rule out the possibility of cell specific effects, downregulation of HSulf-1 in TOV2223 cells with ShRNA (Fig.1F) also showed increased numbers of LDs in TOV2223Sh1 cells compared to TOV2223NTC cells by both Bodipy staining (Fig.1G) and TEM analysis (Fig. 1H) indicating that these metabolic alterations were not unique to the OV202 cell line. Similarly, a high number of AVs was observed in both OV202NTC cells and TOV2223NTC cells as compared to corresponding HSulf-1 depleted cells. The quantification of LDs and AVs in TOV2223

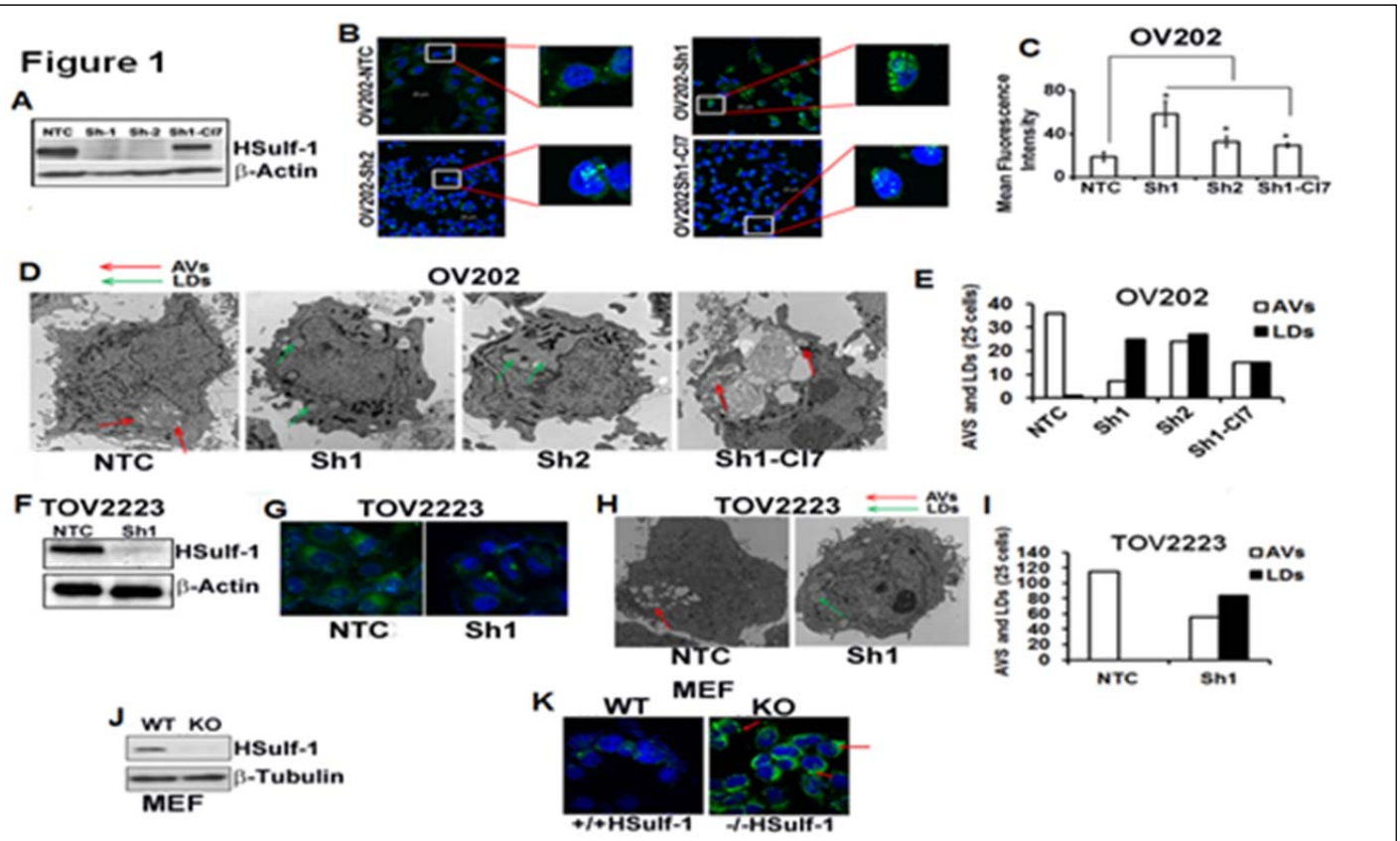

Figure1: HSulf-1 loss promotes lipid droplet biogenesis and defective autophagy in OV202, TOV2223 and in HSulf-1 knockout mouse embryonic fibroblast cells: Protein expression of HSulf-1 was assessed by western blot in OV202 clones (NTC, Sh1, Sh2 and Cl7 cells). Actin was probed as a loading control. **B**. OV202-NTC, Sh1, Sh2 and Cl7 cells were labeled with Bodipy 493/503 (green) and DAPI (Blue) to determine the cytoplasmic lipid droplets (LD) and nuclei respectively. **C.** Mean fluorescence of Bodipy in NTC, Sh1, Sh2 and Cl7 is measured using Carl Zeiss Zen (2009) software and the data is plotted as a bar diagram. **D.** Representative trans-electron microscopic (TEM) images of NTC, Sh1, Sh2 and Cl7 cells are shown; cytoplasmic LDs are marked with green arrows, whereas red arrows indicate autophagic vesicles (AV). **E.** LDs and AVs quantified in NTC, Sh1 and Sh2 cells (total 25 cells counted in each category) demonstrated in bar graph. **F.** Protein expression of HSulf-1 in TOV2223 NTC and Sh1 cells is detected by immunoblot analysis; b-actin is probed as a loading control. **G**. Bodipy staining performed in TOV2223 NTC and Sh1 cells to detect LDs. **H**. Representative TEM images of TOV2223 NTC and Sh1 cells were shown. **I.** AVs and LDs in TOV2223 cells are quantified **J.** Protein expression of HSulf-1 in Mouse Embryonic Fibroblast (MEF) wild type (WT) and HSulf-1 knock out (Sulf-1 $^{-/-}$) cells is detected by western blotting. b-Tubulin has been used as a loading control. **K**. MEF cells were labeled with Bodipy 493/503 (green) to determine the cytoplasmic lipid droplets (LD).

cells is shown in Fig. 1I. Furthermore, HSulf-1 knockout (KO) mouse embryonic fibroblasts (MEFs) also displayed increased numbers of LDs compared to wild-type cells.

Similarly upon ectopic expression of HSulf-1 in SKOV3 cells, there was a significant decrease in the numbers of LDs compared to vector transfected controls (Fig.S1). In contrast, vector transfected SKOV3 cells exhibited higher degree of AVs as quantified through TEM analysis, compared to HSulf-1 transfected SKOV3 cells (Figs S1B and D respectively). Quantification of LDs and AVs in 25 cells is shown in Fig.S1C.

Fig S1: A. Protein expression of HSulf-1 was determined by western blot in SKVO3 vector and cl7 cells. GAPDH was probed as loading control **B.** Representative electron micrograph images of SKOV3 vector and cl7 cells are shown; LDs and AVs are indicated by green and red arrows respectively. **C.** Quantification of LDs and AVs from electron micrograph images are determined in SKOV3 vector and cl7 cells and are demonstrated in a bar diagram. **D.** SKOV3 vector and cl7 cells were labeled with Bodipy 493/503 (green) and DAPI (blue) to determine the cytoplasmic LDs and nuclei respectively

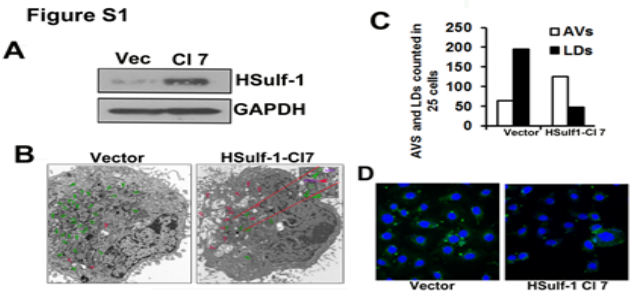

Milestone 2:

Task 1: Determine if increased ERK activity in OVCA cells results in increased cPLA2α activity

Our data indicate that downregulation of HSulf-1 in OV202 cells results in increased ERK activity (He et al Int J Cancer). Conversely, re-expression of HSulf-1 in HSulf-1 deficient cells results in attenuation of growth factor mediated Erk activity (*2-4*). To determine if increased ERK activity is required for the activation of cPLA2α as previously reported (*5, 6*) we had proposed to treat OV202Sh1 and HSulf-1 deficient parental SKOV3 cells (with higher levels of p-ERK) with MAPK inhibitor PD98059 in a dose and time dependent manner and determine if this will result in the inhibition of cPLA2α activity by western blot analysis. We had proposed to determine under the optimal condition of ERK inhibition by BODIPY staining and TEM analysis. Additionally, to determine if growth factor mediated upregulation of ERK activity is critical for increased cPLA2α activity, we had proposed to treat OV202 NTC and Sh1 cells and HSulf-1 deficient parental SKOV3 vec and Cl7 cells with HSulf-1 expression with HB-EGF (50ng/ml) for 12 to 24 h and examine the LD accumulation. Shorter treatment (10-60min) with HB-EGF will be used to examine cPLA2α activity using p-cPLA2α (Ser505) antibody by immunoblot. Thus the **rationale** for this experiment is to inhibit the activity of ERK which has been shown to activate cPLA2α at serine 505 critical for LD biogenesis. Our western blot analysis showed that SKOV3 cells express very low levels of total cPLA2 and no p-cPLA2.

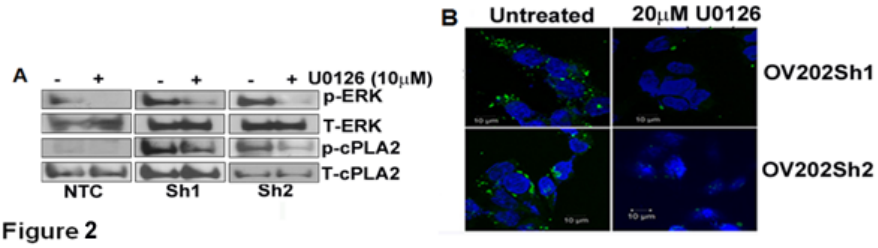

Figure 2

Figure 2: Inhibition of growth factor mediated signaling reduced p-cPLA2 and LD biogenesis: **A.** OV202 NTC, Sh1 and Sh2 cells were treated with 20mm of U0126, an MEK inhibitor for 24 hrs followed by western blot analysis to detect the protein expressions of phospho-ERK, total-ERK, phospho-cPLA2 and total-cPLA2. **B.** Bodipy staining for LDs in OV202Sh1 and Sh2 cells after treatment with 20 mM U0126.

cPLA2 is activated by phosphorylation at Ser residues 505, 515, and 727(*7*). Within these sites, Ser-505 phosphorylation leads to increased catalytic activity, (*8*) which depends on MAPK, ERK and p38.(*8-10*) We previously showed that downregulation of HSulf-1 in OV202 cells results in increased ERK activity.(*11*) Conversely, re-expression of HSulf-1 in HSulf-1 deficient cells results in attenuation of growth factor mediated ERK activity.(*3, 12, 13*) To determine if inhibition of ERK activity will alter p-cPLA2 levels, OV202NTC, Sh1 and Sh2 cells were treated with 10μM U0126 (MEK inhibitor) for 24 hrs. As shown in figure 2A (Panels 2 and 4), treatment with U0126 resulted in the attenuation of p-ERK and p-cPLA2^{ser505} levels in OV202Sh1 and Sh2 cells compared to NTC cells. Bodipy staining of OV202 Sh1-and -Sh2 cells show figure 3B shows reduced LD accumulation as a result of U0126 mediated inactivation of ERK and p-cPLA2 (F ig.2B).

Task 2: Identification of role of cPLA2 in regulating LD biogenesis in OVCA cells.

Milestone 3: Pharmacological approach: We will examine if cPLA2α plays an important role in LD biogenesis in OV202NTC and Sh clones, and in SKOV3 vector and Cl7. Using the pharmacological inhibitor approach, we had proposed to use cPLA2 specific inhibitors including methyl arachidonyl fluorophosphonate (MAFP), arachidonyl trifluoromethyl ketone (AACOCF3) from Calbiochem. To examine if these inhibitors are inhibiting cPLA2α activity, OV202 NTC Sh clones and SKOV3 -vec and Cl7 cells will be labeled with 0.1μci of radioactive arachidonic acid (AA) ([3H] AA, ARC) overnight. Next day, cells will be washed with PBS three times and then cells will be treated with 10μM of MAFP and AACOCF3. Release of radioactive AA will be examined in cell supernatant at various time periods from 2-24h. After standardization, we will examine the number of LD in treated and untreated Sh clones with cPLA2 inhibitors after 24h of treatment to determine if inhibition of cPLA2 leads to abrogation of LD biogenesis. As a control for these experiments, we will determine AA release under similar experimental conditions in the HSulf-1 rescued Sh1C7 cells.

Our western blot analysis showed that SKOV3 cells express very low levels of total cPLA2 and no p-cPLA2. For this reason, we scanned other ovarian cancer cell lines with loss of HSulf-1 expression and determined that OV2008 express high levels of p-cPLA2 and decided to use this cell line in addition to OV202Sh cells.

cPLA2 is activated/phosphorylated in HSulf-1 depleted ovarian cancer cells Since our initial observation indicated increased lipid droplet accumulation upon HSulf-1 depletion in ovarian cancer cells, we next wanted to determine the underlying mechanisms. LD often accumulates from anabolic process known as lipid biosynthesis. Previously we showed that lipid droplet associated proteins were upregulated in HSulf-1 depleted cells (*1*). Among them, one of the key proteins involved in lipid droplet formation is cPLA2α previously shown to be essential for LD biogenesis.(*14*) cPLA2α is activated and phosphorylation at Ser505 by p-ERK has been shown to be critical for cPLA2 mediated LD biogenesis.(*15*) Therefore, we first determined the activated/ phosphorylated levels of cPLA2α by Immunoblot analysis. Our data show that p-cPLA2^{ser505} was clearly increased in OV202Sh1 and to a lesser extent in OV202Sh2 cells (Fig. 3A). Re-expression of HSulf-1 also reduced the cPLA2 phosphorylation, indicating that phosphorylation was reversed by increasing levels of HSulf-1.

To further investigate the role of cPLA2 activation and lipid droplet accumulation/biosynthesis, we treated OV202Sh1 and OV2008 cells with a cPLA2 specific inhibitor, AACOCF3 (10 and 20μM). Western blot analysis show decreased levels of p- cPLA2 in inhibitor treated cells (Figs.3B and C). Bodipy staining upon inhibition of cPLA2 activity with 10μM of AACOCF3 and MAFP (another cPLA2 inhibitor) in OV202Sh1 and -2 cells (Fig. 3D) showed almost complete inhibition of LD biogenesis in these cells compared to untreated control cells. Consistent with this data, TEM analysis of OV202Sh1 cells with AACCOF3 and MAFP also revealed significantly lower number of LDs (Fig.3E, with quantitation of LDs in 25 cells shown next to the representative TEM images). Furthermore, transient downregulation of cPLA2 expression with two different ShRNA (ShcP-1 and ShcP-2) against cPLA2 (Fig. 3F) in OV202Sh1 cells resulted in the decrease of LDs as revealed by Bodipy staining (Fig. 3G). Similarly, stable downregulation of cPLA2 in OV2008 cells (Fig.3H) also resulted in reduced numbers of LDs (Fig.3I). To determine whether cPLA2 inhibitors were able to inhibit cPLA2 activity, we

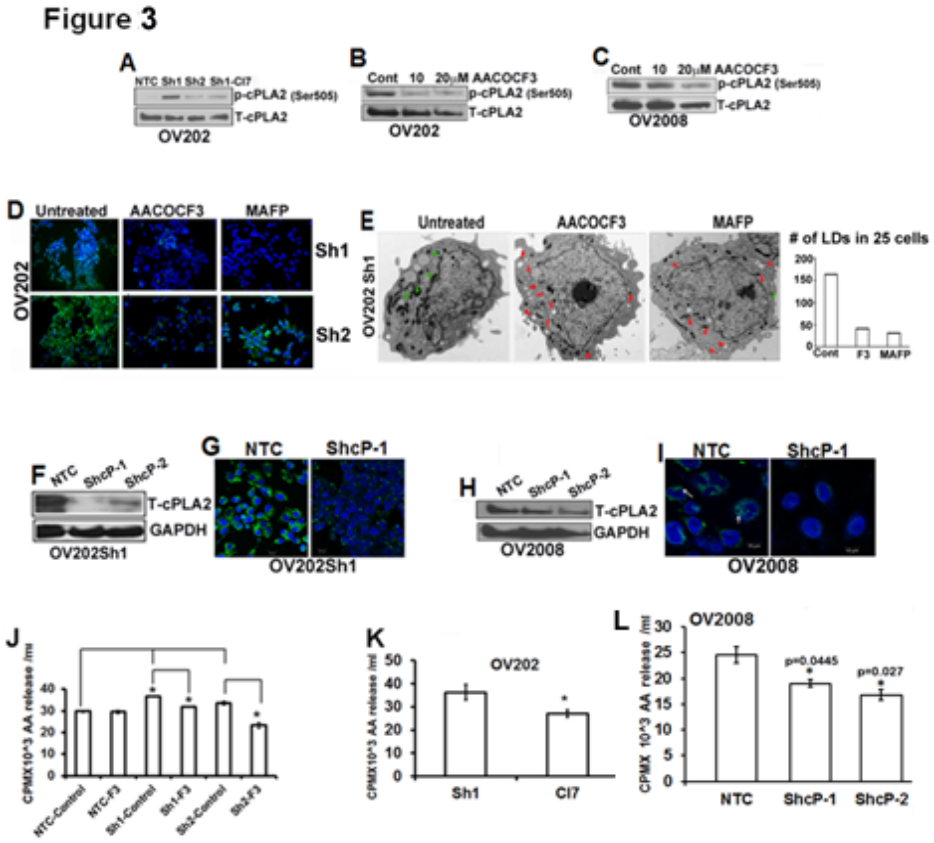

Figure 3: Inhibition of cPLA2 attenuates LD biogenesis in OV202Sh1 cells. A. Immunoblot analysis shows phospho-cPLA2 and total-cPLA2 levels in OV202 NTC, Sh1, Sh2 and Cl7 cells. **B.** & **C**. Immunoblot analysis shows phospho-cPLA2 and total-cPLA2 levels in OV202 Sh1 and OV2008 cells after treatment with 10mM and 20mM of cPLA2 inhibitor, AACOCF3. **D.** Sh1 and SH2 cells were treated with either 10mM AACOCF3 or MAFP for 24 hrs followed by Bodipy (493/503) staining to show the LDs. **E.** Representative TEM images of OV202 Sh1 cells untreated and treated with 10mM AACOCF3 and MAFP for 24 hrs. LDs are marked with green arrows, whereas red arrows indicate autophagic vesicles (AV). LDs are quantified from 25 cells from untreated and treated cells from TEM images and demonstrated in a bar diagram. **F.** & **H**. Total cPLA2 expression was transiently downregulated with two different ShRNAs targeting the open reading frame of cPLA2 in OV202Sh1 and OV2008 cells. Immunoblot analysis shows total cPLA2 expression in non-targeted control transduced (NTC), ShcP-1 and ShcP-2 cells. **G. & I.** Bodipy staining of LDs in OV202 Sh1 and OV2008 cells after transiently transfecting them with either empty vector or sh-cPLA2. **J.** Arachidonic acid (AA) release is evaluated in OV202 NTC, Sh1, Sh2 and Cl7 cells treated or untreated with 10mM AACOCF3. Cells were incubated with H^3-AA under serum starved condition for 24 hrs. Fresh medium was added to the cells after washing and aliquots of growth medium were measured for radioactivity after 24 hrs. Radioactivity is shown as counts per minute (cpm)/ml. **K and L.** AA release is evaluated in OV202 Sh1 and Cl7 cells and in OV2008 NTC, ShcP-1 and -2.

performed arachidonic acid (AA) release assay in OV202Sh1 and Sh2 cells. Cells treated with 10μM of AACOCF3 showed significant reduction of AA release indicating that activity of cPLA2 was inhibited (Figs. 3J, K and L).

Milestone 4: Molecular approach. 4a) Generate stable clones using inactive cPLA2α expression vector mutated at Ser 505 at active site (cPLA2S505) in OV202Sh clones.
Our several attempts in generating the mutant (cPLA2S505A) clones in OV202Sh1/Sh2 were not successful.

Milestone 5: **Task 3:** *Mitochondrial beta oxidation to assess the role of LD to supply energy source in in OVCA cells*.

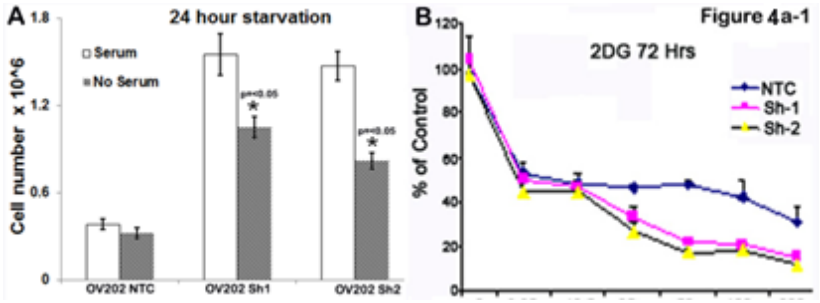

Rationale: Once we established the relationship between cPLA2α and LD in Sh clones, we next examined the role of LD in Sh clones. Lipid droplets consist of a core of neutral lipids, mainly triacylglycerol (TAG) and sterol esters, that are surrounded by a monolayer of polar lipids (*16*). TAG is a mechanism for storing unused calories and free fatty acids (FFA) can be released from Sn-2 position of TAG by action of cPLA2α. Resulting FFA, depending upon the size, can be metabolized by mitochondrial beta oxidation to generate ATP as energy source.

4a) To determine if LDs are used as an energy source under stress conditions. Plate OV202NTC, Sh clones and SKVO3 vector and Cl7 cells were exposed various stress conditions including serum starvation, glucose free media for several days (1-5 days). Cell survival was determined using MTT assay and number of LDs by staining with BODIPY.

OV202NTC, Sh1 and Sh2 cells were grown in the absence of serum **(Fig.4a1-A**) and in the presence of 2DG to inhibit glucose uptake **(Fig.4a1-B**). In the absence of serum and or glucose uptake the Sh1 and Sh2 cells underwent more cell death than NTC cells **(Fig. 4a-1-A and B**).

OV202Sh1 cells were grown in EBSS medium for the indicated time and the amount of LDs were determined by BODIPY staining. The number of LDs increasingly became less and less when cells were grown in EBSS (no aminoacids) **(Fig.4a-2)** indicating that LDs may be utilized for producing energy under these conditions. This was tested in the next task indicated below.

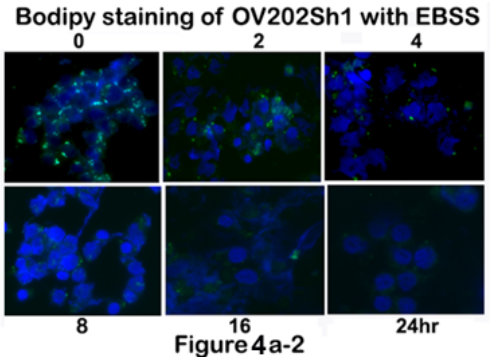

4b) Under similar experimental conditions and time points, we had proposed to assess mitochondrial beta oxidation. 6.0μM [1-14C] palmitic acid in HBSS along with α-cyclodextrin will be added for 30 min to OV2O2NTC and Sh batch clonal cells. Stop reaction with 1M KOH. Remove denatured protein and incubate supernatant at 600C for 1hr, neutralize with 6M HCl and partition. The upper aqueous phase will be taken for measurement of [1-14C] palmitic radioactivity. $^{14}CO_2$, a radioactive end product of the oxidation reaction

Instead of the above method, we used a non radioactive method as described below to measure beta oxidation with and without AACOCF3 treatment of NTC and Sh1 cells. Using the XF analyzer the oxygen consumption rate (OCR) reflective of oxygen consumption was used to measure fatty acid oxidation (FAO) in response to AACOCF3 treatment (*17*).

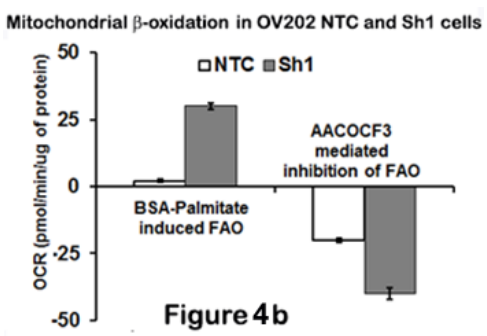

Fatty acid oxidation: Oxygen consumption rate was measured using a Seahorse Bioscience XF24 flux analyzer. $5x10^4$ cells were seeded per well in triplicates in MEM-α containing 20% FBS in an XF24 well culture microplates and incubated overnight in a 37°C/10% CO_2 incubator. The

assay medium for FAO is low-buffered KHB buffer (110 mM NaCl, 4.7 mM KCl, 2 mM MgSO4 1.2 mM Na2HPO4, 2.5 mM glucose adjusted to pH7.4) supplemented with 0.5mM carnitine. For induction of FAO, BSA conjugated palmitate was injected to a final concentration of 50 µM. XF analyses were performed in the XF Extracellular Flux Analyzer (Seahorse Bioscience, Billerica, MA). Three basal rates were measured prior to automated injection of palmitic acid (50 µM) coupled to BSA vehicle or BSA vehicle alone. After treatment for 55 min, the cPLA2 inhibitor AACOCF3 (10 µM), was added. Oxygen consumption rates were measured by using time-resolved method (Seahorse Bioscience XF24) (21). Data were normalized to protein content (assayed after completion of measurements). Changes in the FAO induction in Sh1 cells are compared with that of NTC cells. AACOCF3 induced inhibition of FAO in Sh1 cells are compared with the FAO inhibition in NTC ($P \leq 0.01$ and $P \leq 0.001$) are shown in **figure 4b**. The results clearly indicate that Sh1 cells have higher level of beta oxidation which is inhibited when LD biogenesis is inhibited with AACOCF3 treatment.

4c) Total levels of intracellular ATP will also be examined to correlate with beta oxidation in mitochondria using ATP kit from Promega. Higher levels of ATP in Sh1 and Sh2 compared to NTC cells, while this phenotype is reversed in Sh1-Cl7 associated with increased glycolysis in these cells was reported in a manuscript describing the role of loss of HSulf -1 promoting increased glycolysis Figs. 2E-F (*18*) (See manuscript attached).

Milestone 6: Task 4: *Determine the in vitro effects of cPLA2α inhibitors on migration and invasion of OVCA cells. Since we saw no metastatic invasion in our invivo model (See Figure 5 below)- we did not pursue these studies in vitro.*

Aim 2: Examine the role of lipid droplets in chemoresistance and metastasis using in vitro (Milestones 7- task 1) and in vivo models. Milestones 8 and 9- tasks 2 and 3

Task 1: *Establish relationship between LD and chemoresistance in ovarian cancer using cell culture based study*. To examine the role of cPLA2α-LD axis on chemotherapy-induced cytotoxicity, isogenic cell lines with and without HSulf-1 (OV202NTC, Sh1, Sh2 and SKOV3 vec and Cl7 cells) will be treated with optimal concentration of cPLA2 inhibitor AACCOF3 alone (determined under experimental set 2) with increasing cisplatin concentration. Parallel experiments will determine the percentage of cells undergoing apoptosis under these treatment conditions. Chemotherapy-induced cytotoxicity will be determined by trypan blue staining and clonogenic survival assays (*19*). Data will be expressed as the percentage of total cells that are apoptotic after each treatment.

We did not pursue SKOV3 cells since they do not express p-cPLA2 and very low levels of total cPLA2.We initially established IC50 values for carboplatin, cisplatin and AACCOF3 (F3 in figure 5) in OV202NTC, Sh1 cells by MTT assays (48hrs) (Figs. 5A-F). Using the IC50 for F3, we treated the Sh1 cells with increasing concentrations of

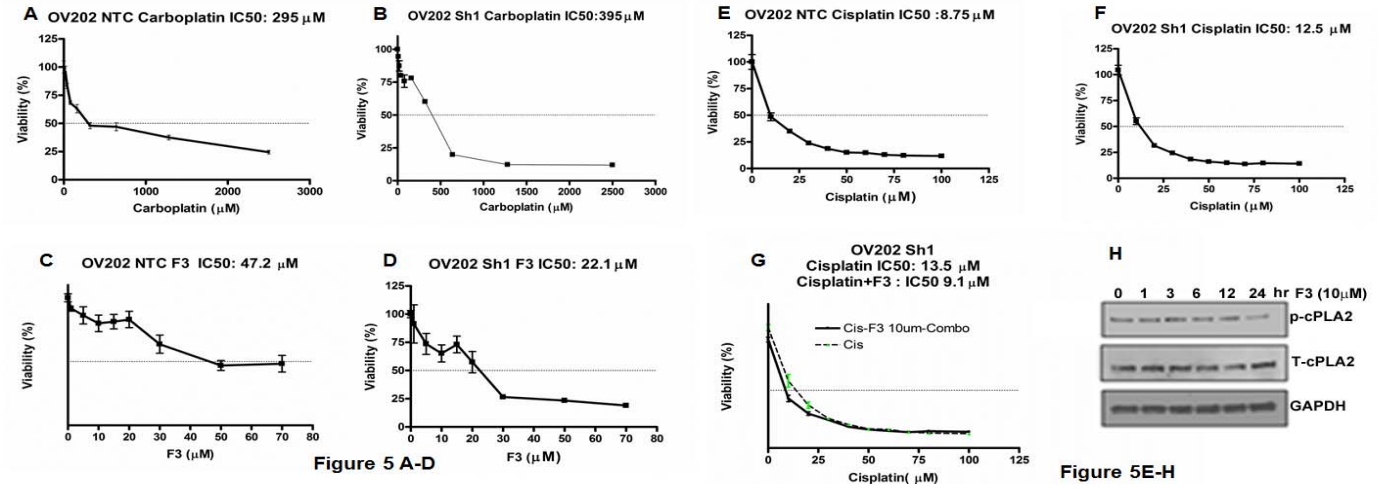

Figure 5 A-D

Figure 5E-H

cisplatin *in vitro* to determine if F3 treatment would sensitize the cells to cisplatin induced cytotoxicity. To our surprise, we did not observe a significant difference in the inhibition of proliferation in the combination compared to F3 treatment alone (Fig.5G). Interestingly, we did observe a time dependent decrease in the levels of p-cPLA2 upon F3 treatment in the Sh1 cells (Fig.5H). Although, we did not see an effect of the combination of platinum with F3 in vitro, our in vivo data shown in Figure 6 clearly showed increased TUNEL staining and decrease in Ki67 staining in the F3 and the combination treated groups compared to untreated control or carboplatin treated groups alone (Fig 6H -J).

Task 2: *Examine the in vivo efficacy of cPLA2 inhibitor in potentiating cisplatin induced cytotoxicity in athymic immunodeficient mice using Sh clones.*

We had proposed to examine the effect of cPLA2α inhibitor treatment in a mouse xenograft model of intraperitoneal (i.p.) carcinomatosis using Sh clone with anticipation that administration of cPLA2 inhibitor will attenuate LDs biogenesis *in vivo* which will sensitize tumor using OV202Sh1 cells as a ovarian cancer model shown in (*20*). All experimental use of animals were complied with the guidelines of Animal Care at the Mayo Foundation, in accordance with approved protocols. $5X10^6$ Sh clones expressing luciferase cells in serum-free RPMI 1640 will be injected intraperitoneally into female athymic nu/nu mice at 4 to 5 wk of age (National Cancer Institute-Frederick Animal Production Area (Frederick, MD). Once i.p implant s are visible via non-invasive imaging (about day 30), animals will receive cisplatin alone or in combination with cPLA2α inhibitor randomly assigned to three groups of 10 from day 1 after i.p. tumor detection via non-invasive imaging.

To determine whether blocking cPLA2 activities via AACOCF3 confer any advantage in attenuating tumor growth in combination with chemotherapeutic agent such as carboplatin, we performed testing of these agents in vivo using a mouse model. The effect of AACOCF3 alone and in combination with carboplatin (CBP) on primary tumor growth was evaluated in OV202Sh1 cells bearing nude mice i.p. (intraperitoneally). $5X10^6$ Sh clones expressing luciferase cells in serum-free RPMI 1640 were injected intraperitoneally into female athymic nu/nu mice at 4 to 5 wk of age (National Cancer Institute-Frederick Animal Production Area (Frederick, MD). Once i.p implants were visible via non-invasive imaging (4 days after

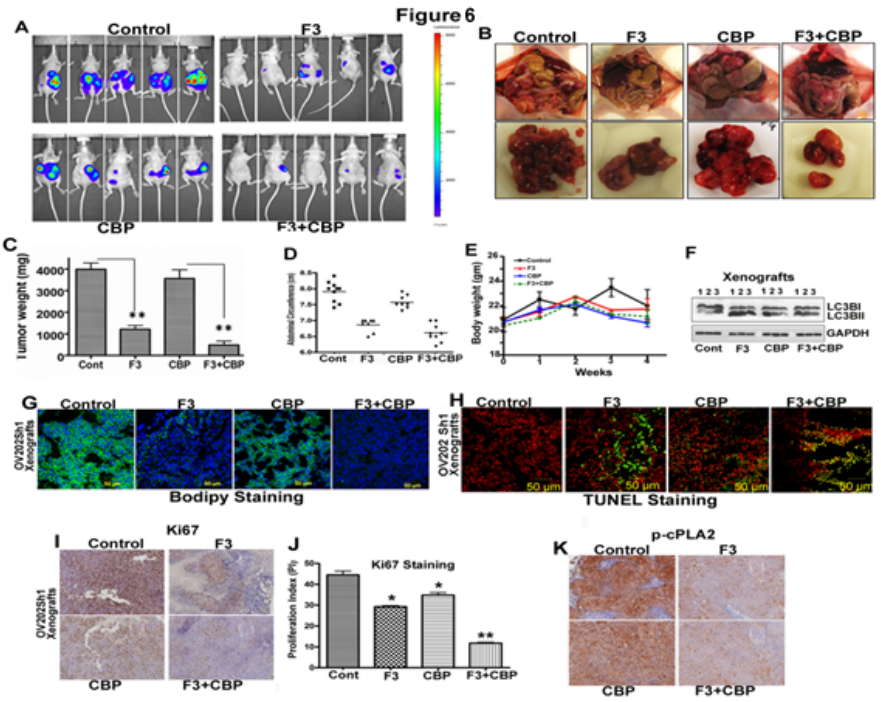

Figure 6: AACOCF3 alone and in combination with carboplatin suppresses tumor growth, and inhibits lipid droplet biogenesis *in vivo*

A. Randomized OV202Sh1 tumor-bearing mice (n=10), were treated with water or AACOCF3 (F3) (10mg/kg), or carboplatin (CBP) (51mg/kg) or with a combination of AACOCF3 and CBP for 4 weeks and after 28 days mice were euthanized. Representative images of the mice prior to sacrifice from control, F3 treated, CBP treated and CBP+F3 combination treatment groups using IVIS luminescence imaging system series 2000. Color bar shows photon intensity. **B.** Representative images of excised tumors from OV202 Sh1 xenografts. **C**. Excised tumor weights from control, F3, CBP and CBP+F3 combination treatment groups. **D**. Abdominal circumference from different groups of mice measured on the day of sacrifice. **E.** Total body weight of untreated control and treated with F3, CBP, CBP+F3. **F.** Immunoblot analysis of LC3BI/II in lysates from untreated, F3, CBP and F3+CBP treated Xenografts with GAPDH as loading control. **G.** Tumor xenografts were stained with Bodipy to detect lipid droplets; DAPI was used to stain the nuclei. **H.** Representative images of TUNEL staining of frozen section of xenografts from different treatment groups and untreated control. Green fluorescence indicates TUNEL and red fluorescence indicates propidium iodide (PI) staining. **I.** Representative images of immunohistochemical staining of Ki67, **J.** Bar graph showing the Ki67 proliferation index (*p=<0.05 and **p=<0.01). Proliferation index (PI) of Ki-67 staining was measured using ImmunoRatio, from public domain image analysis software. **K.** phospho-cPLA2 in FFPE sections of treated and untreated xenografts.

inoculation), mice were randomized (10 mice/group) and treated i.p. with the 10mg/kg body weight (b.w.) of cPLA2 inhibitor AACOCF3 (referred to as F3 in the figures) every other day till the end of the study, 51mg/kg b.w. carboplatin (CBP) every 5 days till the end of the study and a combination of CBP+F3 every 5 days, with vehicle treated group as control. Luciferase imaging of the representative mice from four groups is shown in Fig.6A. Higher luciferase intensity in the control group and CBP group indicates increased tumor volume, progression and metastasis. Representative excised tumor from one of the mouse in each group is shown in Fig.6B. At necropsy, the measured tumor weight and circumference of mice in each group showed that the combination treatment was more effective at reducing cancer progression compared to all of the other groups

(Figs.6C-D). There was no significant body weight loss in F3 or combination treated group compared to control group suggesting both F3 and CBP treatment were well tolerated without apparent toxicity to the animal (Fig.6E). More importantly, Bodipy staining of frozen sections of the xenografts clearly showed high levels of lipid droplets (Fig.6G) in the control and the CBP treated group and significantly less LDs in the F3 and combination treated group consistent with the *in vitro* data shown in figure 2D, top panel. In contrast, TUNEL staining showed increased TUNEL staining in the F3 and the combination treated groups compared to untreated control or CBP treated groups alone (Fig.6H) Anti-tumor effects of AACOCF3 monotherapy and combination with CBP correlated with significant reductions in tumor cell proliferation marker, Ki67 and phospho-cPLA2 as determined by IHC staining using the specific antibodies to these proteins (Figs. 6I and K).

Aim 3:* Milestone 10: *Determine the expression of phospho-cPLA2α in primary ovarian tumors and correlate with clinical parameters.

To determine if cPLA2α is a potential target in ovarian cancer, we had proposed to evaluate the expression of p-cPLA2α s505-in 200 ovarian cancer specimens by immunohistochemistry and correlate to clinical outcome such as progression free survival, overall survival, grade, stage and histology and also determine if p-cPLAαs505 predict responsiveness to adjuvant chemotherapy in ovarian cancer. *Although we had proposed to* evaluate the expression of p-cPLA2α s505-in 200 ovarian cancer specimens, we determined p-cPLA2 expression in 512 ovarian tumors by IHC. These tumors are all from patients before they commenced standard chemotherapy. We initially established the conditions for IHC in the Pathology Research Core at the Mayo Clinic. Immunohistochemistry was performed by the Mayo Clinic Pathology core on 5 different TMAs with 512 tumors in triplicates. The images were digitized and the expression levels were blindly read by three different investigators including a pathologist. The scores were averaged and the expression level was correlated with clinical outcome. To our surprise, we saw that patient tumors with high level of p-cPLA2 had a better progression free survival and overall survival compared to patient tumors with low levels of p-cPLA2.

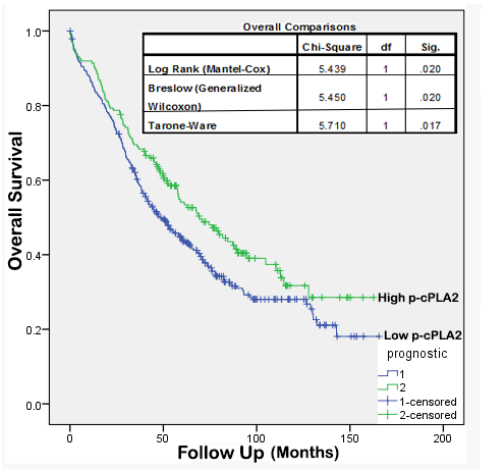

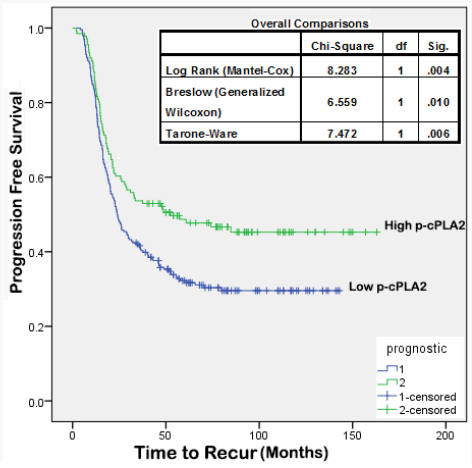

We also saw an inverse correlation in the expression of HSuf-1 and p-cPLA2 in a subset of tumors that expressed either of these proteins in the same tumors. 163 out of 512 tumors expressed both Hsulf-1 and p-cPLA2. 72 of 163 (44%) of these tumors showed an inverse correlation. However, this inverse correlation in expression shown in Fig. 7 below did not correlate with clinical response.

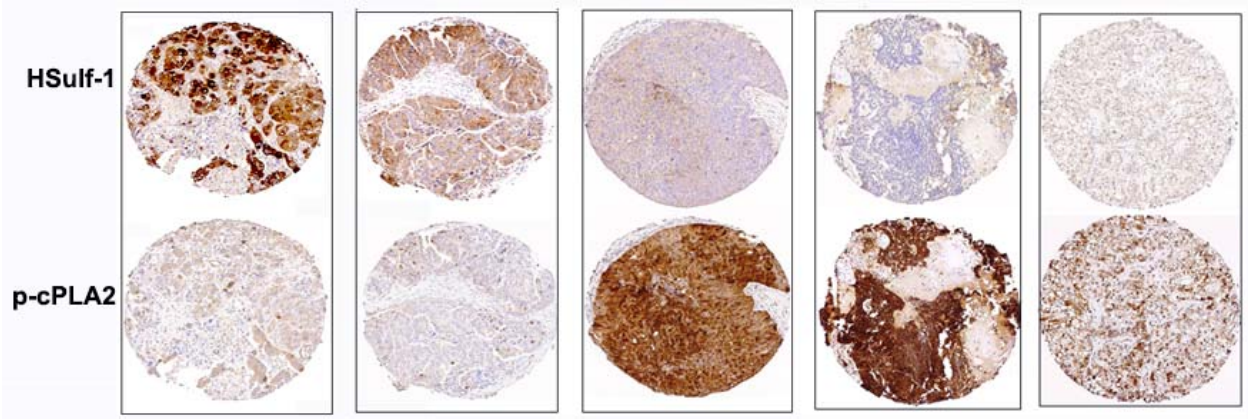

Milestone 11- Manuscript Preparation

Please see appendix for the two manuscripts where we have acknowledged the current support from the DOD.

4. KEY RESEARCH ACCOMPLISHMENTS: We have determined that

- Using two different isogenic cell lines OV202 NTC vs Sh1 and OV2008 cells with high levels of p-cPLA2 vs OV2008ShcP2 cells with genetic downregulation of total cPLA2, we have determined that increased ERK activity in OVCA cells results in increased cPLA2 activity. These results show the contribution of loss of HSulf-1 with high pERK leading to LD biogenesis, also a direct contribution of p-cPLA2 in promoting LD biogenesis in ovarian cancer.

- We have also shown using specific inhibitors of p-cPLA2, AACOCF3 and MAFP that LD biogenesis is attenuated. LD inhibition by these inhibitors also sensitizes these cells to cisplatin mediated cytotoxicity implicating LDs as a disease marker that can be therapeutically targeted. Additionally, we have determined that downregulation of p-cPLA2 sensitizes OV2008 cells to cisplatin mediated cytotoxicity. Taken together, these data indicate that high levels of p-cPLA2 may promote cisplatin resistance.

- Our *in vivo* data using a specific cPLA2 inhibitor, AACOCF3 showed less tumor burden compared to the untreated control indicating that a higher level of cPLA2 itself can play a crucial role in ovarian tumorigenesis. Interestingly, AACOCF3 and carboplatin combination therapy was more effective to reduce tumor growth than carboplatin alone. This is a first report to show that HSulf-1 loss associated ovarian tumor formation is regulated by higher activity of cPLA2. More studies are required to test the synergistic effect, absorption and bioavailability of AACOCF3 alone versus the combination with carboplatin in the mouse model. Our findings indicate that cPLA2 inhibition is a potent therapeutic approach to synergize with conventional chemotherapies to reduce ovarian tumor growth.

- More importantly, we have determined the expression level of p-cPLA2 in more than 500 ovarian tumors on a tissue microarray by immunohistochemistry. These tumors are all from patients before they commenced standard chemotherapy. To our surprise, we saw that patient tumors with high level of p-cPLA2 had a better progression free survival and overall survival compared to patient tumors with low levels of p-cPLA2.

Conclusion: HSulf-1 and its tumor suppressor activities are long been a research interest of our group. We have established the protective role of HSulf-1 in the regulation of growth factor mediated tumor growth in ovarian cancer. Recently, we have shown that HSulf-1 loss also connects to metabolic alterations which play a critical role for tumor growth (*18, 20*). Among several metabolites, lipid and glycolytic metabolites were the one which altered most significantly. When we studied the specific changes among the lipid metabolites, we observed significant phenotypical changes in HSulf-1 knockout cell lines, i.e. lipid droplets (LDs). LDs are unique organelles which primarily act as storage of neutral lipids and cholesterol and recent findings from various investigators connected its role with disease progression including cancer and metabolic diseases. To our surprise, we have observed that LDs are associated with various proteins which are all enhanced in their mRNA and protein level upon loss of HSulf-1. Further, we targeted one specific LD associated protein, cPLA2 and used its functional inhibitors to therapeutically target the cells with loss of HSulf-1 and higher LD content. We have shown that, inhibition of cPLA2 activity not only reduces LDs but also reduces cell proliferation, release of free fatty acid, inhibition of beta oxidation, and most importantly attenuates the tumor growth *in vivo*. These data support our hypothesis that lipid droplet can be used as a disease marker in ovarian cancer. In other cells with loss of HSulf-1, other lipogenic gene may be playing a role such as FASN, SREBP1C and PLA2G3 playing a role in promoting lipid droplet biogenesis or a lipogenic phenotype. This is not surprising since loss of HSulf-1 in ovarian cancer affects many genes involved in the lipogenic pathway as we have shown in our recent study *(1)*. Targeting the lipogenic phenotype in ovarian cancer with targeted inhibitors of the pathway or other broad acting inhibitors that can reduce the number of lipid droplets may have a beneficial effect on patients with this deadly disease. Although obesity perse has not been linked to ovarian cancer, our data suggest that targeting the lipogenic pathway may be of interest in the future trials for ovarian cancer. The results from this study will be equally applicable to all women with ovarian cancer, both civil and women serving in the army and their relatives afflicted with ovarian cancer.

Future Directions

We have extended our understanding on the role of HSulf-1 in the regulation of autophagy and lipid metabolism that has opened up newer research avenues to investigate the impact of tumor suppressor activities of HSulf-1 in regard to autophagic regulation od LDs.

6. PUBLICATIONS, ABSTRACTS, AND PRESENTATIONS:

(1) Lay Press: **Nothing to report**

(2) Peer-Reviewed Scientific Journals: All attached in the Appendix

- Roy, Mondal and Shridhar et ., -Loss of HSulf-1 promotes altered lipid metabolism in ovarian cancer Cancer and Metabolism IN PRESS, 2014.
- Mondal et.al., - HSulf-1 deficiency dictates a metabolic reprograming of glycolysis and TCA cycle in ovarian cancer- Oncotarget, 2015
- Manuscript under revision – Roy et al- Loss of HSulf-1-The Missing Link between Autophagy and Lipid Droplets in Ovarian Cancer- Autophagy, 2016

(3) Invited Articles: Nothing to report

a. Abstracts: All five abstracts attached in the appendix section

1. Debarshi Roy, Xiaoping He, Ashwani Khurana, Susmita Mondal, Deok-Beom Jung, Sung Kim, Thomas Dierks, Clifford Folmes, Andre Terzic and Viji Shridhar. HSulf-1 loss in ovarian cancer cells induces lipid droplet biogenesis 105th AACR Annual Meeting San Diego, CA, April 5-9, 2014.Abstract Number: 1293.
2. Debarshi Roy, Chen Wang, Shailendra Giri, Xiaoping He, Ashwani Khurana , Susmita Mondal, Deok-Beom Jung, Han Ihn, Sung Kim, Shaun Riska, Ann Oberg, Jeremy Chien and Viji Shridhar. Loss of HSulf-1 Promotes Altered Cellular Metabolism of Ovarian Cancer. The 17 International Conference on Korean Medicine. Cancer Preventive Material Development Research Center (CPMDRC) & Institute, Kyunghee University, 2013.
3. Viji Shridhar. The Missing Link between Lipid Droplets and Autophagy in Ovarian Cancer. 1st annual Meeting International Ovarian Cancer Consortium Tumor Microenvironment and Drug Discovery, Oklahoma City, OK.
4. Viji Shridhar. The Missing Link between Lipid Droplets and Autophagy in Ovarian Cancer. **GCC Global Cancer Conference & Medicare summit.** September 15-17, 2014 Hyderabad International Convention Centre, India.
5. Debarshi Roy, Susmita Mondal, Ashwani Khurana, Xiaoping He, Edward Hammond, Keith Dredge, and Viji Shridhar. Loss of HSulf-1 Promotes Defective Autophagy and Increased Lipid Droplet Biogenesis *in vitro* and *in vivo* in Ovarian Cancer. American Association of Cancer Research, May 18-22, 2015, Philadelphia, PA. ABSTRACT #-2413.

b. Presentations: Invited Presentations-Local, National and International

(1) 2014-09/15- Title: The Missing Link between Lipid Droplets and Autophagy in Ovarian Cancer. Global Cancer Conference – Hyderabad, India.

(2) 2014-02/07 Title: The Missing Link between Lipid Droplets and Autophagy in Ovarian Cancer. 1st annual Meeting International Ovarian Cancer Consortium Tumor Microenvironment and Drug Discovery, Oklahoma City, OK.

(3) 2014-01/28 Title: The Link between lipid droplets and autophagy in Ovarian Cancer-Division of Experimental Pathology, Mayo Clinic, Rochester, MN.

(4) 2013-11/14 Title: Identification of HSulf-1 as a regulator of altered cellular metabolism in ovarian cancer*****. Gyn/Onc Cancer Seminar series, Mayo Clinic, Rochester, MN.

(5) 2013-11/26 Title: Loss HSulf-1 promotes altered Cellular Metabolism of Ovarian Cancer*. 2013, the 17 International Conference on Korean Medicine. Cancer Preventive Material Development Research Center (CPMDRC) & Institute, Kyunghee University.

(6) 2013-11/07 Title: Story of HSulf-1: From Genomics to Glycomics to Metabolomics**.** University of Louisville, James Graham Brown Cancer Center, KY.

(7) 2013-06: Title: Metabolic Alterations Mediated by Loss of HSulf-1 in Ovarian Cancer*****, University of Kansas Medical Center, Kansas City, Kansas.

7. INVENTIONS, PATENTS AND LICENSES: Nothing to Report.

8. REPORTABLE OUTCOMES: Provide a list of reportable outcomes that have resulted from this research. Reportable outcomes are defined as a research result that is or relates to a product, scientific advance, or research tool that makes a meaningful contribution toward the understanding, prevention, diagnosis, prognosis, treatment and /or rehabilitation of a disease, injury or condition, or to improve the quality of life. This list may include development of prototypes, computer programs and/or software (such as databases and animal models, etc.) or similar products that may be commercialized. **Nothing to report**

9. OTHER ACHIEVEMENTS:

a. We have developed isogenic non-targeted control transduced OV2008 NTC cell line and a batch clonal line of ShRNA downregulated cPLA2 cell line (OV2008ShcP2).
b.
c. Funding applied for based on work supported by this award- LOI to OCRF postdoctoral award by Dr. Roy in 2013- But was not invited back to apply for the full proposal.

10. REFERENCES:

1. D. Roy *et al.*, Loss of HSulf-1 promotes altered lipid metabolism in ovarian cancer. *Cancer Metab* 2, 13 (2014).
2. J. Lai *et al.*, Loss of HSulf-1 up-regulates heparin-binding growth factor signaling in cancer. *The Journal of biological chemistry* 278, 23107 (Jun 20, 2003).
3. J. P. Lai *et al.*, HSulf-1 modulates HGF-mediated tumor cell invasion and signaling in head and neck squamous carcinoma. *Oncogene* 23, 1439 (Feb 19, 2004).
4. K. Narita *et al.*, HSulf-1 inhibits angiogenesis and tumorigenesis in vivo. *Cancer research* 66, 6025 (Jun 15, 2006).
5. C. C. Leslie, Properties and regulation of cytosolic phospholipase A2. *The Journal of biological chemistry* 272, 16709 (Jul 4, 1997).
6. R. A. Nemenoff *et al.*, Phosphorylation and activation of a high molecular weight form of phospholipase A2 by p42 microtubule-associated protein 2 kinase and protein kinase C. *The Journal of biological chemistry* 268, 1960 (Jan 25, 1993).
7. M. Ghosh, D. E. Tucker, S. A. Burchett, C. C. Leslie, Properties of the Group IV phospholipase A2 family. *Prog Lipid Res* 45, 487 (Nov, 2006).
8. Z. Pavicevic, C. C. Leslie, K. U. Malik, cPLA2 phosphorylation at serine-515 and serine-505 is required for arachidonic acid release in vascular smooth muscle cells. *J Lipid Res* 49, 724 (Apr, 2008).
9. C. Guijas *et al.*, Simultaneous activation of p38 and JNK by arachidonic acid stimulates the cytosolic phospholipase A2-dependent synthesis of lipid droplets in human monocytes. *J Lipid Res* 53, 2343 (Nov, 2012).
10. P. L. de Souza, M. Castillo, C. E. Myers, Enhancement of paclitaxel activity against hormone-refractory prostate cancer cells in vitro and in vivo by quinacrine. *Br J Cancer* 75, 1593 (1997).
11. M. Artesi *et al.*, Connexin 30 expression inhibits growth of human malignant gliomas but protects them against radiation therapy. *Neuro Oncol*, (Aug 25, 2014).
12. J. Lai *et al.*, Loss of HSulf-1 up-regulates heparin-binding growth factor signaling in cancer. *J Biol Chem* 278, 23107 (Jun 20, 2003).

13. J. Staub *et al.*, Epigenetic silencing of HSulf-1 in ovarian cancer:implications in chemoresistance. *Oncogene* 26, 4969 (Jul 26, 2007).
14. A. Gubern *et al.*, Group IVA phospholipase A2 is necessary for the biogenesis of lipid droplets. *J Biol Chem* 283, 27369 (Oct 10, 2008).
15. J. H. Kwon, J. H. Lee, K. S. Kim, Y. W. Chung, I. Y. Kim, Regulation of cytosolic phospholipase A2 phosphorylation by proteolytic cleavage of annexin A1 in activated mast cells. *J Immunol* 188, 5665 (Jun 1, 2012).
16. T. C. Walther, R. V. Farese, Jr., The life of lipid droplets. *Biochim Biophys Acta* 1791, 459 (Jun, 2009).
17. L. S. Pike, A. L. Smift, N. J. Croteau, D. A. Ferrick, M. Wu, Inhibition of fatty acid oxidation by etomoxir impairs NADPH production and increases reactive oxygen species resulting in ATP depletion and cell death in human glioblastoma cells. *Biochim Biophys Acta* 1807, 726 (Jun, 2011).
18. S. Mondal *et al.*, HSulf-1 deficiency dictates a metabolic reprograming of glycolysis and TCA cycle in ovarian cancer. *Oncotarget* 6, 33705 (Oct 20, 2015).
19. J. Chien *et al.*, Serine protease HtrA1 modulates chemotherapy-induced cytotoxicity. *The Journal of clinical investigation* 116, 1994 (Jul, 2006).
20. X. He, A. Khurana, D. Roy, S. Kaufmann, V. Shridhar, Loss of HSulf-1 expression enhances tumorigenicity by inhibiting Bim expression in ovarian cancer. *Int J Cancer* 135, 1783 (Oct 15, 2014).

11. APPENDICES: Five Abstracts and Three Manuscripts* attached

Please note that of the three Manuscripts, the third Manuscript in Autophagy is tentatively accepted with revisions that we are currently doing

Abstract 1: 105th AACR Annual Meeting San Diego, CA, April 5-9, 2014.Abstract Number:1293.

HSulf-1 loss in ovarian cancer cells induces lipid droplet biogenesis

Debarshi Roy, Xiaoping He, Ashwani Khurana, Susmita Mondal, Deok-Beom Jung, Sung Kim, Thomas Dierks, Clifford Folmes, Andre Terzic, Viji Shridhar.

We have previously shown that a frequent loss of endosulfatase HSulf-1 in ovarian cancer enhances the heparin binding growth factor signaling which subsequently induces and potentiates tumorigenesis. Our recent data indicate that knockdown of HSulf-1 in ovarian cancer cells significantly alter levels of several metabolites which is comparable to the deranged metabolite profiles in primary ovarian tumors. Here we report that the metabolites associated with lipid metabolism are altered in such a way that the cells start manifesting a "lipogenic phenotype" characterized by an increased fatty acid synthesis, storage and mitochondrial beta oxidation. The lipogenic phenotype is associated with an accumulation of cytoplasmic lipid droplets (LDs) in a stably HSulf-1 knockdown cells [OV202 (Sh1/2) and OV2223 cells]. Presence of LDs is evidenced by BODIPY staining and transmission electron microscopy (TEM) analysis in Sh1/2 and a non-transduced control (NTC) cells. Conversely, enhanced expression of HSulf-1 in TOV21G, SKOV3, and C13 cells also resulted in reducing the number of LDs. More importantly, MEFs (mouse embryonic fibroblasts) from HSulf-1 knockout mice also showed an increased LD biogenesis compared to the wild type MEFs. Microarray analysis identified cytoplasmic phospholipase A_2 ($cPLA_2$; an enzyme involved in LD biogenesis) as one of the genes that was significantly upregulated in OV202 Sh1 and Sh2 cells. We found that Sh1 and Sh2 cells show an increased phosphorylation (ser505) of cytoplasmic phospholipase A_2 ($p\text{-}cPLA_2$) compared to NTC cells. Phosphorylation at ser505 is vital for the enzyme activity of $cPLA_2$ and also necessary for LD biogenesis. We inhibited the LD biogenesis in Sh1 cells by a pharmacological inhibitor of $cPLA_2$ (AACOCF3 and MAFP) as well by shRNA mediated knockdown of endogenous $cPLA_2$. Further, we stimulated NTC and Sh1 cells with heparin binding growth factor (50ng/ml) for different time points and found an elevated phosphorylation of $cPLA_2$ and extracellular signal related kinase (ERK), which is also inhibited by a pre-treatment of cells with $cPLA_2$ inhibitor. Interestingly, inhibition of phospho-ERK by U0126 (MEK inhibitor) also inhibits the phosphorylation of $cPLA_2$. These findings strongly suggest that loss of HSulf-1 promotes lipid metabolism in the ovarian cancer cells via activation of $cPLA_2$ via an ERK dependent pathway. The present work highlights a novel role HSulf-1 in

regulating lipid metabolism which could lead to a better understanding of tumorigenesis and identification of new targets for tumor therapy.

Abstract 2 : presented at the 17 International Conference on Korean Medicine. Cancer Preventive Material Development Research Center (CPMDRC) & Institute, Kyunghee University, 11/26/2013.

Loss of HSulf-1 Promotes Altered Cellular Metabolism of Ovarian Cancer

Debarshi Roy, Chen Wang, Shailendra Giri, Xiaoping He, Ashwani Khurana , Susmita Mondal, Deok-Beom Jung, Han Ihn, Sung Kim, Shaun Riska, Ann Oberg, Jeremy Chien and Viji Shridhar*

Loss of the endosulfatase HSulf-1 is common in ovarian cancer, upregulates heparin binding growth factor signaling and potentiates tumorigenesis and angiogenesis. Since growth factor signaling is closely tied to metabolic signaling, we determined the extent to which HSulf-1 loss affects cancer cell metabolism. We performed untargeted global metabolite profiling in the HSulf-1 ShRNA knockdown cells compared to isogenic non-targeted control transduced cells and identified ~ 338 metabolites using gas chromatography and mass spectrometry (GC/MS) and liquid chromatography tandem mass spectrometry (LC/MS/MS platforms). Knockdown of HSulf-1 in OV202 cells led to significant changes in 156 metabolites pertaining to several metabolic pathways including amino acid, glycolysis, lipids, glutathione and extracellular matrix remodeling. Combining ingenuity pathway analysis of the gene expression changes of these isogenic cell lines and Kyoto Encyclopedia of Genes and Genomics (KEGG) database analysis of commonly altered metabolites indicated that, specifically changes in the metabolites associated with lipid metabolism leading to a "lipogenic phenotype" characterized by an increase in fatty acid synthesis, storage and mitochondrial beta oxidation. Evaluation of the elevated lipid metabolites upon HSulf-1 knockdown in ovarian cancer cells indicated that these were similar to the metabolites reported to be elevated in primary ovarian tumors, thereby alluding to the possibility that loss of HSulf-1 could potentially contribute to the metabolic alterations associated with the progression of ovarian pathogenesis, specifically impacting the lipogenic phenotype of ovarian cancer cells.

Abstract 3: 1st annual Meeting International Ovarian Cancer Consortium Tumor Microenvironment and Drug Discovery, Oklahoma City, OK, 02/07/2014

The Missing Link between Lipid Droplets and Autophagy in Ovarian Cancer

Viji Shridhar, Ph.D.
Department of Experimental Pathology and Laboratory Medicine, Mayo Clinic, Rochester, MN.

Excess free fatty acids are stored as triglycerides in lipid droplets (LD) to be used for energy under nutrient deprived conditions. A second cellular response to starvation is autophagy, in which the cell digests its own components to provide nutrients. Stable downregulation of HSulf-1 in OV202 (Sh1/2) and OV2223 lead to increased LDs as evidenced by BODIPY staining and transmission electron microscopy (TEM) analysis compared to non-transduced control (NTC) cells. Conversely, enhanced expression of HSulf-1 in TOV21G, and SKOV3 cells resulted in reducing the number of LDs compared to vector transfected controls. More importantly, MEFs from HSulf-1 KO mice also showed increased LD biogenesis compared the WT MEFs. Microarray analysis identified $cPLA_2$, a protein involved in LD biogenesis as one of the genes that was significantly upregulated OV202 Sh1 and Sh2 cells. Pharmacological inhibition and ShRNA downregulation of $cPLA_2$ activity resulted in decreasing the # of LDs in OV202Sh1cells. TEM analysis showed that all HSulf-1 proficient cells displayed increased number of autophagic vesicles compared to isogenic HSulf-1 deficient cells. Pharmacological inhibition of $cPLA_2$ promoted autophagy in OV202 Sh1cells and elevated DAPK and LC3BII levels suggesting a novel cross-talk between LD biogenesis and autophagy in ovarian cancer cells. Enhanced expression of WT DAPK reduced LD formation and induced autophagy related markers such as LC3BII, Beclin, ATG12 and 5 in OV202Sh1 cells. HS mimetic PG545, a tumor microenvironment targeting drug that mimics the action of HSulf-1, reduced LDs and promoted autophagy in Sh1 and Sh2 cells. Collectively, these results identify the critical role of HSulf-1, a major regulator of growth factor mediated signaling in the tumor microenvironment as the missing link in regulating both autophagy and LDs in ovarian cancer.

Abstract 4: American Association of Cancer Research, May 18-22, 2015, Philadelphia, PA. ABSTRACT #-2413

Loss of HSulf-1 Promotes Defective Autophagy and Increased Lipid Droplet Biogenesis *in vitro* and *in vivo* in Ovarian Cancer

[1] Debarshi Roy , [1] Susmita Mondal, [1] Ashwani Khurana, [1] Xioping He, [2] Edward Hammond, [2] Keith Dredge, and [1] Viji Shridhar.
[1] Department of Laboratory Medicine and Pathology, Mayo Cancer Center, Mayo Clinic, Rochester, MN; [2] Progen pharmaceuticals, Brisbane, Australia

Abstract

Dysregulation of autophagy and altered metabolic pathways are frequently observed in cancer. Due to these alterations, pharmacological targeting of these two pathways simultaneously could provide a viable therapeutic option. Although the association between these two pathways is well characterized in metabolic disorders, it is not well defined in ovarian cancer (OVCA). In this regard, we found that loss of endosulfatase HSulf-1, a known putative tumor suppressor, suppresses LC3-GFP foci formation and promotes increased lipid droplet (LD) biogenesis suggesting that absence of HSulf-1 in OVCA affects both autophagy and lipid metabolism. While isogenic cells with genetic ablation of HSulf-1 (OV202Sh1/2 and TOV2223Sh1 cells) displayed LDs, the nontargeted control transduced (NTC) OV202 and TOV2223 cells had significantly less LDs. In contrast, Transmission Electron Micrographs (TEMs) showed that OV202 and TOV2223 NTC cells had significantly more autophagic vacuoles (AVs) compared to their isogenic ShRNA targeted cells. Conversely, ectopic expression of HSulf-1 in SKOV3 cells decreased the number of LDs and increased the number of AVs compared to vector transfected controls. Here we report that OV202Sh1 cells and HSulf-1 deficient OV2008 cells have increased p-cPLA$_{2\alpha}^{(ser505)}$ levels that are associated with biogenesis of large number of LDs with reduced AVs. Interestingly, pharmacological inhibition of cPLA$_{2\alpha}$ with AACOCF3 in OV202Sh1 cells resulted in reduced LD biogenesis, inhibited colony formation and reduced tumorigenesis *in vivo*. More importantly, treatment of HSulf-1 deficient cells with HS mimetic PG545 which can compensate for loss of HSulf-1, reduced LD biogenesis, promoted autophagy and inhibited tumor growth *in vivo*. Collectively, these results show a critical role of HSulf-1 in regulating both autophagy and LD biogenesis in ovarian cancer.

Abstract 5: GCC Global Cancer Conference & Medicare Summit , September 15-17, 2014 Hyderabad International Convention Centre, India

THE MISSING LINK BETWEEN LIPID DROPLETS AND AUTOPHAGY
IN OVARIAN CANCER
Viji Shridhar, Ph.D.

It is increasingly being recognized that altered lipid metabolism is an early event in carcinogenesis and a central hallmark of many cancers. Under nutrient deprived conditions, excess free fatty acids are stored as triglycerides in lipid droplets (LD) to be used for energy. A second cellular response to starvation is autophagy, in which the cell digests its own components to provide nutrients. Microarray and Metabolomics profiling identified the lipid pathway as one the major pathways modulated by loss of HSulf-1 in ovarian cancer (OVCA). HSulf-1 deficient cells (OV202 Sh1/sh2, OV2223 and Sulf-1 KO MEFs) possess high levels of lipid droplets (LD) that are absent in the HSulf-1 proficient isogenic cells (TOV21G and SKOV3). More importantly, TEM analysis showed that all HSulf-1 proficient cells displayed increased number of autophagic vesicles compared to isogenic HSulf-1 deficient cells. Pharmacological inhibition and ShRNA downregulation of cPLA$_2$ activity, a protein involved in LD biogenesis resulted in decreasing the # of LDs and promoted autophagy in OV202 Sh1cells and elevated the autophagy inducing protein DAPK and autophagy related markers including LC3BII levels suggesting a novel cross-talk between LD biogenesis and autophagy in ovarian cancer cells. HS mimetic PG545, a tumor microenvironment targeting drug that mimics the action of HSulf-1, reduced LDs and promoted autophagy in Sh1 and Sh2 cells. Collectively, these results identify the critical role of HSulf-1, a major regulator of growth factor mediated signaling in the tumor microenvironment as the missing link in regulating both autophagy and LDs in OVCA.

Cancer & Metabolism

RESEARCH Open Access

Loss of HSulf-1 promotes altered lipid metabolism in ovarian cancer

Debarshi Roy[1†], Susmita Mondal[1†], Chen Wang[2†], Xiaoping He[1], Ashwani Khurana[1], Shailendra Giri[3], Robert Hoffmann[1], Deok-Beom Jung[4], Sung H Kim[4], Eduardo N Chini[5], Juliana Camacho Periera[5], Clifford D Folmes[6], Andrea Mariani[7], Sean C Dowdy[7], Jamie N Bakkum-Gamez[7], Shaun M Riska[2], Ann L Oberg[2], Edward D Karoly[8], Lauren N Bell[8], Jeremy Chien[9] and Viji Shridhar[1*]

A correction to this article has been published: http://www.cancerandmetabolism.com/content/2/1/24

Abstract

Background: Loss of the endosulfatase HSulf-1 is common in ovarian cancer, upregulates heparin binding growth factor signaling and potentiates tumorigenesis and angiogenesis. However, metabolic differences between isogenic cells with and without HSulf-1 have not been characterized upon HSulf-1 suppression *in vitro*. Since growth factor signaling is closely tied to metabolic alterations, we determined the extent to which HSulf-1 loss affects cancer cell metabolism.

Results: Ingenuity pathway analysis of gene expression in HSulf-1 shRNA-silenced cells (Sh1 and Sh2 cells) compared to non-targeted control shRNA cells (NTC cells) and subsequent Kyoto Encyclopedia of Genes and Genomics (KEGG) database analysis showed altered metabolic pathways with changes in the lipid metabolism as one of the major pathways altered inSh1 and 2 cells. Untargeted global metabolomic profiling in these isogenic cell lines identified approximately 338 metabolites using GC/MS and LC/MS/MS platforms. Knockdown of HSulf-1 in OV202 cells induced significant changes in 156 metabolites associated with several metabolic pathways including amino acid, lipids, and nucleotides. Loss of HSulf-1 promoted overall fatty acid synthesis leading to enhance the metabolite levels of long chain, branched, and essential fatty acids along with sphingolipids. Furthermore, HSulf-1 loss induced the expression of lipogenic genes including FASN, SREBF1, PPARγ, and PLA2G3 stimulated lipid droplet accumulation. Conversely, re-expression of HSulf-1 in Sh1 cells reduced the lipid droplet formation. Additionally, HSulf-1 also enhanced CPT1A and fatty acid oxidation and augmented the protein expression of key lipolytic enzymes such as MAGL, DAGLA, HSL, and ASCL1. Overall, these findings suggest that loss of HSulf-1 by concomitantly enhancing fatty acid synthesis and oxidation confers a lipogenic phenotype leading to the metabolic alterations associated with the progression of ovarian cancer.

Conclusions: Taken together, these findings demonstrate that loss of HSulf-1 potentially contributes to the metabolic alterations associated with the progression of ovarian pathogenesis, specifically impacting the lipogenic phenotype of ovarian cancer cells that can be therapeutically targeted.

Keywords: HSulf-1, Lipogenesis, Lipolysis, Lipid droplets, Microarray and metabolite profiling

* Correspondence: shridhar.vijayalakshmi@mayo.edu
†Equal contributors
[1]Department of Experimental Pathology, Mayo Clinic College of Medicine, Rochester, MN 55905, USA
Full list of author information is available at the end of the article

BioMed Central

© 2014 Roy et al.; licensee BioMed Central Ltd. This is an Open Access article distributed under the terms of the Creative Commons Attribution License (http://creativecommons.org/licenses/by/4.0), which permits unrestricted use, distribution, and reproduction in any medium, provided the original work is properly credited. The Creative Commons Public Domain Dedication waiver (http://creativecommons.org/publicdomain/zero/1.0/) applies to the data made available in this article, unless otherwise stated.

Background

Metabolic re-programming has recently emerged as a new hallmark of cancer. Alteration of cellular metabolism in cancer cells is proposed to increase the availability of essential building blocks that support uncontrolled cellular proliferation [1]. Most cancer cells, although diversified by etiology and type, reprogram their metabolism to accumulate metabolic intermediates as sources of building blocks [2]. The Warburg effect is one of the most important metabolic alteration in cancer, in which neoplastic cells exhibit higher glucose uptake and utilization by altering glucose metabolism even in the presence of oxygen to produce lactate from glucose and thereby decouples glycolysis from mitochondrial oxidation [3]. Although alterations in fatty acids (FAs) and lipid metabolism have received less attention, recently, their importance in cancer metabolism is being increasingly recognized. The total lipid pools required for membrane synthesis of dividing cells are derived mainly from FAs and in part from acetyl CoA [4]. Cancer cells meet their FAs demand mainly by increasing *de novo* FA synthesis rather than from exogenous sources and partly from acetyl CoA [5,6]. The activated FAs can then be utilized in the synthesis of membrane phospholipids (PLs) including phosphatidylcholine (PC), phosphatidylethanolamine (PE) in addition to sterols, sphingolipids, and lysolipids to meet the energy demands and proliferation. The rest of the activated FAs then function as signaling molecules or esterified as triglycerols or sterol esters and stored in lipid droplets (LDs) [7,8].

Accumulating evidence suggest that activation of oncogenes such as *MYC*, NF-kB, *K-RAS* [2,9] and loss of tumor suppressor genes (*P53*, *LKB1/AMPK*) [10-12] forms a basis for altered metabolism of cancer cells. The oncogenic activation of c-MYC turns on the Ras-Raf-MAPK signaling pathway along with HIF1α and PI3K-Akt-mTOR axis which transcriptionally stimulate the expression of most glycolytic and glutaminolytic genes and subsequently activate lipid metabolism [13]. Similarly, loss of tumor suppressors forms the basis of the Warburg effect leading to carcinogenesis. For example, p53 activates TIGAR to reduce the cellular accumulation of fructose 2,6 bisphosphate, an allosteric activator of phosphofructo kinase, a critical control point in glycolysis leads to decreased glycolysis [10]. Moreover, growth factor-mediated phosphorylation of pyruvate kinase isoform 2 (PKM2) [14] and mutations of genes in IDH1/2 [15] in the metabolic pathways such as glycolysis and the TCA cycle respectively have been identified that support growth of the rapidly proliferating cells and survive metabolic stress [16,17].

Human Sulfatase 1 (HSulf-1), an endosulfatase established as a putative tumor suppressor in ovarian cancer, has been shown to modulate the signaling of growth factors and cytokines in tumor microenvironment [18]. Our previous work demonstrated that loss of HSulf-1 modulates heparin-binding growth factors such as bFGF, VEGF, HGF, PDGF, and heparin binding EGF (HB-EGF) signaling, which plays an important role in tumor progression, metastasis, and angiogenesis [19-22]. Moreover, serous tumors with moderate to high levels of HSulf-1 had better prognosis in terms of overall survival, implicating its critical role in the progression of ovarian cancer [23]. Our more recent data demonstrated that HSulf-1 knockdown clones in the OV202 ovarian cancer cell line (OV202Sh1 and Sh2 cells) have significantly increased the ability to form anchorage-independent colonies *in vitro* and enhanced tumorigenicity *in vivo* [24]. Also, in breast cancer, HSulf-1 is negatively regulated by HIF1α, but positively by von Hippel-Lindau tumor suppressor gene [23,25,26]. These findings led us to hypothesize that HSulf-1 might play a unique role to alter tumor microenvironment raising the possibility that its loss might alter the cellular metabolism and levels of the resulting metabolites as a downstream effect of altered growth factor signaling.

In the current study, global changes in metabolism were investigated in HSulf-1 silenced OV202 cells by microarray, metabolic data analysis, and Western blotting. Here, we for the first time report that loss of HSulf-1 promotes overall fatty acid synthesis and oxidation leading to a lipogenic phenotype to promote cancer growth in ovarian cancer.

Methods

Cell culture

OV202 cell line was low-passage primary line established at the Mayo Clinic [27]. OV202NTC, Sh1, Sh2, and Cl 11 cells were cultured in 5% CO_2-95% air humidified atmosphere at 37°C with minimal essential medium supplemented with 20% fetal bovine serum and 1 μg/ml puromycin, with non-essential amino acids. All cell lines were tested using a PCR-based assay and found to be free of Mycoplasma contamination.

ShRNA

HSulf-1 short-hairpin (sh) RNA1 (Sh1- AGCTACCCT GGGTTCCTTTGT) which targets the 3′-untranslated region (UTR) was cloned into lentiviral vector pLKO.1-puro as described previously [27]. HSulf-1 shRNA2 (Sh2-CGTCGAATTTGAAGGTGAAAT) and nontargeted control shRNAs (NTC shRNA- ACTTACGAGTGAC AGTAGATT) cloned into the lentivirus vector pLKO.1-puro were chosen from the human library (MISSION TRC-Hs 1.0) and purchased as glycerol stock from Sigma. Transfection with Fugene (Roche) was performed according to the manufacturer's instructions. Transducted cells were selected with 1 μg/ml puromycin.

Rescue of HSulf-1 in Sh1 cells

pcDNA-HSulf-1 plasmid was cloned as described previously [19]. Since Sh1 shRNA targeted the 3′UTR of HSulf-

1, we rescued the expression of HSulf-1 in this cell line with CMV-driven WT expression construct and selected stable clone C11 as previously described [19]. Vector only transfected cells served as controls.

Microarray expression data analysis

OV202 NTC, Sh1, and Sh2 cells in triplicates were profiled using Illumina Human HT-12 3.0 Expression Beadchip array as previously described [28]. Microarray expression data were analyzed on the log2 scale. Data quality was assessed via box and whisker plots along with residual and pair-wise MVA plots before and after normalization [29,30]. All arrays were normalized together using fastlo, a non-linear normalization similar to cyclic loess which runs in a fraction of the time [31]. Both supervised and unsupervised analyses were performed. Supervised analysis to determine differentially expressed genes was performed using Significance Analysis of Microarrays (SAM) [32]. For SAM analysis for unpaired samples, Biometric Research Branch (BRB)-ArrayTools (Version 3.7.0, developed by Dr. Richard Simon and Amy Peng Lam.) was used with Delta set to 0.822, resulting in false discovery rate <5%. Unsupervised clustering was performed using the one minus correlation metric with average linkage. Heat maps were generated for visualization. Pathway analysis was performed using Ingenuity Pathway Analysis (Ingenuity® Systems, www.ingenuity.com).

Liquid chromatography/mass spectrometry (LC/MS, LC/MS^2)

The LC/MS portion of the platform was based on a Waters ACQUITY UPLC and a Thermo-Finnigan LTQ mass spectrometer, which consisted of an electrospray ionization (ESI) source and linear ion-trap (LIT) mass analyzer. The sample extract was split into 2 aliquots, dried, then reconstituted in acidic or basic LC-compatible solvents, each of which contained 11 or more injection standards at fixed concentrations. One aliquot was analyzed using acidic positive ion optimized conditions and the other using basic negative ion optimized conditions in two independent injections using separate dedicated columns. Extracts reconstituted in acidic conditions were gradient eluted using water and methanol both containing 0.1% Formic acid, while the basic extracts, which also used water/methanol, contained 6.5 mM ammonium bicarbonate. The MS analysis alternated between MS and data-dependent MS^2 scans using dynamic exclusion.

Gas chromatography/mass spectrometry (GC/MS)

The samples destined for GC/MS analysis were re-dried under vacuum desiccation for a minimum of 24 h prior to being derivatized under dried nitrogen using bistrimethylsilyl-triflouroacetamide (BSTFA). The GC column was 5% phenyldimethyl silicone and the temperature ramp is from 40°C to 300°C in a 16-min period. Samples were analyzed by a Thermo-Finnigan Trace DSQ fast-scanning single-quadrupole mass spectrometer using electron impact ionization. The instrument was tuned and calibrated for mass resolution and mass accuracy on a daily basis. The information output from the raw data files was automatically extracted as discussed below.

Data extraction and compound identification

Peaks were identified using Metabolon's proprietary peak integration software. Compounds were identified by comparison to library entries of purified standards or recurrent unknown entities. Identification of known chemical entities was based on comparison to metabolomic library entries of purified standards. As of this writing, more than 2,600 commercially available purified standard compounds had been identified and registered into LIMS for distribution to both the LC and GC platforms for determination of their analytical characteristics. The combination of chromatographic properties and mass spectra gave an indication of a match to the specific compound or an isobaric entity. Metabolon data analysts use proprietary visualization and interpretation software to confirm the consistency of peak identification among the various samples. Library matches for each compound were checked for each sample and corrected if necessary.

Normalization

Raw data from each sample was normalized to protein concentration as measured by Bradford assay prior to statistical analysis.

Sample accessioning

Each sample received was accessioned into the Metabolon LIMS system and was assigned by the LIMS, a unique identifier, which was associated with the original source identifier only. This identifier was used to track all sample handling, tasks, and results. The samples (and all derived aliquots) were bar-coded and tracked by the LIMS system. All portions of any sample were automatically assigned their own unique identifiers by the LIMS when a new task was created; the relationship of these samples was also tracked. All samples were maintained at −80°C until processed.

Sample preparation

The sample preparation process was carried out using the automated MicroLab STAR® system from Hamilton Company (Reno, NV, USA). Recovery standards were added prior to the first step in the extraction process for QC purposes. Sample preparation was conducted using a proprietary series of organic and aqueous extractions to remove the protein fraction while allowing maximum recovery of small molecules. The resulting extract was

divided into four fractions; two for analysis by LC and one for analysis by GC and a forth as a spare. Samples were placed briefly on a TurboVap® (Zymark, Hopkinton, MA, USA) to remove the organic solvent. Each sample was then frozen and dried under vacuum. Samples were then prepared for the appropriate instrument, either LC/MS or GC/MS.

QA/QC

For QA/QC purposes, a number of additional samples are included with each day's analysis. Furthermore, a selection of QC compounds is added to every sample, including those under test. These compounds are carefully chosen so as not to interfere with the measurement of the endogenous compounds. These QC samples are primarily used to evaluate the process control for each study as well as aiding in the data curation.

Metaboanalyst

Differently expressed metabolites between Sh1/Sh2 and baseline conditions were firstly mapped to KEGG metabolites IDs according to Human Metabolome Database (HMDB; URL: http://www.hmdb.ca/) [33]. Then, pathway analysis was performed to highlight relevant metabolic pathways defined in KEGG database (http://www.genome.jp/kegg/), using an on-line tool named MetaboAnalyst (http://www.metaboanalyst.ca/) [34,35]. Specifically, two types of pathway analysis were done: one is over-representation analysis using hypergeometric test [35], asking if differentially expressed metabolites are particularly enriched in a same pathway; the other is pathway topology analysis summarizing relative-betweeness centrality [34], investigating potential pathway impact of observed metabolite changes based on known pathway topology relationships.

Western blot analysis

Western blot analysis was performed as described previously [36]. Whole cell lysates were analyzed with the following antibodies: FASN, ASCL1 (Cell signaling), SREBP1c, PLA2G3, HSulf-1 (Abcam, AB96533), CPT1A, HSL, DAGLA, β-tubulin (GeneTex) and β-actin (Sigma-Aldrich).

Real-time PCR

Quantitative real-time PCR (qRT-PCR) was carried out using SYBR-Green PCR Master Mix (Applied Biosystems, Foster City, CA, USA), with specific primers for the genes shown in this study. GAPDH or 18S ribosomal subunit (Applied Biosystems) were used as internal control in a Light Cycler kit (BioRad Chromo 4). Normalization across samples was carried out using the average of the constitutive human gene 18S and/or GAPDH primers and calculated as previously described [18]. Binding efficiencies of primer sets for both target and reference genes were similar.

Bodipy staining

Cells (50,000) were seeded on a coverslip in a 24-well plate and were grown for 24 hours in the presence of complete growth medium. Cells were washed and fixed in 4% paraformaldehyde for 10 min at room temperature before staining with 1 μg/ml BODIPY (493/503; Sigma, St. Louis, MI, USA) in PBS for 10 min at room temperature. Coverslips were washed with PBS and mounted in a slide with Prolong Gold Antifade Reagent (Invitrogen). BODIPY stained cells were examined under inverted confocal fluorescence microscope (Zeiss).

Transient transfection

To determine the effect of PLA2G3 on lipid droplet biogenesis OV202 NTC cells were transiently transfected with plasmids containing empty vector or cDNA encoding PLA2G3. After 24 h of transfection, we performed BODIPY staining to visualize lipid droplets. PLA2G3 plasmid was obtained on a MTA from Addgene.

Fatty acid synthesis

Cells were washed twice in cold PBS and resuspend in lysis buffer (50 mM Tris-HCl, pH 7.4, 1 mM EDTA, 150 mM NaCl and PMSF. Cells were sonicated and homogenized by dounce homogenizer followed by centrifugation at 13,000 rpm for 15 min at 4°C. The supernatant was collected and proteins were measured by Bradford assay, and 100 μg of protein was used to conduct FASN activity assay. FASN activity was measured by protocol described by Vazquez-Martin et al. [37]. Briefly, 100 μg of protein was incubated with 240 μM NADPH, 30 μM acetyl CoA and 50 μM malonyl CoA in assay buffer (200 mM potassium phosphate, pH 6.6, 1 mM DTT, 1 mM EDTA) and oxidation of NADPH was measured by monitoring the absorbance at 340 nM over the period of the time. Results presented here compares FASN activity monitored for 10 min. Values are presented as nanomolar NADPH oxidized per minute per milligram of protein.

Fatty acid oxidation

Oxygen consumption rate was measured using a Seahorse Bioscience XF24 flux analyzer. 5×10^4 cells were seeded per well in triplicates in MEM-α containing 20% FBS in an XF24 well culture microplates and incubated overnight in a 37°C/10% CO_2 incubator. The assay medium for FAO is low-buffered KHB buffer (110 mM NaCl, 4.7 mM KCl, 2 mM $MgSO_4$, 1.2 mM Na_2HPO_4, 2.5 mM glucose adjusted to pH 7.4) supplemented with 0.5 mM carnitine. For induction of FAO, BSA conjugated palmitate was injected to a final concentration of 50 μM. XF analyses were performed in the XF Extracellular Flux Analyzer

(Seahorse Bioscience, Billerica, MA, USA). Three basal rates were measured prior to automated injection of palmitic acid (50 μM) coupled to BSA vehicle or BSA vehicle alone. After treatment for 55 min, the carnitine palmitoyl transferase-1 inhibitor, Etomoxir (ETO, 50 μM), was added. Oxygen consumption rates were measured by using time-resolved method (Seahorse Bioscience XF24) (21). Data were normalized to protein content (assayed after completion of measurements).

Proliferation assay

Equal number of cells (1×10^5) was plated in triplicate in 12-well plates. OV202NTC, Sh1, and Sh2 cells were counted after 24, 48, and 72 h using a cellometer (Nexelom, Lawrence, MA, USA). For Etomoxir treatment, Equal number of cells (1×10^5) were seeded in 12-well plates in triplicate and treated with increasing concentration of Etomoxir (0 to 100 μM) for 24 h and total cell numbers were counted using cellometer.

Results

Loss of HSulf-1 comprehensively altered major metabolic pathways

We recently reported that HSulf-1 knockdown clones in the OV202 ovarian cancer cell line (OV202Sh1 and Sh2 cells) have significantly increased ability to form anchorage-independent colonies *in vitro* and enhanced tumorigenicity *in vivo* [24]. Consistent with these observations, our growth assays showed enhanced growth rate in Sh1 and Sh2 cells compared to NTC cells (Additional file 1: Figure S1). Here, to elucidate the function of putative tumor suppressor HSulf-1 in the metabolism of ovarian cancer, we performed gene expression profiling of stably knockdown HSulf-1 clonal lines OV202 Sh1 and Sh2 cells (referred to from hereon as Sh1 and Sh2) compared to HSulf-1 expressing non-targeted control cells (OV202NTC, referred to as NTC) [26] in triplicates using Illumina HumanHT 12 v3 platform [28]. Unbiased hierarchical clustering and heat maps showed that genes in several different pathways were differentially expressed in Sh1 and Sh2 compared to NTC cells (Figure 1A). We found that over 1,645 and 780 genes were differentially expressed in Sh1 and Sh2 cells, respectively, compared to NTC at 2.6 FC (p and FDR <0.0001). We identified 500 and 280 altered genes in Sh1 and Sh2 cells respectively by significance analysis of microarrays (SAM) [32] from the comprehensive list of 2,752 genes which encoded all known human metabolic enzymes and transporters reported by Possemato et al. [38]. Ingenuity pathway analysis (http://www.ingenuity.com) for these genes showed that most genes were differentially regulated in the fatty acid/lipid pathways in Sh1 and Sh2 cells compared to NTC cells (Additional file 2: Table S1, Figure 1B). We next explored the 271 genes in the lipid related pathways from our microarray data by unsupervised clustering (Figure 1C) and found that 26% (73 of 271) genes were differentially expressed in Sh1 and Sh2 cells compared to NTC cells (Figure 1D), indicating that tumor suppressor HSulf-1 possibly regulates the lipid metabolism in ovarian cancer cells.

Loss of HSulf-1 altered global metabolic profile in ovarian cancer cells

To determine whether loss of HSulf-1 has effect in cellular metabolism, we performed unbiased global metabolic profiling using the Metabolon platform (Metabolon Inc, Durham, NC, USA) in Sh1 and Sh2 cells compared to NTC. The samples were extracted using Metabolon's standard solvent extraction method from cells in logarithmic phase with 5 biological replicates for each sample and distributed into equal parts for analysis on the GC/MS and LC/MS/MS platforms. Hierarchical clustering revealed that metabolite levels of Sh1 and Sh2 cells cluster together separately from control NTC (Figure 2A). Our initial principal component analysis (PCA) [39] revealed that Sh1 and Sh2 cells had specific group of metabolites which were different from NTC cells (Figure 2B). Additionally, t test in each principal component dimension showed that PCA differences between Sh1-Sh2 and NTC cells mainly reside in the first and second principal components, with statistically significant p values of 1.8e – 10 and 4.5e – 6, respectively. Consistent with this, two-dimensional PCA plots showed differences between Sh1-Sh2 and NTC are mainly in the first and second PC dimensions (Figure 2C,D,E). We also performed linear regression analysis to evaluate association of each principal component vs. major metabolite classes, to determine if lipid class is one of the dominant factors determining the first and second principal components. The association was evaluated in a multivariate regression model (Additional file 3: Figure S2), where coefficients of first/second PCs were treated as dependent variable, and metabolite class labels were regarded as independent variables. This analysis showed that the lipid class has statistically significant association with both first and second PC dimensions, with p values = 5.0e – 3 and 1.4e – 3, respectively. Interestingly, the peptide class, despite its relatively small size, also has significant associations with both first and second PC dimensions, while the amino acid class has significant association with the first principal component.

Moreover, this analysis showed a total of 338 known metabolites altered by the loss of HSulf-1 in Sh1 and Sh2 cells. Among them, Sh1 and Sh2 cells had a total of 193 and 188 biochemical, respectively, which were significantly altered ($p < 0.05$, Welch's t test) compared to NTC cells (Figure 2F, Additional file 4: Table S2, and Additional file 5: Table S3). Additionally, with the loss of

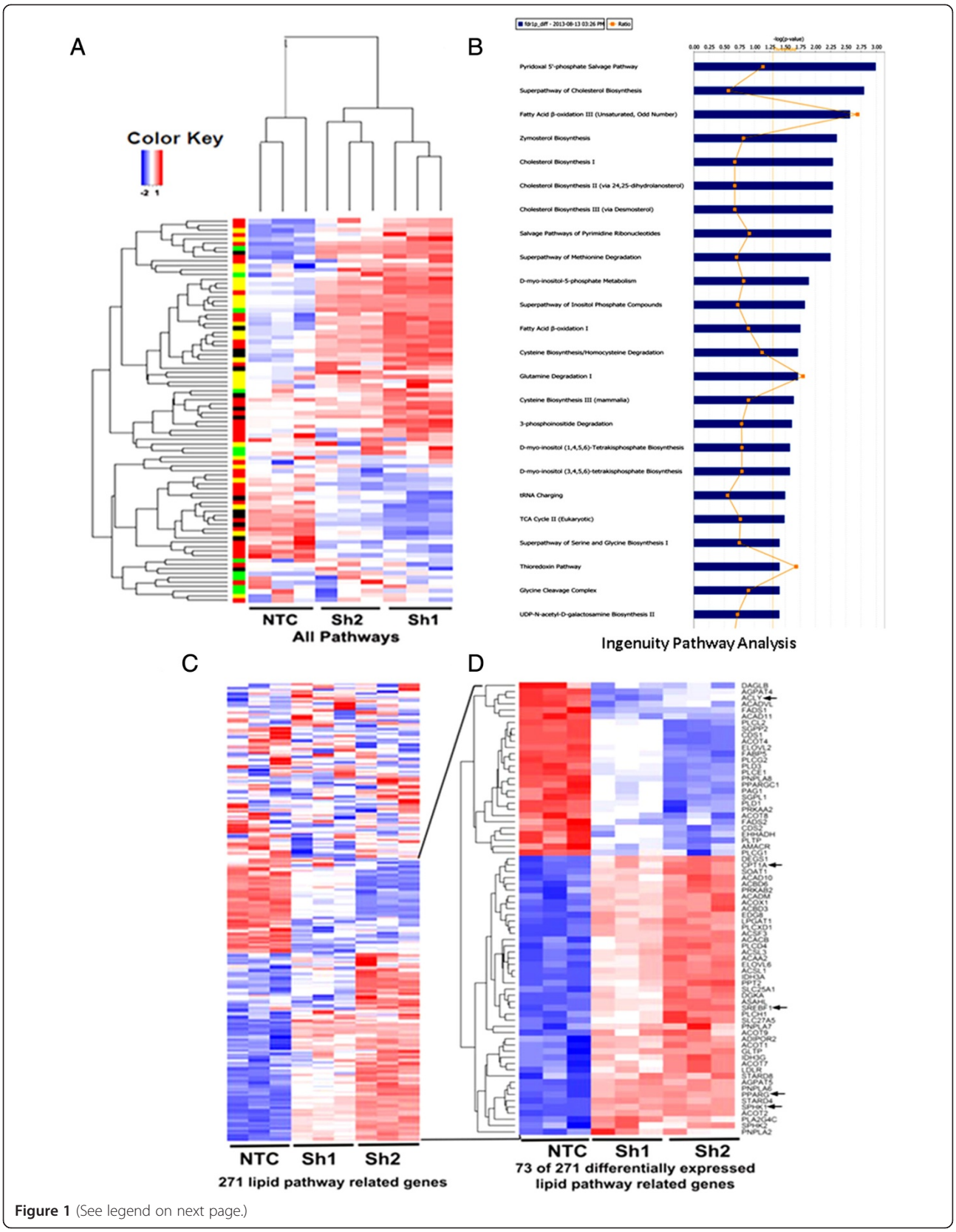

Figure 1 (See legend on next page.)

(See figure on previous page.)

Figure 1 Microarray analysis of differentially expressed genes in OV202NTC, Sh1, and Sh2 cells. (A) Unsupervised hierarchical clustering normalized expression values of 20,090 selected probe sets for NTC, Sh1, and Sh2. Each class is represented by three biological replicates. *Red*: expression values above the average across all samples; *blue*: expression values below the average across all samples. **(B)** Ingenuity pathway analysis of metabolic genes. The most statistically significant metabolic pathways identified in the confirmed cell-specific marker list are listed according to their *p* value (−Log) (*blue bars*) and the ratio of list genes found in each pathway over the total number of genes in that pathway (Ratio, orange squares). The threshold line corresponds to a pathway enrichment *p* value of 0.05. **(C)** Unsupervised hierarchical clustering normalized expression values of 271 selected lipid pathway related probe sets for NTC, Sh1, and Sh2. Each class is represented by three biological replicates. *Red*: expression values above the average across all samples; *blue*: expression values below the average across all samples. **(D)** The most differentially expressed lipid pathway related genes (73 of the 271 genes in A, FDR = <1%). The statistical difference was tested according to *t* test using 'genefilter' package in R, and multi hypothesis-testing corrected FDR was estimated using 'fdrtool' package in R. The *black arrow* indicates genes analyzed by real-time and/or western blot analysis in this study.

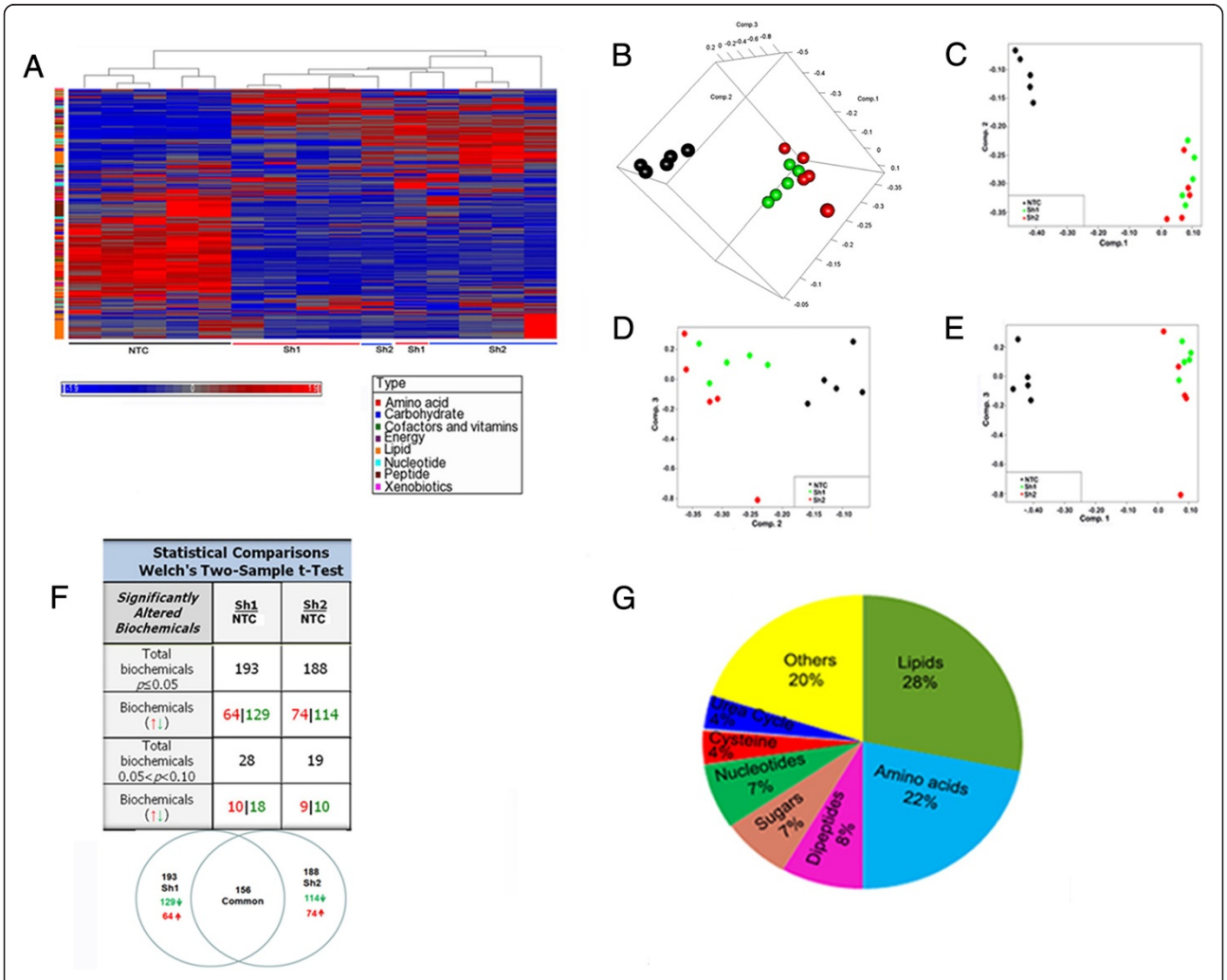

Figure 2 Metabolite profile of ovarian cell line expressing HSulf-1 (NTC) and HSulf-1 downregulates Sh1 and Sh2 cells. (A) Heatmap showing 338 biochemicals in lysates from 5 replicates each of OV202 cells expressing HSulf-1 (NTC), HSulf-1 Sh1 and Sh2 cells arranged by unsupervised clustering. **(B)** Three-dimensional sample PCA plot of log-transformed normalized concentration of 338 biochemicals, where samples were colored by NTC, Sh1, and Sh2 cell-types. **(C, D, E)** 2-D PCA plots: two-dimensional PCA plots between paired principal components (first PC vs. second PC; second PC vs. third PC; first PC vs. third PC). *x-/y*-axis corresponds to loadings of specified PC dimension and each point is a metabolite sample, with *black*, *green*, and *red colors* indicating NTC, Sh1, and Sh2 conditions, respectively. **(F)** Table showing significantly altered biochemical in Sh1 and Sh2 cells compared to NTC cells. Welch's two-sample *t* test was used to identify biochemicals that differed significantly between experimental groups. A summary of the numbers of biochemicals that achieved statistical significance ($p \leq 0.05$), as well as those approaching significance ($0.05 < p < 0.10$), are shown along with the Venn diagram of shared metabolites between Sh1 and Sh2 cells. **(G)** Pie chart of percentage of common altered metabolites in Sh1 and Sh2 cells in major pathways.

HSulf-1, 129 and 114 metabolites were downregulated, whereas 64 and 74 metabolites were upregulated in Sh1 and Sh2 cells, respectively. Also, 40% of these biochemicals were altered in the same direction in Sh1 and Sh2 cells compared to NTC cells ($p = <0.05$, with false discovery rate (FDR) <0.05, Additional file 6: Table S4). Interestingly, we found that among all the metabolites altered, 28% were lipids, 22% were amino acids, whereas sugar and dipeptide comprised 7% (Figure 2G), implicating that loss of HSulf-1 mediates a global metabolic alteration in ovarian cancer with changes in the lipid class being a major contributor.

However, some metabolites were differentially altered in the Sh1 and Sh2 cells. The differentially changed metabolites between these ShRNAs could also be a function of the level of knockdown and where the ShRNAs could have integrated. The extent of knockdown in Sh1 targeting the 3'UTR was close to 100%. However, with Sh2 RNA targeting the open reading frame, there was still some level of HSulf-1 present (Figure 1A, [24]).

Alteration of lipid metabolites upon HSulf-1 loss

The lipogenic phenotype characterized by the activation of lipid metabolism is recognized as a universal feature of most cancers [40,41]. Apart from the fatty acid (FA) uptake, cancer cells requires de novo FA biosynthesis to synthesize new membranes, to store energy in lipid droplets and to form the lipidic platform for signaling in membrane level in lipid rafts for increased signaling of cell growth receptors [42,43]. Moreover, circulating lipids also play a significant role in cancer cell growth, migration, and invasion [44,45]. Of the 156 common metabolites altered in Sh1 and Sh2 cells, 44 (28%) metabolites belonged to the lipid class including long-chain FAs, lysolipids, sphingolipids, glycerolipids, eicosanoids, and carnitine (Additional file 6: Table S4), in which 20 metabolites were upregulated (45%). Using the Kyoto Encyclopedia of Genes and Genomics (KEGG) database, we mapped these metabolites to major pathways impacted with alterations in the key junctions [34,35]. These included linoleic acid, glycerophospholipid, arachidonic acid (Additional file 7: Figure S3), and sphingolipid pathways [46,47]. Consistent with these data, we found that among the 20 long-chain fatty acid metabolites detected, 13 metabolites were significantly increased by 2–6-fold including palmitate, stearate, and oleate, while the remaining 7 long-chain FAs did not show any significant differences in both Sh1 and Sh2 cells (Figure 3A). Of note, docosadienoate (22:2n6), 10-nonadeconoate and eicosenoate (20:1n9) levels were increased approximately sevenfold compared to NTC. Additionally, all the detected branched fatty acid metabolites were augmented (Figure 3B) while five of six essential fatty acids detected were increased 2–5.5-fold (Figure 3C).

The key structural lipids in cell membranes are the glycerol-phospholipids including phosphatidyl-choline, phosphatidyl-ethanolamine, phosphatidyl-serine, phosphatidyl-inositol, and phosphatidic acid in addition to other lipids, such as sterols, sphingolipids, and lysophospholipids. Sphingolipids such as ceramide, sphingosine, and sphingosine-1-phosphate are bioactive lipids which can dictate the signaling including growth factor responses, inflammation, apoptosis, and proliferation [48]. Our metabolite analysis revealed that HSulf-1 deficiency was closely associated with increased levels of sphinganine (FC = 21.79, $p = <0.001$), sphingosine (FC = 5.08, $p = <0.001$), palmitoyl sphingomyelin (FC = 1.62, $p = <0.0047$, and FC = 1.52, $p = <0.001$), and stearoyl sphingomyelin (FC = 6.24, $p = <0.001$ and FC = 5.30, $p = <0.001$) (Figure 3D). Additionally, we found that knockdown of HSulf-1 expression also largely affected the metabolite levels of choline/inositol pathway (Figure 3E) and lysophospholipids (Figure 3F) including reduced glycerophosphorylcholine (GPC) (FC = −1.5, $p = 0.0940$ in Sh1 cells only) and glycerol 3-phosphate (G3P) (FC = −1.6, $p = 0.0154$ and FC = −1.9, $p = <0.001$). Altogether, these results implicated a key role of HSulf-1 in increased lipid metabolism and signaling.

Deficiency of HSulf-1 in ovarian cancer induced higher expression of 'lipogenic genes'

All the lipid molecules in cells are derived in part from acetyl CoA, and many contain FAs. These FA building blocks come from either exogenous sources or from de novo FA synthesis. Thus, malignant cells synthesize their own FA de novo and thereby exhibit a preference over exogenous FA uptake, while most normal human cells prefer exogenous sources [49]. Our microarray analysis showed that mRNA levels of lipogenic enzymes fatty acid synthase (*FASN),* sphingosine kinase 1 (*SPHK1*), *PLA2G4A, PLA2G3,* sterol regulatory element-binding transcription factor 1 (*SREBF1*), and peroxisome proliferator-activated receptor (*PPARγ*) are also upregulated upon loss of HSulf-1 (Figure 4A). Consistent with the increased levels of these genes and lipid metabolites, qRT PCR and immunoblotting showed enhanced mRNA (Figure 4B) and protein (Figure 4C) expressions of *FASN*, *SPHK1*, *PLA2G4A*, *PLA2G3*, *SREBF1*, and *PPARγ* in the Sh1 and Sh2 cells compared to the NTC cells. The increase in the mRNA and protein expression of *FASN* along with the increased production of several long chain FAs in Sh1 and Sh2 cells indicated that fatty acid synthesis was enhanced in HSulf-1 silenced cells. To confirm, we also measured the enzymatic activity of FASN and found almost twofold higher activity of FASN in Sh1 and Sh2 cells compared to NTC cells (Figure 4D). These data suggest that loss of HSulf-1 can increase the activity of FASN to enhance FA synthesis.

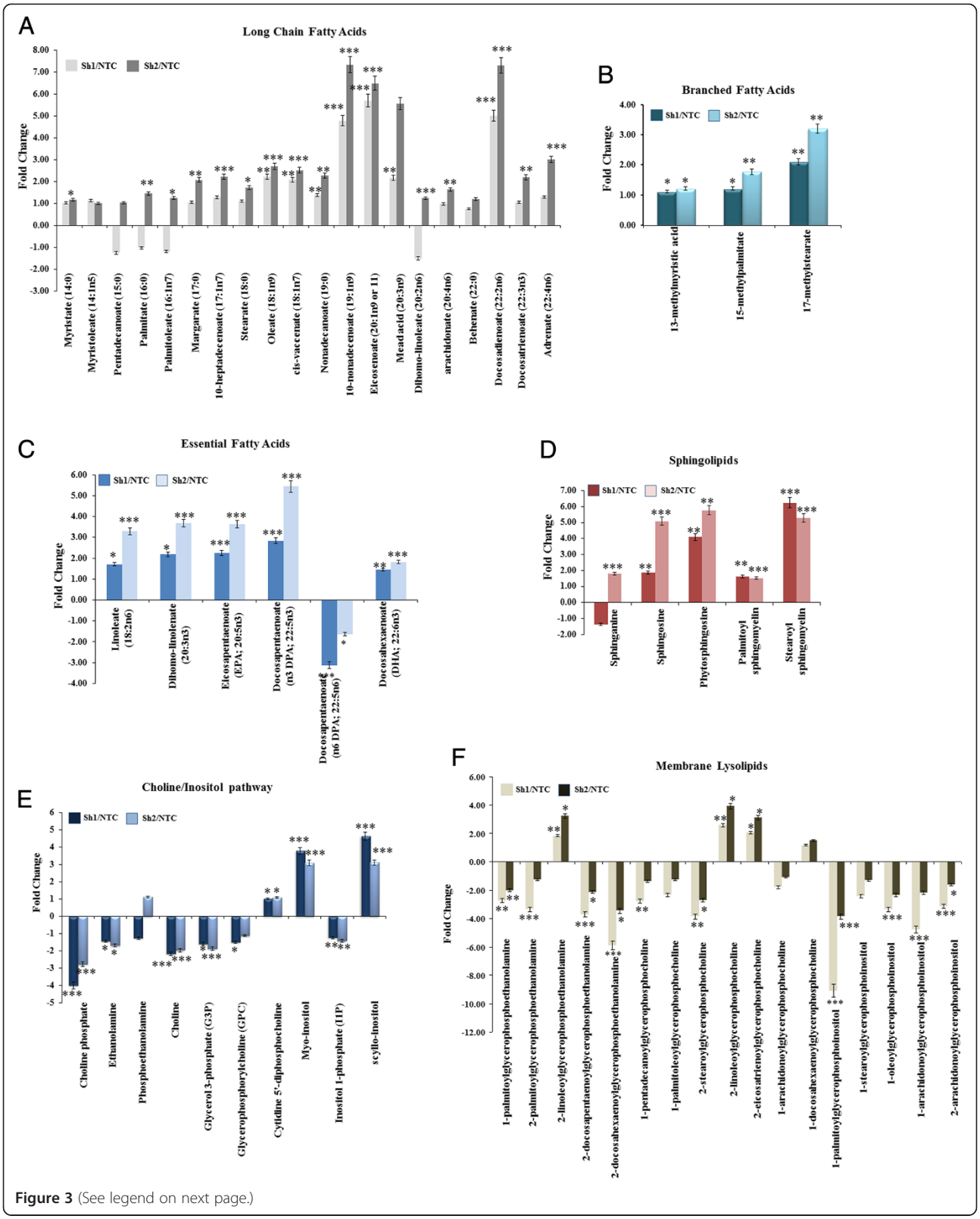

Figure 3 (See legend on next page.)

(See figure on previous page.)
Figure 3 Loss of HSulf-1-mediated increase in fatty acids, sphingolipids, and lysolipids. The samples were extracted using Metabolon's standard solvent extraction method from cells in logarithmic phase having five biological replicates for each sample and distributed into equal parts for analysis on the GC/MS and LC/MS/MS platforms. **(A)** Fold increase of long-chain fatty acids were calculated by the average metabolite level of Sh1/NTC and Sh2/NTC. *$p = 0.02$ to 0.09; **$p = 0.002$ to 0.01; ***$p < 0.001$ compared to NTC. **(B)** Branched chain fatty acids and (**C**) essential fatty acids were calculated by the average metabolite level of Sh1/NTC and Sh2/NTC. *p* values for both branched chain fatty acids and essential fatty acids were *$p = 0.01$ to 0.02; **$p = 0.002$ to 0.01; ***$p < 0.001$ compared to NTC. **(D)** Fold increase of sphingolipids were calculated by the average metabolite level of Sh1/NTC and Sh2/NTC. *$p = 0.01$ to 0.09; **$p = 0.002$ to 0.008; ***$p < 0.001$ compared to NTC. **(E)** Choline/inositol pathway metabolites' fold change and **(F)** membrane lysolipids were calculated as mentioned earlier. *P* values for choline/inositol pathway was *$p = 0.009$ to 0.09; **$p = 0.002$ to 0.008; ***$p < 0.001$ whereas *$p = 0.01$ to 0.02; **$p = 0.002$ to 0.009; ***$p < 0.001$ for membrane lysolipids compared to NTC.

Interestingly, FASN, SPHK1, PLA2G4A, PLA2G3, SRE BF1, and PPARγ are the key enzymes which are localized and involved in the biogenesis of lipid droplets (LD) [50-54]. The FAs are activated by covalent modification by CoA via fatty-acyl-CoA synthetases and esterified to glycerol generating triglycerides or sterol esters that are stored in lipid droplets [42]. Accumulation of cytoplasmic LDs forms a basis of increased growth and chemoresistance in neoplastic cells [40,55]. To explore whether increased expression of above enzymes resulted in LD formation, we imaged the LDs by bodipy staining which clearly showed increased LDs in Sh1 and Sh2 cells. As expected, there were very few LDs in the NTC cells (Figure 4E). To confirm whether HSulf-1 was directly involved in LD biogenesis, we also rescued the expression of HSulf-1 in Sh1 cells by stable transfection of CMV-driven HSulf-1 expression construct (clone 11) with vector-transfected Sh1 cells served as controls (Figure 4F,G). Bodipy staining revealed that rescue of HSulf-1 significantly reduced the number of lipid droplets in Sh1 (Sh1 clone 11) compared to Sh1 vector control with many LDs (Figure 4G) demonstrating that loss of HSulf-1 promotes LD biogenesis. Additionally, transient transfection of PLA2G3 into OV202NTC cells showed increased LDs in these cells compared to vector-transfected controls (Figure 4H), suggesting a role of PLA2G3 in loss of HSulf-1 mediated LD biogenesis.

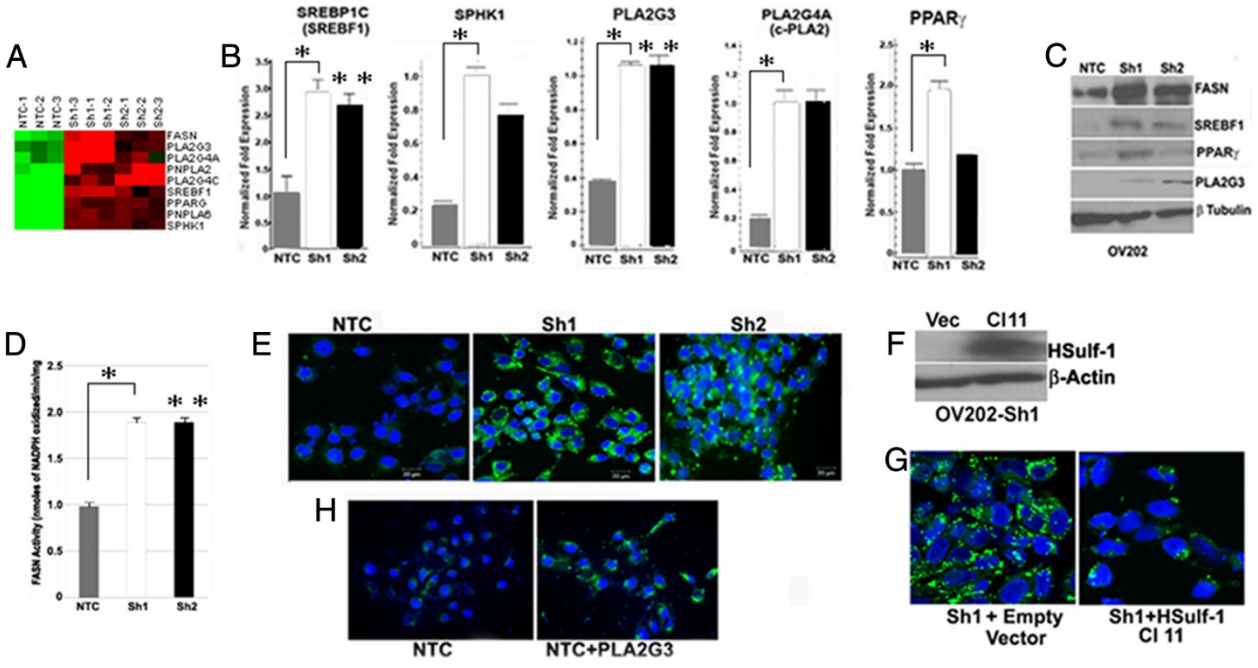

Figure 4 Enhanced expression of lipogenic genes in ovarian cancer. (A) Heat map of a subset of significantly altered lipid pathway-related genes by supervised clustering (*Red*, overexpressed and *green*, downregulated genes in Sh1 and Sh2 compared to NTC cells). **(B)** Normalized levels of *SREBP1c* (*SREBF1*), *SPHK1*, *PLA2G3*, *PLA2G4A* (*c-PLA2*) and PPARγ mRNA by quantitative RT-PCR in NTC and Sh1 and Sh2 cells. *$p < 0.05$; **$p < 0.01$; ***$p < 0.001$ compared to NTC cells. **(C)** Western blot analysis of FASN, SREBF1, PPARγ, PLA2G3 with beta tubulin as loading control. **(D)** FASN activity is expressed as fold change in Sh1 and Sh2 cells compared to NTC cells. Results are means (*columns*) of two independent experiments made in triplicate. One-factor ANOVA was used to analyze the differences in FASN activity between each experimental condition. All statistical tests were two-sided (**$p \leq 0.01$). **(E)** Bodipy (*green*) and DAPI (*blue*) staining of the lipid droplets in NTC, Sh1, and Sh2 cells imaged in Carl Zeiss LSM 510S confocal microscope. **(F)** Immunoblot analysis of HSulf-1 in Sh1 vec, and Sh1 Cl 11, where β-actin was used as loading control. **(G)** Bodipy (*green*) and DAPI (*blue*) staining of lipid droplets and nuclei respectively in Sh1 vec and Sh1 Cl 11 cells. **(H)** Bodipy staining of LDs following enhanced expression of empty vector compared to PLA2G3 construct by transient transfection in OV202NTC cells shows LDs only in PLA2G3 transfected cells.

Loss of HSulf-1 facilitates enhanced β-oxidation and lipolysis

The analysis of metabolite data additionally revealed the increased levels of acetylcarnitine (FC = 3.74, $p = <0.001$ and FC = 3.22, $p = <0.001$), butyrylcarnitine, hexanoylcarnitine and octanoylcarnitine in HSulf-1 silenced cells. Moreover, increased levels of oleolycarnitine were 16.84- and 6.64-fold in Sh1 and Sh2, respectively (Figure 5A). Carnitine is important for shuttling FAs across mitochondrial membranes for oxidation and so the escalation of carnitine level enhances β-oxidation support the increased growth of ovarian cancer. To determine if β-oxidation was enhanced in Sh1 and Sh2 cells, we measured the mRNA and protein level of carnitine palmitoyltransferase 1 (*CPT1A*) and the results showed a higher level of CPT1A in both in Sh1 and Sh2 cells (Figure 5B). The increase in the expression of *CPT1A* mRNA along with increased production of several of the long chain FAs in Sh1 and Sh2 cells indicated that these cells may utilize long chain FAs by β-oxidation to generate more ATP to accommodate increase proliferation. Next, to confirm this notion, we determined the fatty acid oxidation (FAO), and results showed that FAO was higher both in Sh1 and Sh2 compared to NTC cells upon addition of palmitate (Figure 5C). Subsequently, we demonstrated that Etomoxir, a specific inhibitor of CPT1A, decreased FAO more significantly in Sh1 and Sh2 cells compared to NTC cells. We also demonstrated that Sh1 and Sh2 cells were more sensitive toward Etomoxir treatment than NTC confirming a major role of FAO in their survival (Additional file 8: Figure S4).

Since FAs are stored in lipid droplets and released by the action of lipolytic enzymes, we determined the expression of monoacylglycerol lipase (MAGL), diacylglycerol lipase alpha (DAGLA), long-chain acyl-CoA synthetase (ACSL1), and hormone-sensitive lipase (HSL). Immunoblot analysis showed that the expression of these enzymes was upregulated in Sh1 and Sh2 cells compared to NTC cells (Figure 5D), demonstrating that loss of HSulf-1 activates beta oxidation and lipolysis.

Altered metabolism in amino acid and peptide super pathways in cells with loss of HSulf-1

In addition to the altered lipid metabolism, the metabolomic analysis revealed that amino acids and their derivatives were the second most class of metabolites altered in HSulf-1 knockdown cells (Additional file 4: Table S2). Most of the amino acids including serine, threonine, aspartate, asparagine, alanine, phenylalanine, tyrosine, tryptophan, arginine, ornithine, proline, and methionine were decreased in the range of −1.36- to −3.33-fold ($p < 0.05$) in both OV202 Sh1 and Sh2 cells. In contrast, glycine was increased marginally in Sh1 and Sh2 cells (range 1.08- to 1.1-fold; $p < 0.001$ for each). Interestingly, we found significant upregulation of cysteine (eight to tenfold, $p < 0.001$) and its derivatives, hypotaurine (FC = 2.38, $p = <0.001$ and FC = 1.99, $p = <0.0244$) and taurine (FC = 9.91, $p = <0.0032$ and FC = 5.38, $p = <0.0090$) in both Sh1 and Sh2 cells (Additional file 4: Table S2). We also observed alterations of *N*-acetylated amino acids including *N*-acetyl-alanine, serine, and threonine resulted from the action of *N*-acetyltransferases on acetyl-CoA and L-amino acids where all the six *N*-acetylated amino acid tested were downregulated. The amino acid-derived antioxidant, both reduced and oxidized glutathione levels were lower in HSulf-1-deficient cells. Additionally, among different dipeptide molecules, gamma-glutamylglutamate (FC = 3.73, 2.77 in Sh1 and Sh2, $p = <.0001$) and gamma-glutamylmethionine (FC = 7.31, 6.23 in Sh1 and Sh2 respectively, $p = <.0001$) levels were increased upon loss of HSulf-1. This enhancement may be particularly relevant as increased expression of gamma-glutamylglutamate is reported to be associated with tumor progression and drug resistance observed in human malignancies [56]. Additionally, a significant increase of pro-hydroxy-proline, (FC = 2.05, $p = 0.0057$ and FC = 1.92, $p = 0.0088$) a dipeptide, also demonstrated in Sh1 and Sh2 cells. Pro-hydroxy-proline is a marker of collagen and extracellular matrix degradation (Additional file 4: Table S2).

Discussion

Aberrant cellular metabolism in cancer is now well known and is directly related to tumorigenesis in most of the cancers [57,58]. Multiple signaling pathways and several molecules are involved in the synthesis and degradation of the lipids and also the activities of lipid metabolizing enzymes are regulated by a complex interplay between metabolic, tumor suppressor, and oncogenic signaling [59]. Though loss of HSulf-1, a putative tumor suppressor gene, was well known to promote tumorigenesis, angiogenesis [22,23], and invasion [20] in breast [18,21] and ovarian [23,24] cancers, the role of HSulf-1 was never elucidated in altered metabolism of ovarian cancer cells so far. Thus, in the present study, we have shown that loss of the putative tumor suppressor, HSulf-1 promotes altered metabolic pathways including lipid, amino acid, and nucleotide. Of the several pathways altered by loss of HSulf-1, the lipid and amino acid pathway-related metabolites accounted for 50% of the total altered metabolites identified. In ovarian cancer, altered lipid metabolism was detected in patients during early and late stages of disease compared to healthy controls [60,61]. In contrast to lipid pathway-related metabolites, there are very few reports on the alteration in the amino acid levels in OVCa. We found a significant downregulation of most of the amino acids with loss of HSulf-1 consistent with Zhang et al.'s report where they showed

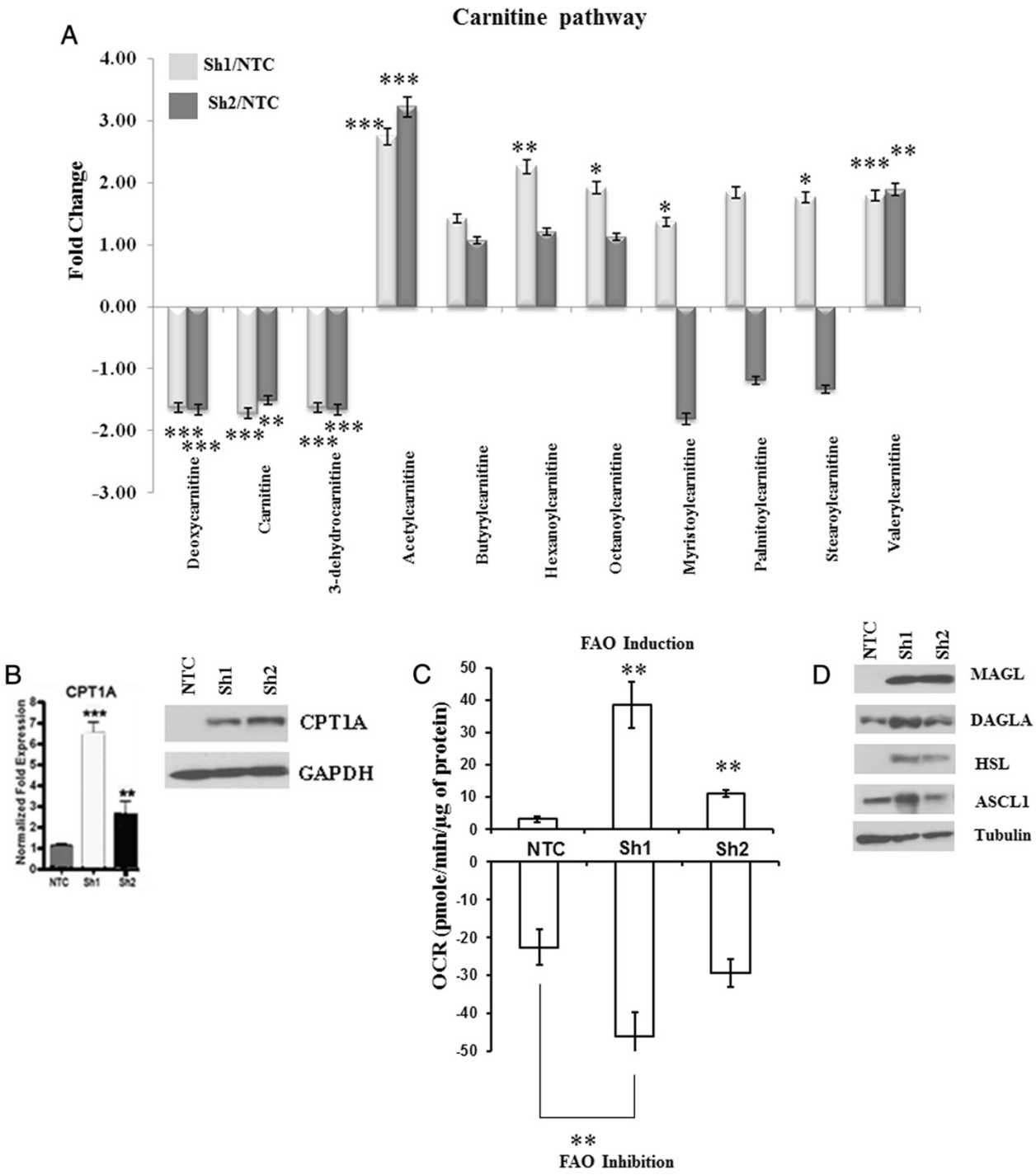

Figure 5 Loss of HSulf-1 induced enhanced β-oxidation and lipolytic enzymes. (A) The samples were extracted using Metabolon's standard solvent extraction method from cells in logarithmic phase having five biological replicates for each sample and distributed into equal parts for analysis on the GC/MS and LC/MS/MS platforms. Fold increase of carnitine and its derivatives were calculated by the average metabolite level of Sh1/NTC and Sh2/NTC. *$p = 0.01$ to 0.09; **$p = 0.001$ to 0.009; ***$p < 0.001$ compared to NTC. **(B)**. Levels of *CPT1A* in NTC, Sh1, and Sh2 cells determined by real-time PCR and Western blot analysis. *$p < 0.05$; **$p < 0.01$; ***$p < 0.001$ compared to NTC. **(C)** FAO in terms of OCR in pmol/min/mg of protein was monitored using a Seahorse Bioscience Extracellular Flux Analyzer in real time (mean ± S.D., $n = 3$). Cells treated with etomoxir (50 μM), an inhibitor of carnitine palmitoyltransferase 1, served as a positive control. Changes in the FAO induction in Sh1 and Sh2 cells are compared with that of NTC cells. Etomoxir-induced inhibition of FAO in Sh1 and Sh2 cells are compared with the FAO inhibition in NTC ($p \leq 0.01$ and $p \leq 0.001$). **(D)** Immunoblot analysis of MAGL, DAGLA, HSL, ASCL1 in NTC, Sh1, and Sh2 where tubulin used as internal loading control.

presence of lower levels of amino acids in the serum of patients with esophageal adenocarcinomas [62]. This downregulation could be due to differences in uptake from the media, increased utilization, and/or catabolism since increased demand for utilization of amino acids has been reported in other cancers [63,64]. Other studies have shown an increase in amino acid levels in the serum of patients with colon and breast cancers [65,66]. While the majority of amino acids were downregulated, we found significant upregulation of cysteine and its derivatives hypotaurine and taurine in Sh1 and Sh2 cells. Significant upregulation in cysteine, taurine, and hypotaurine could be the result of increased levels of cysteine dioxygenase type I (CDO1) [67-69] in Sh1 and Sh2 cells (data not shown). While taurine is reported to be downregulated in cancer [70], it is also reported to be increased in tumors of the prostate, squamous cell carcinoma and liver metastasis [71,72]. Additionally, levels of myo-inositol and taurine concentrations both *in vivo* and *in vitro* are correlated with cell density of the tumors [73].

Additionally, we also saw an increase in the dipeptide pro-hydroxy-pro in Sh1 and Sh2 cells. Increase in pro-hydroxy-proline is consistent with the report that major cartilage ECM proteins type II collagen and aggrecan were significantly lower in *HSulf*$^{-/-}$ chondrocytes suggesting that loss of HSulf-1 may regulate the overall balance of cartilage matrix synthesis and degradation [74]. Consistent with this, significant alterations in several UDP-glycosylation moieties, including UDP-acetylglucosamine/UDP-acetylgalactosamine UDP-glucose, UDP-glucuronate, and UDP-galactose are also supportive of changes in extracellular matrix remodeling with reduced HSulf-1 expression.

The major pathway identified by both ingenuity pathway analysis and metabolic profiling was the alterations in the lipid pathway. Lipids are as important building blocks as carbohydrates to form the basic skeleton of rapidly dividing cells, and therefore, large amounts of FAs are required to accommodate high rates of proliferation in cancer cells [4]. Additionally, the source of FAs may determine the phospholipid composition of membranes. Moreover, it was reported that in high-grade ovarian cancer, long-chain fatty acids were elevated [75]. Our results indicate that with the loss of HSulf-1, there was a significant increase in the long-chain FAs along with branched and essential FAs in ovarian cancer. These high levels of FAs in ovarian cancer with the absence of HSulf-1 indicate a major role of HSulf-1 in FA synthesis. This enhanced production of FAs might meet the structural needs of highly proliferative ovarian cancer cells' requirement, when the tumor suppressor HSulf-1 is lost.

Sphingolipids and lysolipid or lysophospholipids are bioactive lipid molecules which play pivotal role in cancer pathogenesis. The most important sphingolipids are ceramide and sphingosine-1-phosphate and the balance between these two define the cell's fate. In cancer, sphingolipid metabolism is altered and includes changes in the levels of sphingolipids and the enzymes involved in their metabolism [76]. Lysolipids with their various FA side chains are also bioactive lipids which mainly function as growth-stimulating factor and induce cell proliferation, differentiation, and cell migration [77]. Herein, we report an increase in sphingolipids including sphinganine, sphingosine, palmitoylsphingomyelin along with altered choline/inositol and lysolipid content. Interestingly, according to the KEGG database, metabolite mapping and glycerophospholipid, arachidonic, and sphingolipid metabolisms were identified as key junctions. These results clearly indicate that with the loss of HSulf-1, the cell remodeled its own lipid synthesis in a manner to supply both structural and signaling lipids to malignant cells.

In cancer cells, the increased lipid synthesis is due to the higher expression and activity of lipogenic enzymes [78,79]. Changes in the expression and activity of enzymes involved in lipid metabolism are regulated by metabolic and oncogenic signalling pathways [80,81]. We identified enhanced expression of FASN, SREBF1, SPHK1, and PPARγ related to lipid biogenesis. Upregulation of these key lipogenic enzymes with the loss of HSulf-1 were further corroborated by their mRNA and protein expressions. Moreover higher enzymatic activity of FASN strongly supports the enhanced biogenesis of FAs with HSulf-1 loss. Additionally, phospholipase-related genes PLA2G3, PLA2G4A, PNPLA2, PLA2G4C, and PNPLA6 involved in lipolysis were also found to be higher in Sh1 and Sh2. Interestingly, PLA2G3 is an important enzyme in lipid metabolism and implicated in LD biogenesis [50,52]. Recently, it was reported that cancer cells contain increased numbers of lipid droplets compared with normal tissue [82] which are storage sites for triglycerides and cholesterol to be used as energy source. Loss of HSulf-1 induced an increase in PLA2G3 expression that may lead to the accumulation of LD in ovarian cancer. Furthermore, reduction in the number of LDs with the rescue of HSulf-1 expression in Sh1 cells establishes a direct connection to the loss of a putative tumor suppressor HSulf-1 and enhanced LD biogenesis in ovarian cancer.

In accordance with these results, we also demonstrated lower level of carnitine along with higher level of carnitine derivatives suggestive of enhanced transport of FAs through the mitochondrial membrane. More importantly, the augmented CPT1A level in Sh1 and Sh2 cells strongly support the possibility of enhanced β-oxidation. Increased and altered FA synthesis in cancer is a well-accepted phenomenon; however, enhanced expression and activity of lipolytic enzymes in tumor cells is a recent observation. In prostate cancer, malignant cells solely rely on FAO as their energy resource [83]. Here, we report that

loss of HSulf-1 also promotes enhanced FAO in Sh1 and Sh2 cells compared to NTC. Consistent with increased lipolysis, our results indicated a significant increase in the expression of important lipolytic enzymes including MAGL, DAGLA, HSL, and ASCL1 in Sh1 and Sh2 cells compared to NTC cells. Higher MAGL expression has been shown to stimulate pro-tumorigenic signals and promotes survival, tumor growth, and migration [84]. In this regard, the relationship between synthesis, storage, and utilization of free fatty acids (FFA) through beta oxidation for energy production is very poorly understood. While the prevailing belief that cells that have increased FA synthesis usually do not undergo beta oxidation, it has also been suggested that newly synthesized FFA are immediately converted into neutral lipids and stored in lipid droplets [84]. The FFAs are released by the action of lipases such as mono-acyl glycerol (MAGL) which is then used for new membrane synthesis, lipid signaling and beta oxidation for energy production for the anabolic reactions. Our data seems to support this hypothesis since the Sh1/Sh2 cells have both increased the rate of FA synthesis and beta oxidation compared to NTC cells. The FFA may be immediately converted to neutral lipids and stored in lipid droplets to be released under stress conditions.

Increasing evidence indicates that metabolic alterations induced by loss of tumor suppressor genes are common in cancer [16]. These alterations are critical for growth and survival of cancer cells. This is the first comprehensive report on metabolic alterations induced by loss of HSulf-1, a putative tumor suppressor gene in ovarian and breast cancer. Our results clearly indicate that loss of HSulf-1 remodels lipid metabolism in ovarian cancer. It is well accepted that HSulf-1 is a major regulator of growth factor-mediated signaling and altered the tumor microenvironment in ovarian cancer; however, how HSulf-1 directly reconstructs the lipid metabolism in terms of FA synthesis, lipolysis, and enhanced LD formation is yet to be unraveled. A better understanding of the function of HSulf-1, its role in energy metabolism (glycolysis, TCA cycles, PPP) and its regulation on target genes involved in altered cellular metabolism could lead to a better understanding of tumorigenesis as well as development of new targeted therapy.

Conclusions

HSulf-1 is reported to be an important tumor-suppressor gene and its expression is lost in a majority of ovarian tumors. This study demonstrates a significant alteration of cellular metabolism upon loss of HSulf-1 in OV202 cells. Microarray analysis and metabolite profiling is performed to ascertain the impact of HSulf-1 on the overall metabolic changes including alterations in lipid and amino acid pathways. The major finding from our study shows the metabolic reprogramming of cells toward an enhanced lipid metabolism upon absence of HSulf-1. Cells adopt a lipogenic phenotype which is manifested with an excess fatty acid synthesis and an upregulated beta-oxidation. Furthermore, HSulf-1-deficient cells accumulate a huge amount of cytoplasmic lipid droplets to accommodate the excessive fatty acid syntheses. The present findings are supported by the increasing evidences of enhanced lipid metabolism in cancer cells facilitating cell survival, proliferation, and signaling. Our results indicate that, loss of HSulf-1 is enabling the cells to synthesize more lipids to expedite the high proliferation rate and survival.

Additional files

Additional file 1: Figure S1. Loss of HSulf-1 induced enhanced proliferation in OV202 cells. Equal number of cells of NTC, Sh1, and Sh2 were plated in triplicates (1×10^5) and counted after 24, 48, and 72 h. The increase in cell count in both Sh1 and Sh2 were statistically significant in 48 h ($*p < 0.05$) and 72 hr ($**p < 0.001$). These experiments were repeated twice.

Additional file 2: Table S1. Microarray analyses of OV202 cells upon HSulf-1 loss.

Additional file 3: Figure S2. Multivariate regression results between major metabolite classes. The eight major metabolite classes are amino acid, carbohydrate, cofactors and vitamins, energy, lipid, nucleotide, peptide, and xenobiotics. 'Estimate' and 'Std. Error' are estimate of regression coefficient and estimation of standard-deviation error; '*t* value' is the *t* statistics for each coefficient estimate, and 'Pr(>|t|)' is the corresponding *p* value for each coefficient estimate.

Additional file 4: Table S2. Changes in major metabolic pathways including amino acids, lipids and nucleotides. List of metabolites identified through mass spectrometry and the super-pathway and sub-pathway for them are shown. The green- and red-shaded boxes are metabolites that are downregulated and/or upregulated in Sh1 and Sh2 cells compared to NTC cells respectively. The *p* values and the platform used to identify these metabolites are also shown.

Additional file 5: Table S3. Global metabolic changes upon HSulf-1 loss. List of significantly altered metabolites in Sh1 and Sh2 cells compared to NTC cells in different pathways (XLS). Heat map of statistically significant biochemical profiles in this study. By paired comparisons, shaded cells indicate $p \leq 0.05$ (red indicates that the mean values are significantly higher compared untreated control; green values significantly lower). Blue-bolded text indicates $0.05 < p < 0.10$. All data were normalized using Bradford protein concentration (red—upregulated, green—downregulated, and blue—approaching significance).

Additional file 6: Table S4. Alterations in lipid metabolites. Lipid metabolic pathways in Sh1 and Sh2 cells compared to NTC cells. Heat map of statistically significant ($p \leq 0.05$, FDR < 0.05) biochemicals are shown. Red indicates that the mean values are significantly higher by comparison with untreated control; green values significantly lower. All data were normalized using Bradford protein concentration (red—upregulated, green—downregulated.

Additional file 7: Figure S3. Metaboanalyst pathway analysis. **(A)** Statistics for pathways with major change based on high impact (linoleic acid metabolism) or *p* value (pathways glycerophospholipid, arachidonic, and sphingolipid metabolic pathways). **(B)** Of the 12 highly significant KEGG pathways plotted according to global test *p* value (intensity of color in the vertical axis) and impact factor (size of the circles in the horizontal axis), all 4 belong to the lipid pathways.

Additional file 8: Figure S4. Effect of etomoxir on cellular growth with increasing concentration of Etomoxir treatment (0 to 100 μM) in NTC, Sh1, and Sh2 cells ($n = 2$). At 60 μM and onwards, the cell growth inhibition was statistically significant ($p < 0.05$) in both Sh1 and Sh2 cells compared to NTC.

Abbreviations

ACSL1: long-chain acyl-CoA synthetase; CPT1A: carnitine palmitoyltransferase 1; DAGLA: diacylglycerol lipase alpha; FDR: false discovery rate; FA: fatty acid; FAO: fatty acid oxidation; FASN: fatty acid synthase; GC/MS: LC/MS/MS: PCA: principal component analysis; HSL: hormone sensitive lipase; KEGG: Kyoto Encyclopedia of Genes and Genomics; LD: lipid droplet; MAGL: monoacylglycerol lipase; NTC: OV202: non-targeted control cells; PPARγ: peroxisome proliferator-activated receptor gamma; SAM: significance analysis of microarray; Sh1: stably knockdown HSulf-1 clonal line 1 in OV202; Sh2: stably knockdown HSulf-1 clonal line 2 in OV202; SPHK1: sphingosine kinase 1; SREBF1: sterol regulatory element-binding transcription factor 1.

Competing interests

EDK and LNB are employees of Metabolon, Inc. and, as such, have affiliations with or financial involvement with Metabolon, Inc. These authors have no other relevant affiliations or financial involvement with any organization or entity with a financial interest in or financial conflict with the subject matter or materials discussed in the manuscript apart from those disclosed. The rest of the authors declare that they have no competing interests.

Authors' contributions

DR technically performed the experiments in Figures 4C,E,G,H and 5B,C,D. He also wrote portions of the manuscript and the 'Methods' section for FASN and beta oxidation section and was involved in the discussions. SM wrote a major part of the Introduction and Results and discussion, provided figures related to lipid metabolites, western blots in Figure 2E, and performed beta oxidation-related studies in Figure 5C. CW did the bioinformatics analysis of the KEGG pathway of the metabolites, the ingenuity pathway analysis of the microarray data and provided the following figures: Figure 1B,D, Additional file 3: Figure S2, Figure 2, Additional file 7: Figure S3, and wrote the corresponding section in the MS. XH generated the OV202NTC, Sh1, and Sh2 cells and the rescue clone Sh1 Cl11. AK performed the FASN activity assay and edited the manuscript. SG edited the manuscript and provided input regarding the metaboanalyst analysis. RH and DBJ extracted RNA and provided cDNAs for real-time PCR analysis. SK edited the manuscript and provided financial support for visiting student DBJ. EC and JCP were involved in the discussions and editing of the manuscript. CF trained DR and SM in the use of Seahorse-related experiments for beta oxidation. AM, SD, and JBG edited the manuscript and provided funds to support a technician involved in the study. SR and AO designed the microarray study and normalized the microarray data, provided the write-up related to these methods in the 'Methods' section, and reviewed the final manuscript. EDK edited the manuscript. LNB provided the initial write-up on the analysis of the overall metabolomics data and edited the manuscript. JC did the SAM analysis and was involved in the discussion and editing of the manuscript. VS was involved in the design, execution and analysis and did the QPCR of the lipid-related genes and wrote the manuscript with SM and DR. All authors read and approved the final manuscript.

Acknowledgements

The work is supported in part by the grants from the National Institutes of Health P50CA136393, CA106954, CA123249, Department of Defense Ovarian Cancer Research Program (W81XWH-13-1-0119, OC120250) and Mayo Clinic CCaTS grant number UL1TR000135 (VS) and CNPQ/Brazil and the Korea Science and Engineering Foundation (KOSEF) grant funded by the Korea government (MEST 2012–0005755) to JCP and SHK, respectively. The authors wish to acknowledge Dr. Andre Terzic (Mayo Clinic) for the use of seahorse equipment.

Author details

[1]Department of Experimental Pathology, Mayo Clinic College of Medicine, Rochester, MN 55905, USA. [2]Division of Biomedical Statistics and Informatics, Mayo Clinic, Rochester, MN 55905, USA. [3]Henry Ford Health System, Detroit, MI 48202, USA. [4]Cancer Preventive Material Development Research Center (CPMRC), College of Oriental Medicine, Kyunghee University, Seoul 130-701, Republic of Korea. [5]Department of Anesthesiology, Mayo Clinic College of Medicine, Rochester, MN 55905, USA. [6]Department of Cardiovascular Disease, Mayo Clinic College of Medicine, Rochester, MN 55905, USA. [7]Department of Obstetrics and Gynecology, Mayo Clinic College of Medicine, Rochester, MN 55905, USA. [8]Metabolon, Inc, Durham, NC 27713, USA. [9]Department of Cancer Biology, University of Kansas Medical Center, Kansas City, KN 66160, USA.

Received: 22 February 2014 Accepted: 21 July 2014
Published: 18 August 2014

References

1. Hanahan D, Weinberg RA: **Hallmarks of cancer: the next generation.** *Cell* 2011, **144**(5):646–674.
2. Fan TW, Lane AN, Higashi RM, Farag MA, Gao H, Bousamra M, Miller DM: **Altered regulation of metabolic pathways in human lung cancer discerned by (13)C stable isotope-resolved metabolomics (SIRM).** *Mol Cancer* 2009, **8**:41.
3. Warburg O: **On the origin of cancer cells.** *Science* 1956, **123**(3191):309–314.
4. Menendez JA, Lupu R: **Fatty acid synthase and the lipogenic phenotype in cancer pathogenesis.** *Nat Rev Cancer* 2007, **7**(10):763–777.
5. Medes G, Thomas A, Weinhouse S: **Metabolism of neoplastic tissue. IV A study of lipid synthesis in neoplastic tissue slices in vitro.** *Cancer Res* 1953, **13**(1):27–29.
6. Ookhtens M, Kannan R, Lyon I, Baker N: **Liver and adipose tissue contributions to newly formed fatty acids in an ascites tumor.** *Am J Physiol* 1984, **247**(1 Pt 2):R146–153.
7. Tauchi-Sato K, Ozeki S, Houjou T, Taguchi R, Fujimoto T: **The surface of lipid droplets is a phospholipid monolayer with a unique Fatty Acid composition.** *J Biol Chem* 2002, **277**(46):44507–44512.
8. Wilfling F, Wang H, Haas JT, Krahmer N, Gould TJ, Uchida A, Cheng JX, Graham M, Christiano R, Frohlich F, Liu X, Buhman KK, Coleman RA, Bewersdorf J, Farese RV Jr, Walther TC: **Triacylglycerol synthesis enzymes mediate lipid droplet growth by relocalizing from the ER to lipid droplets.** *Dev Cell* 2013, **24**(4):384–399.
9. Yun J, Rago C, Cheong I, Pagliarini R, Angenendt P, Rajagopalan H, Schmidt K, Willson JK, Markowitz S, Zhou S, Diaz LA, Velculescu VE, Lengauer C, Kinzler KW, Vogelstein B, Papdopoulos N: **Glucose deprivation contributes to the development of KRAS pathway mutations in tumor cells.** *Science* 2009, **325**(5947):1555–1559.
10. Bensaad K, Tsuruta A, Selak MA, Vidal MN, Nakano K, Bartrons R, Gottlieb E, Vousden KH: **TIGAR, a p53-inducible regulator of glycolysis and apoptosis.** *Cell* 2006, **126**(1):107–120.
11. Matoba S, Kang JG, Patino WD, Wragg A, Boehm M, Gavrilova O, Hurley PJ, Bunz F, Hwang PM: **p53 regulates mitochondrial respiration.** *Science* 2006, **312**(5780):1650–1653.
12. Shackelford DB, Shaw RJ: **The LKB1-AMPK pathway: metabolism and growth control in tumour suppression.** *Nature Rev* 2009, **9**(8):563–575.
13. Levine AJ, Puzio-Kuter AM: **The control of the metabolic switch in cancers by oncogenes and tumor suppressor genes.** *Science* 2010, **330**(6009):1340–1344.
14. Luo W, Semenza GL: **Emerging roles of PKM2 in cell metabolism and cancer progression.** *Trends Endocrinol Metab* 2012, **23**(11):560–566.
15. Reitman ZJ, Jin G, Karoly ED, Spasojevic I, Yang J, Kinzler KW, He Y, Bigner DD, Vogelstein B, Yan H: **Profiling the effects of isocitrate dehydrogenase 1 and 2 mutations on the cellular metabolome.** *Proc Natl Acad Sci USA* 2011, **108**(8):3270–3275.
16. Jones RG, Thompson CB: **Tumor suppressors and cell metabolism: a recipe for cancer growth.** *Genes Dev* 2009, **23**(5):537–548.
17. Vogelstein B, Kinzler KW: **Cancer genes and the pathways they control.** *Nat Med* 2004, **10**(8):789–799.
18. Khurana A, Liu P, Mellone P, Lorenzon L, Vincenzi B, Datta K, Yang B, Linhardt RJ, Lingle W, Chien J, Baldi A, Shridhar V: **HSulf-1 modulates FGF2- and hypoxia-mediated migration and invasion of breast cancer cells.** *Cancer Res* 2011, **71**(6):2152–2161.
19. Lai J, Chien J, Staub J, Avula R, Greene EL, Matthews TA, Smith DI, Kaufmann SH, Roberts LR, Shridhar V: **Loss of HSulf-1 up-regulates heparin-binding growth factor signaling in cancer.** *J Biol Chem* 2003, **278**(25):23107–23117.
20. Lai JP, Chien J, Strome SE, Staub J, Montoya DP, Greene EL, Smith DI, Roberts LR, Shridhar V: **HSulf-1 modulates HGF-mediated tumor cell invasion and signaling in head and neck squamous carcinoma.** *Oncogene* 2004, **23**(7):1439–1447.
21. Narita K, Chien J, Mullany SA, Staub J, Qian X, Lingle WL, Shridhar V: **Loss of HSulf-1 expression enhances autocrine signaling mediated by amphiregulin in breast cancer.** *J Biol Chem* 2007, **282**(19):14413–14420.
22. Narita K, Staub J, Chien J, Meyer K, Bauer M, Friedl A, Ramakrishnan S, Shridhar V: **HSulf-1 inhibits angiogenesis and tumorigenesis in vivo.** *Cancer Res* 2006, **66**(12):6025–6032.

23. Liu P, Khurana A, Rattan R, He X, Kalloger S, Dowdy S, Gilks B, Shridhar V: **Regulation of HSulf-1 expression by variant hepatic nuclear factor 1 in ovarian cancer.** *Cancer Res* 2009, **69**(11):4843–4850.
24. He X, Khurana A, Roy D, Kaufmann SH, Shridhar V: **Loss of HSulf-1 expression enhances tumorigenicity through inhibiting Bim expression in ovarian cancer.** *Int J Cancer* 2014, **135**(8):1783–1789.
25. He X, Khurana A, Maguire JL, Chien J, Shridhar V: **HtrA1 sensitizes ovarian cancer cells to cisplatin-induced cytotoxicity by targeting XIAP for degradation.** *Int J Cancer* 2012, **130**(5):1029–1035.
26. Khurana A, Beleford D, He X, Chien J, Shridhar V: **Role of heparan sulfatases in ovarian and breast cancer.** *Am J Cancer Res* 2013, **3**(1):34–45.
27. Staub J, Chien J, Pan Y, Qian X, Narita K, Aletti G, Scheerer M, Roberts LR, Molina J, Shridhar V: **Epigenetic silencing of HSulf-1 in ovarian cancer: implications in chemoresistance.** *Oncogene* 2007, **26**(34):4969–4978.
28. Chien J, Fan JB, Bell DA, April C, Klotzle B, Ota T, Lingle WL, Gonzalez Bosquet J, Shridhar V, Hartmann LC: **Analysis of gene expression in stage I serous tumors identifies critical pathways altered in ovarian cancer.** *Gynecol Oncol* 2009, **114**(1):3–11.
29. Cunningham JM, Oberg AL, Borralho PM, Kren BT, French AJ, Wang L, Bot BM, Morlan BW, Silverstein KA, Staggs R, Zeng Y, Lamblin AF, Hilker CA, Fan JB, Steer CJ, Thibodeau SN: **Evaluation of a new high-dimensional miRNA profiling platform.** *BMC Med Genomics* 2009, **2**:57.
30. Eckel JE, Gennings C, Therneau TM, Burgoon LD, Boverhof DR, Zacharewski TR: **Normalization of two-channel microarray experiments: a semiparametric approach.** *Bioinformatics* 2005, **21**(7):1078–1083.
31. Ballman KV, Grill DE, Oberg AL, Therneau TM: **Faster cyclic loess: normalizing RNA arrays via linear models.** *Bioinformatics* 2004, **20**(16):2778–2786.
32. Tusher VG, Tibshirani R, Chu G: **Significance analysis of microarrays applied to the ionizing radiation response.** *Proc Natl Acad Sci USA* 2001, **98**(9):5116–5121.
33. Wishart DS, Jewison T, Guo AC, Wilson M, Knox C, Liu Y, Djoumbou Y, Mandal R, Aziat F, Dong E, Bouatra S, Sinelnikov I, Arndt D, Xia J, Liu P, Yallou F, Bjorndahl T, Perez-Pinero R, Eisner R, Allen F, Neveu V, Greiner R, Scalbert A: **HMDB 3.0–the human metabolome database in 2013.** *Nucleic Acids Res* 2013, **41**(Database issue):D801–807.
34. Aittokallio T, Schwikowski B: **Graph-based methods for analysing networks in cell biology.** *Brief Bioinform* 2006, **7**(3):243–255.
35. Goeman JJ, Buhlmann P: **Analyzing gene expression data in terms of gene sets: methodological issues.** *Bioinformatics* 2007, **23**(8):980–987.
36. He X, Ota T, Liu P, Su C, Chien J, Shridhar V: **Downregulation of HtrA1 promotes resistance to anoikis and peritoneal dissemination of ovarian cancer cells.** *Cancer Res* 2010, **70**(8):3109–3118.
37. Vazquez-Martin A, Colomer R, Brunet J, Lupu R, Menendez JA: **Overexpression of fatty acid synthase gene activates HER1/HER2 tyrosine kinase receptors in human breast epithelial cells.** *Cell Prolif* 2008, **41**(1):59–85.
38. Possemato R, Marks KM, Shaul YD, Pacold ME, Kim D, Birsoy K, Sethumadhavan S, Woo HK, Jang HG, Jha AK, Chen WW, Barrett FG, Stransky N, Tsun ZY, Cowley GS, Barretina J, Kalaany NY, Hsu PP, Ottina K, Chan AM, Yuan B, Garraway LA, Root DE, Mino-Kenudson M, Brachtel EF, Driggers EM, Sabatini DM: **Functional genomics reveal that the serine synthesis pathway is essential in breast cancer.** *Nature* 2011, **476**(7360):346–350.
39. Hervé Abdi ALJW: **Principal component analysis.** *Wiley Int Rev: Comput Stat* 2010, **2**(4):433–459.
40. Hopperton KE, Duncan RE, Bazinet RP, Archer MC: **Fatty acid synthase plays a role in cancer metabolism beyond providing fatty acids for phospholipid synthesis or sustaining elevations in glycolytic activity.** *Exp Cell Res* 2014, **320**(2):302–310.
41. Swinnen JV, Brusselmans K, Verhoeven G: **Increased lipogenesis in cancer cells: new players, novel targets.** *Curr Opin Clin Nutr Metabol Care* 2006, **9**(4):358–365.
42. Currie E, Schulze A, Zechner R, Walther TC, Farese RV Jr: **Cellular fatty acid metabolism and cancer.** *Cell Metab* 2013, **18**(2):153–161.
43. Swierczynski J, Sledzinski T: **[Metabolic and regulatory function of fatty acid synthase].** *Postepy Biochem* 2012, **58**(2):175–185.
44. Zhang F, Du G: **Dysregulated lipid metabolism in cancer.** *World J Biol Chem* 2012, **3**(8):167–174.
45. Zaidi N, Lupien L, Kuemmerle NB, Kinlaw WB, Swinnen JV, Smans K: **Lipogenesis and lipolysis: the pathways exploited by the cancer cells to acquire fatty acids.** *Prog Lipid Res* 2013, **52**(4):585–589.
46. Xia J, Mandal R, Sinelnikov IV, Broadhurst D, Wishart DS: **MetaboAnalyst 2.0–a comprehensive server for metabolomic data analysis.** *Nucleic Acids Res* 2012, **40**(Web Server issue):W127–133.
47. Xia J, Psychogios N, Young N, Wishart DS: **MetaboAnalyst: a web server for metabolomic data analysis and interpretation.** *Nucleic Acids Res* 2009, **37**(Web Server issue):W652–660.
48. Kraveka YAH JM: **Bioactive sphingolipids: an overview on ceramide, ceramide 1-phosphate dihydroceramide, sphingosine, sphingosine 1-phosphate**. In *Handbook of Neurochemistry and Molecular Neurobiology*. Edited by Lajtha A, Tettamanti G, Goracci G. New York: Springer; 2010:373–383.
49. Mashima T, Seimiya H, Tsuruo T: **De novo fatty-acid synthesis and related pathways as molecular targets for cancer therapy.** *Br J Cancer* 2009, **100**(9):1369–1372.
50. Gubern A, Casas J, Barcelo-Torns M, Barneda D, de la Rosa X, Masgrau R, Picatoste F, Balsinde J, Balboa MA, Claro E: **Group IVA phospholipase A2 is necessary for the biogenesis of lipid droplets.** *J Biol Chem* 2008, **283**(41):27369–27382.
51. McDonough PM, Agustin RM, Ingermanson RS, Loy PA, Buehrer BM, Nicoll JB, Prigozhina NL, Mikic I, Price JH: **Quantification of lipid droplets and associated proteins in cellular models of obesity via high-content/high-throughput microscopy and automated image analysis.** *Assay Drug Dev Technol* 2009, **7**(5):440–460.
52. Sato H, Kato R, Isogai Y, Saka G, Ohtsuki M, Taketomi Y, Yamamoto K, Tsutsumi K, Yamada J, Masuda S, Ishikawa Y, Ishii T, Kobayashi T, Ikeda K, Taguchi R, Hatakeyama S, Hara S, Kudo I, Itabe H, Murakami M: **Analyses of group III secreted phospholipase A2 transgenic mice reveal potential participation of this enzyme in plasma lipoprotein modification, macrophage foam cell formation, and atherosclerosis.** *J Biol Chem* 2008, **283**(48):33483–33497.
53. Schadinger SE, Bucher NL, Schreiber BM, Farmer SR: **PPARgamma2 regulates lipogenesis and lipid accumulation in steatotic hepatocytes.** *Am J Physiol Endocrinol Metab* 2005, **288**(6):E1195–1205.
54. Wang H, Maechler P, Antinozzi PA, Herrero L, Hagenfeldt-Johansson KA, Bjorklund A, Wollheim CB: **The transcription factor SREBP-1c is instrumental in the development of beta-cell dysfunction.** *J Biol Chem* 2003, **278**(19):16622–16629.
55. Cheng YX, Hu M, Chen L, Huang JL, Xia LB, Li BS, Zhou LM, Hong L: **The mechanism of lipid raft mediating chemoresistance of cervical cancer.** *Saudi Med J* 2012, **33**(5):508–514.
56. Corti A, Franzini M, Paolicchi A, Pompella A: **Gamma-glutamyltransferase of cancer cells at the crossroads of tumor progression, drug resistance and drug targeting.** *Anticancer Res* 2010, **30**(4):1169–1181.
57. Merida I, Avila-Flores A: **Tumor metabolism: new opportunities for cancer therapy.** *Clin Transl Oncol* 2006, **8**(10):711–716.
58. Sheng H, Niu B, Sun H: **Metabolic targeting of cancers: from molecular mechanisms to therapeutic strategies.** *Curr Med Chem* 2009, **16**(13):1561–1587.
59. Tania M, Khan MA, Song Y: **Association of lipid metabolism with ovarian cancer.** *Curr Oncol* 2010, **17**(5):6–11.
60. Xiao Y, Chen Y, Kennedy AW, Belinson J, Xu Y: **Evaluation of plasma lysophospholipids for diagnostic significance using electrospray ionization mass spectrometry (ESI-MS) analyses.** *Ann N Y Acad Sci* 2000, **905**:242–259.
61. Xu Y, Shen Z, Wiper DW, Wu M, Morton RE, Elson P, Kennedy AW, Belinson J, Markman M, Casey G: **Lysophosphatidic acid as a potential biomarker for ovarian and other gynecologic cancers.** *JAMA* 1998, **280**(8):719–723.
62. Zhang J, Bowers J, Liu L, Wei S, Gowda GA, Hammoud Z, Raftery D: **Esophageal cancer metabolite biomarkers detected by LC-MS and NMR methods.** *PLoS One* 2012, **7**(1):e30181.
63. Wu H, Xue R, Lu C, Deng C, Liu T, Zeng H, Wang Q, Shen X: **Metabolomic study for diagnostic model of oesophageal cancer using gas chromatography/mass spectrometry.** *J Chromatogr B Analyt Technol Biomed Life Sci* 2009, **877**(27):3111–3117.
64. Lai HS, Lee JC, Lee PH, Wang ST, Chen WJ: **Plasma free amino acid profile in cancer patients.** *Semin Cancer Biol* 2005, **15**(4):267–276.
65. Poschke I, Mao Y, Kiessling R, de Boniface J: **Tumor-dependent increase of serum amino acid levels in breast cancer patients has diagnostic potential and correlates with molecular tumor subtypes.** *J Transl Med* 2013, **11**:290.

66. Denkert C, Budczies J, Weichert W, Wohlgemuth G, Scholz M, Kind T, Niesporek S, Noske A, Buckendahl A, Dietel M, Fiehn O: **Metabolite profiling of human colon carcinoma–deregulation of TCA cycle and amino acid turnover.** *Mol Cancer* 2008, **7**:72.
67. Stipanuk MH, Ueki I: **Dealing with methionine/homocysteine sulfur: cysteine metabolism to taurine and inorganic sulfur.** *J Inherit Metab Dis* 2011, **34**(1):17–32.
68. Stipanuk MH, Ueki I, Dominy JE Jr, Simmons CR, Hirschberger LL: **Cysteine dioxygenase: a robust system for regulation of cellular cysteine levels.** *Amino Acids* 2009, **37**(1):55–63.
69. Ueki I, Roman HB, Valli A, Fieselmann K, Lam J, Peters R, Hirschberger LL, Stipanuk MH: **Knockout of the murine cysteine dioxygenase gene results in severe impairment in ability to synthesize taurine and an increased catabolism of cysteine to hydrogen sulfide.** *Am J Physiol Endocrinol Metab* 2011, **301**(4):E668–684.
70. Fong MY, McDunn J, Kakar SS: **Identification of metabolites in the normal ovary and their transformation in primary and metastatic ovarian cancer.** *PLoS One* 2011, **6**(5):e19963.
71. El-Sayed S, Bezabeh T, Odlum O, Patel R, Ahing S, MacDonald K, Somorjai RL, Smith IC: **An ex vivo study exploring the diagnostic potential of 1H magnetic resonance spectroscopy in squamous cell carcinoma of the head and neck region.** *Head Neck* 2002, **24**(8):766–772.
72. Moreno A, Lopez LA, Fabra A, Arus C: **1H MRS markers of tumour growth in intrasplenic tumours and liver metastasis induced by injection of HT-29 cells in nude mice spleen.** *NMR Biomed* 1998, **11**(3):93–106.
73. Lehtimaki KK, Valonen PK, Griffin JL, Vaisanen TH, Grohn OH, Kettunen MI, Vepsalainen J, Yla-Herttuala S, Nicholson J, Kauppinen RA: **Metabolite changes in BT4C rat gliomas undergoing ganciclovir-thymidine kinase gene therapy-induced programmed cell death as studied by 1H NMR spectroscopy in vivo, ex vivo, and in vitro.** *J Biol Chem* 2003, **278**(46):45915–45923.
74. Otsuki S, Hanson SR, Miyaki S, Grogan SP, Kinoshita M, Asahara H, Wong CH, Lotz MK: **Extracellular sulfatases support cartilage homeostasis by regulating BMP and FGF signaling pathways.** *Proc Natl Acad Sci U S A* 2010, **107**(22):10202–10207.
75. Behrouz Z, Justin Bottsford M, Wei H, Rebecca Stone L, Alpa Nick M, Xinna Z, De Koen G, Sood SK: **Metabolic distinctions in high grade epithelial ovarian cancer.** *In Proceedings of the AACR 103rd Annual Meeting, 2012; Chicago, IL. Cancer Res* 2012, **72**(8).
76. Ryland LK, Fox TE, Liu X, Loughran TP, Kester M: **Dysregulation of sphingolipid metabolism in cancer.** *Cancer Biol Ther* 2011, **11**(2):138–149.
77. Sutphen R, Xu Y, Wilbanks GD, Fiorica J, Grendys EC Jr, LaPolla JP, Arango H, Hoffman MS, Martino M, Wakeley K, Griffin D, Blanco RW, Cantor AB, Xiao Y, Krischer JP: **Lysophospholipids are potential biomarkers of ovarian cancer.** *Cancer Epidemiol Biomarkers Prev* 2004, **13**(7):1185–1191.
78. Gansler TS, Hardman W 3rd, Hunt DA, Schaffel S, Hennigar RA: **Increased expression of fatty acid synthase (OA-519) in ovarian neoplasms predicts shorter survival.** *Hum Pathol* 1997, **28**(6):686–692.
79. Pizer ES, Wood FD, Heine HS, Romantsev FE, Pasternack GR, Kuhajda FP: **Inhibition of fatty acid synthesis delays disease progression in a xenograft model of ovarian cancer.** *Cancer Res* 1996, **56**(6):1189–1193.
80. Scaglia N, Chisholm JW, Igal RA: **Inhibition of stearoylCoA desaturase-1 inactivates acetyl-CoA carboxylase and impairs proliferation in cancer cells: role of AMPK.** *PLoS One* 2009, **4**(8):e6812.
81. Yang YA, Han WF, Morin PJ, Chrest FJ, Pizer ES: **Activation of fatty acid synthesis during neoplastic transformation: role of mitogen-activated protein kinase and phosphatidylinositol 3-kinase.** *Exp Cell Res* 2002, **279**(1):80–90.
82. Accioly MT, Pacheco P, Maya-Monteiro CM, Carrossini N, Robbs BK, Oliveira SS, Kaufmann C, Morgado-Diaz JA, Bozza PT, Viola JP: **Lipid bodies are reservoirs of cyclooxygenase-2 and sites of prostaglandin-E2 synthesis in colon cancer cells.** *Cancer Res* 2008, **68**(6):1732–1740.
83. Zha S, Ferdinandusse S, Hicks JL, Denis S, Dunn TA, Wanders RJ, Luo J, De Marzo AM, Isaacs WB: **Peroxisomal branched chain fatty acid beta-oxidation pathway is upregulated in prostate cancer.** *Prostate* 2005, **63**(4):316–323.
84. Nomura DK, Long JZ, Niessen S, Hoover HS, Ng SW, Cravatt BF: **Monoacylglycerol lipase regulates a fatty acid network that promotes cancer pathogenesis.** *Cell* 2010, **140**(1):49–61.

doi:10.1186/2049-3002-2-13
Cite this article as: Roy *et al.*: Loss of HSulf-1 promotes altered lipid metabolism in ovarian cancer. *Cancer & Metabolism* 2014 **2**:13.

Submit your next manuscript to BioMed Central and take full advantage of:

- **Convenient online submission**
- **Thorough peer review**
- **No space constraints or color figure charges**
- **Immediate publication on acceptance**
- **Inclusion in PubMed, CAS, Scopus and Google Scholar**
- **Research which is freely available for redistribution**

Submit your manuscript at
www.biomedcentral.com/submit

BioMed Central

HSulf-1 deficiency dictates a metabolic reprograming of glycolysis and TCA cycle in ovarian cancer

Susmita Mondal[1], Debarshi Roy[1], Juliana Camacho-Pereira[2,7], Ashwani Khurana[1], Eduardo Chini[2], Lifeng Yang[3], Joelle Baddour[3], Katherine Stilles[3], Seth Padmabandu[3], Sam Leung[4], Steve Kalloger[4] , Blake Gilks[4], Val Lowe[5], Thomas Dierks[6], Edward Hammond[8], Keith Dredge[8], Deepak Nagrath[3] and Viji Shridhar[1]

[1] Department of Experimental Pathology, Mayo Clinic College of Medicine, Rochester, MN, USA

[2] Department of Anesthesiology, Mayo Clinic College of Medicine, Rochester, MN, USA

[3] Department of Chemical and Biomolecular Engineering, Rice University, Houston, TX, USA

[4] Department of Pathology and Laboratory Medicine, University of British Columbia, Canada

[5] Department of Nuclear Medicine, Mayo Clinic College of Medicine, Rochester, MN, USA

[6] Department of Chemistry, Biochemistry I, Bielefeld University, Bielefeld, Germany

[7] Institute of Medical Biochemistry Leopoldo de Meis, Federal University of Rio de Janeiro, Rio de Janeiro, RJ, Brazil

[8] Progen Pharmaceuticals Ltd, Brisbane, Queensland, Australia

***Correspondence to**: Viji Shridhar, **email**: shridhar.vijayalakshmi@mayo.edu*

Keywords: HSulf-1, Warburg effect, HB-EGF, ovarian cancer, c-Myc, PG545

***Received**: May 05, 2015* ***Accepted**: August 27, 2015* ***Published**: September 10, 2015*

This is an open-access article distributed under the terms of the Creative Commons Attribution License, which permits unrestricted use, distribution, and reproduction in any medium, provided the original author and source are credited.

ABSTRACT

Warburg effect has emerged as a potential hallmark of many cancers. However, the molecular mechanisms that led to this metabolic state of aerobic glycolysis, particularly in ovarian cancer (OVCA) have not been completely elucidated. HSulf-1 predominantly functions by limiting the bioavailability of heparan binding growth factors and hence their downstream signaling. Here we report that HSulf-1, a known putative tumor suppressor, is a negative regulator of glycolysis. Silencing of HSulf-1 expression in OV202 cell line increased glucose uptake and lactate production by upregulating glycolytic genes such as Glut1, HKII, LDHA, as well as metabolites. Conversely, HSulf-1 overexpression in TOV21G cells resulted in the down regulation of glycolytic enzymes and reduced glycolytic phenotype, supporting the role of HSulf-1 loss in enhanced aerobic glycolysis. HSulf-1 deficiency mediated glycolytic enhancement also resulted in increased inhibitory phosphorylation of pyruvate dehydrogenase (PDH) thus blocking the entry of glucose flux into TCA cycle. Consistent with this, metabolomic and isotope tracer analysis showed reduced glucose flux into TCA cycle. Moreover, HSulf-1 loss is associated with lower oxygen consumption rate (OCR) and impaired mitochondrial function. Mechanistically, lack of HSulf-1 promotes c-Myc induction through HB-EGF-mediated p-ERK activation. Pharmacological inhibition of c-Myc reduced HB-EGF induced glycolytic enzymes implicating a major role of c-Myc in loss of HSulf-1 mediated altered glycolytic pathway in OVCA. Similarly, PG545 treatment, an agent that binds to heparan binding growth factors and sequesters growth factors away from their ligand also blocked HB-EGF signaling and reduced glucose uptake *in vivo* in HSulf-1 deficient cells.

INTRODUCTION

Cancer cell survival and growth vastly depends on the deregulated overlapping signaling cascades which are initiated at the extracellular matrix by a range of growth factors [1]. Constitutive activation of these signals instructs the cells for continual biomass production to accumulate metabolic intermediates as the source of building blocks. Mounting evidence indicates that this altered cell metabolism can be actively regulated by oncogenes and tumor suppressors. Among the tumor suppressors, the roles of P53 and PTEN leading to metabolic reprogramming of cancer are well documented [2, 3]. However, it is unclear whether other putative tumor suppressors also play a critical role in altering the Warburg effect. Thus, a comprehensive understanding of the molecular alterations by other putative tumor suppressors or oncogenes that lead to altered metabolism may not only shed new light on tumorigenesis but also provide novel strategies for therapeutically targeting these alterations.

Majority of the growth factors like FGF-1,-2 [4], VEGF [5], HB-EGF [6] and cytokines including IL-6 [7] and IL-8 [8] depend on heparan sulfate proteoglycans (HSPGs) for binding and signaling through their cognate receptor. Heparan sulfate (HS) is a glycosaminoglycan consisting of repeating unbranched negatively charged disaccharide units variably sulfated at the 3-*O*, 6-*O*, or N sites on glucosamine and the 6-*O* site on glucuronic/iduronic acid [9]. Growth factors and cytokines form the ternary complexes with their cognate receptors and HS resulting in ligand-mediated activation. We had previously reported that HSulf-1 (also known as Sulfatase 1, Sulf-1, KIAA1077 and Extracellular Sulfatase Sulf-1 [6] is downregulated in a majority of ovarian cancer cell lines [6] (Fig.S1) and tumors including serous, endometrioid and clear cell tumors of the ovary [10]. Also, we have demonstrated that loss of HSulf-1modulates the signaling of HS binding growth factors such as FGF-2, VEGF, HGF, and HB-EGF in ovarian [11], head and neck squamous carcinoma [11] and metastatic breast carcinomas [12] respectively and plays an important role in tumor progression, metastasis and angiogenesis [10, 13, 14]. Further, we showed that HIF-1α, a major transcription factor that also promotes altered metabolic signature, negatively regulates HSulf-1 expression in breast cancer [15]. Moreover, HSulf-1 silencing increases the ability to form anchorage-independent colonies *in vitro* and enhanced tumorigenicity *in vivo* [16]. Other studies also demonstrated that HSulf-1 blocks cell proliferation, migration and growth *in vitro* and *in vivo* in hepatocellular carcinoma [17, 18] and suppresses the malignant growth in lung and gastric cancer by inhibiting ERK, AKT and hedgehog signaling respectively [19, 20]. Based on these findings, we hypothesized that HSulf-1, due to its regulation of growth factor mediated signaling, might play a critical role in altering cellular metabolism. Indeed, our recent findings demonstrate that loss of HSulf-1 potentially contributes to the metabolic alterations in the lipogenic phenotype of ovarian cancer cells [21]. Here, we investigated whether HSulf-1 deficiency would also affect other metabolic pathways such as glycolysis and TCA cycle. By combining bioenergetics and metabolic studies, our results show for the first time that growth factor signaling modulated by HSulf-1 loss increases glucose uptake and lactate production and alters the energy metabolism and subsequently promoting c-Myc activation. In this study we utilized PG545, a novel synthetic agent currently in Phase 1 clinical trials (Clinical Trials gov.identifier, NCT02042781) and essentially mimics HSulf-1 function. PG545 functions as HS mimetic by simultaneously blocking HS-mediated growth factor signaling leading to inhibition of angiogenesis and carcinogenesis [22-24] including in ovarian cancer [22]. However, whether PG545 also modulates the glycolytic phenotype has never been explored before. We show for the first time that PG545 treatment resulted in significant reduction in glycolytic phenotype induced by loss of HSulf-1 and downregulated c-Myc and expression of key glycolytic enzymes *in vitro*. More importantly, PG545 decreased *in vivo* glucose uptake, lactate production and markedly inhibited tumor progression.

RESULTS

HSulf-1 reprograms the glycolytic pathway

To understand the impact of HSulf-1 on glycolytic metabolism in OVCA cells, we analyzed the levels of glycolytic genes of OV202 non-targeted control (NTC) and HSulf-1-ShRNA downregulated clones, Sh1 and Sh2 cells [16]. The microarray analysis (accession no-GSE67086) revealed aberrant glycolytic gene expression in Sh1 and Sh2 compared to NTC cells (Figure 1A). Q-PCR validation showed that glycolytic genes including hexokinase II (HKII), 6-phosphofructo-2-kinase/fructose-2,6-biphosphatase 3 (PFKFB3), 6-phosphofructokinase, liver type (PFKL), aldolase C, fructose-bisphosphate (ALDOC) and related genes including glucose transporter 1 (Glut1), and moncarboxylase transporter 4 (MCT4) were upregulated in Sh1 and Sh2 cells (Figure 1B). Similar results were also observed at the protein level by immunoblot including PGAM and PKM2. Importantly, most of the protein levels were rescued after re-expression of HSulf-1 in Sh1 (Cl7) cells (Figure 1C).

To determine if ectopic expression of HSulf-1 will reduce glycolytic enzyme levels, we generated a HSulf-1-overexpressing stable clone in TOV21G (Figure 1D). Results showed that enhanced HSulf-1 expression in TOV21G clonal line (Cl1) resulted in the downregulation of all of these enzymes compared to vector control (Figure

1D). To further substantiate loss of HSulf-1 induced alterations in glycolysis, we checked the enzyme levels in immortalized Wild-Type (WT) and HSulf-1 Knock-Out (KO) MEFs and observed higher Glut 1, HKII and LDHA levels in MEF KO cells (Figure 1E).

To assess the role of putative tumor suppressor HSulf-1 in other cancer, we transiently overexpressed HSulf-1in prostate cancer (PC3), lung cancer (H358) and breast cancer (MDA-231) cells. Results showed a marked reduction in Glut1, HKII and LDHA (Figures 1F-1H) in HSulf-1 expressing cells compared to vector transfected controls. These results suggested that HSulf-1 might play a significant role in promoting glycolysis in cancer.

Loss of HSulf-1 induced enhanced glycolytic phenotype in ovarian cancer *in vitro* and *in vivo*

To evaluate if upregulation of glycolytic genes and enzyme levels upon HSulf-1 loss resulted in increased glucose uptake, we stained the live cells using 2-NBDG a fluorescent glucose analogue which is used to monitor glucose uptake in live cells. Data shows that glucose uptake was enhanced in Sh1 and Sh2 cells by 2.8 and 1.8 fold respectively as compared to NTC cells (Figures 2A-2B). Interestingly, re-expression of HSulf-1 resulted in significant reduction in glucose uptake in Cl7compared to Sh1 cells (Figures 2A-2B). Moreover, *in vivo* imaging using[18]FDG-PET showed a marked increase in glucose uptake in 2 week old Sh1-xenograft but not in the NTC-xenograft model (Figures 2C-2D, S2). Our results also demonstrated a significant increase in lactate secretion and higher levels of ATP in Sh1 and Sh2 compared to

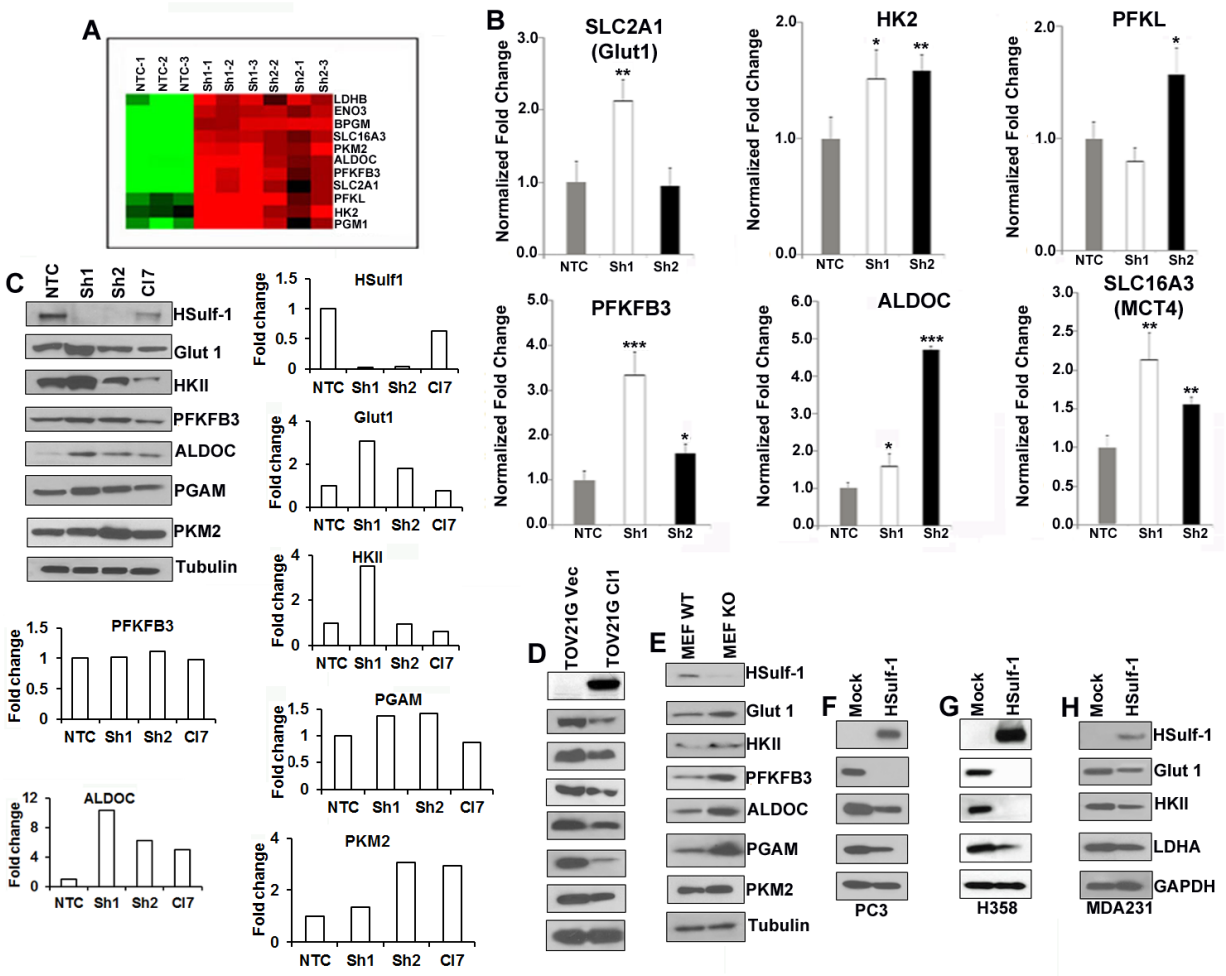

Figure 1: Absence of HSulf-1 augmented glycolytic key enzymes. A. Microarray analysis of glycolytic genes in NTC, Sh1and Sh2 cells in triplicates. **B.** QRT-PCR analysis of relative mRNA levels. **C.** Immunoblot analysis of glycolytic enzymes in NTC, Sh1, Sh2 and Cl7 cells ($N = 2$). Fold change as determined by densitometric analysis of these enzymes in Sh1 and 2 cells compared to NTC cells are shown as bar graph. Immunoblot analysis of glycolytic enzymes in TOV21GVec and Clone 1 cells **D.**, in WT and HSulf-1 KO MEF cells **E.**. Protein levels of glycolytic enzymes after transient over-expression of HSulf-1 in PC3 **F.**, H358 **G.** and MDA231 **H.** cells.

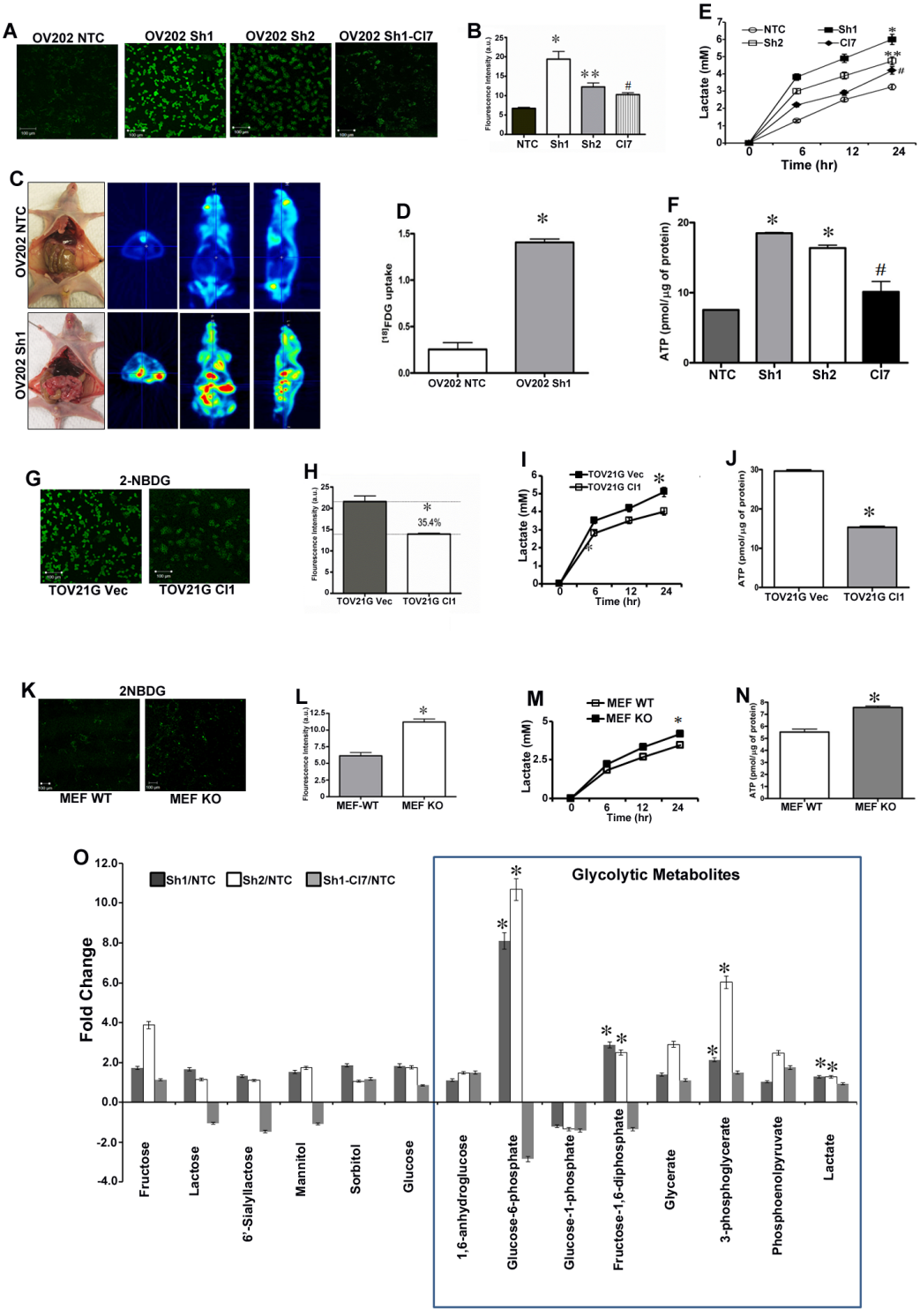

Figure 2: HSulf-1 loss induces enhanced glycolytic phenotype in ovarian cancer. A. Live cell imaging showing glucose uptake in NTC, Sh1, Sh2 and Cl7 using 2-NBDG. **B.** Quantification of fluorescence intensity of the glucose uptake in OV202NTC, Sh1, Sh2 and Cl7 cells. **C.** *In vivo* glucose uptake using ^{18}FDG in OV202NTC and Sh1 xenografts. **D.** *In vivo* glucose uptake was calculated using PMOD Biomedical Image Quantification software, $*p \leq 0.001$. **E.** Lactate secretion in media of OV202NTC, Sh1, Sh2 and Cl7 cells, **F.** Intracellular ATP levels in OV202NTC, Sh1, Sh2 and Cl7 cells, ($*p$ and $**p < 0.05$ compared to NTC, $\#p < 0.05$ compared to Sh1).Glucose uptake **G.**,glucose uptake intensity **H.**, lactate secretion **I.**,and intracellular ATP levels **J.** in TOV21G Vec and Cl cells where $*p < 0.05$. Glucose uptake **K.**, its intensity **L.**, lactate secretion **M.**, and intracellular ATP levels **N.** in WT and KO MEFs, where $*p < 0.05$. **O.** Fold increase/decrease of glycolytic metabolite were evaluated using GC/MS and LC/MS/MS platforms and fold change were calculated by the average metabolite level ofSh1/NTC, Sh2/NTC and Sh1-Cl7/Sh1. $*p < 0.05$.

NTC cells, while this phenotype is reversed in Sh1-Cl7 (Figures 2E-2F). Conversely, forced expression of HSulf-1 in TOV21G (Cl1) showed a significant reduction (35.4%) in glucose uptake, lactate production (21.5%) and ATP levels (50%) (Figures 2G-2J). Similarly, HSulf-1 KO MEFs showed 84% increase in glucose uptake when compared to WT-MEFs (Figures 2M-2N), and exhibited 22% increase in lactate secretion and 37% increase in ATP content (Figures 2K-2N), further substantiating that loss of HSulf-1-induced aerobic glycolysis. Also, transient overexpression of HSulf-1 in PC3, H358 and MDA231 cancer cell lines reduced lactate secretion (Figure S3). Additionally, our metabolite analysis demonstrated that HSulf-1 deficiency was closely associated with increased levels of glycolytic metabolites including glucose 6-phosphate [fold change (FC) compared to NTC (FC =10.68 p =< 0.001)], fructose 1,6 bisphosphate (FC=2.89, p=0.03), 3-phosphoglycerate (FC = 6.02, p = 0.01) and intracellular lactate (FC = 1.5, p = 0.002) (Figure 2O). Altogether, these results suggest a key role of HSulf-1 in modulating the glycolytic phenotype.

HSulf-1 decouples the energy flow from glycolysis to TCA cycle

To elucidate the role of HSulf-1 in the next level of glucose oxidation, we examined the inhibitory phosphorylation of PDH (S-293) along with PDK1 expression as PDH and PDK regulates the entry of acetyl CoA into TCA cycle [23]. Our results showed increased p-PDH in E1 complex in Sh1 and Sh2 compared to NTC cells (Figure 3A). Similar results were observed in TOV21G Vec/Cl1 (Figure 3B) and in MEFs (Figure 3C). It is well established that increased levels of pyruvate that accumulate due to higher aerobic glycolysis is either converted to acetyl CoA or lactate [24]. Since the level of

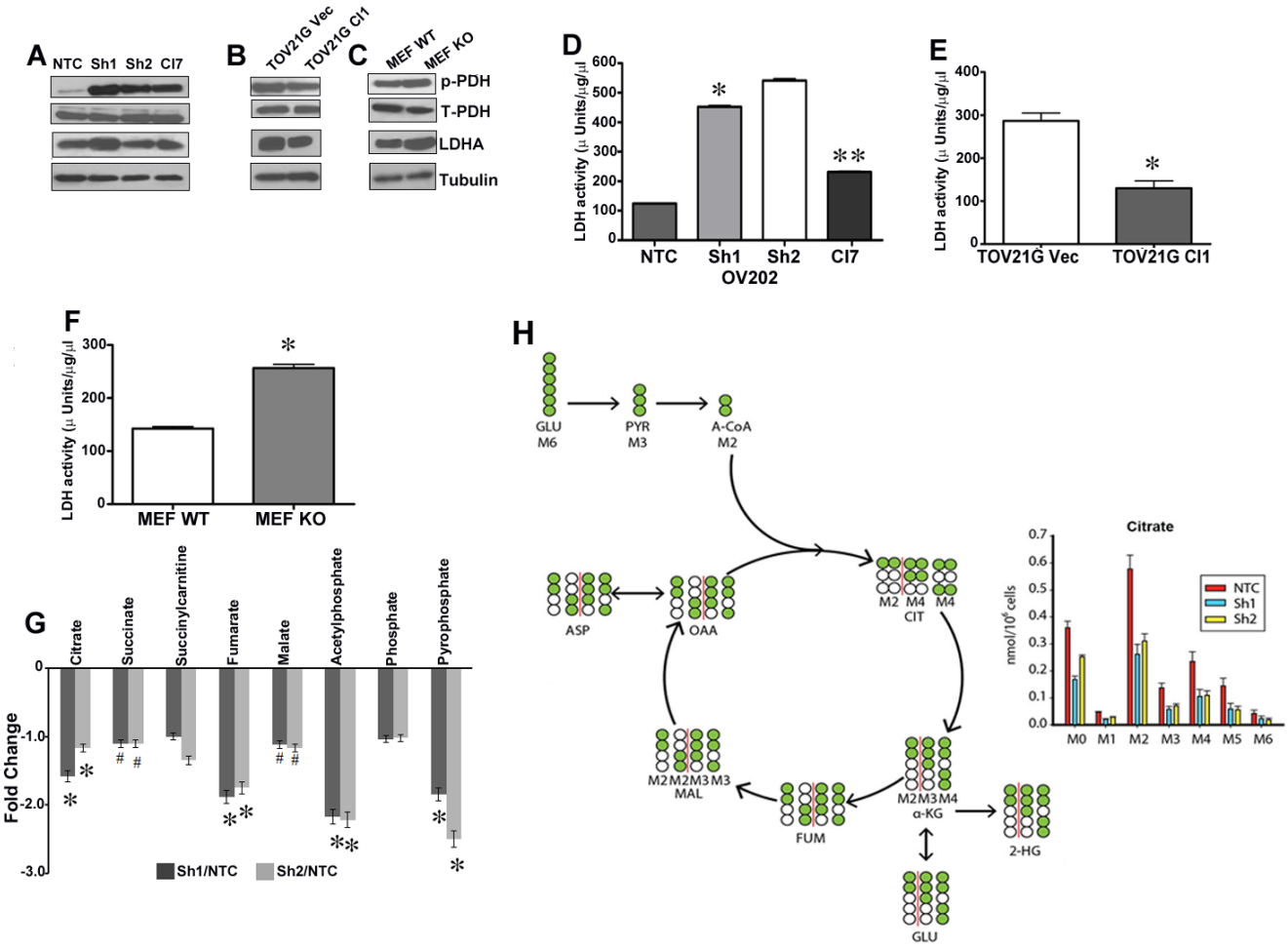

Figure 3: Disruption of energy flow from glycolysis to TCA cycles. Immunoblot analysis of p-PDH, PDH, and LDHA in OV202 clonal cells **A.**, TOV21G vec and Cl1 **B.** and HSulf-1 WT and KO MEF cells **C.**. LDH activity in OV202 clonal lines **D.**, TOV21G vec and Cl1 **E.** and in MEFs **F.** where*p< 0.05 and **p< 0.05 compared to Sh1 cells and /or compared to vector transfected and WT- MEF cells respectively. **G.** Fold increase/ decrease of TCA metabolites evaluated on metabolon platform and fold change were calculated by the average metabolite level of Sh1/NTC, Sh2/NTC and Sh1-Cl7/Sh1, *p < 0.05 and #p < 0.9. **H.** Isotope tracer analysis using $^{13}C_6$ labeled glucose to estimate glucose's contribution towards TCA cycle metabolites level. Data is normalized by cell number for OV202 NTC, Sh1 and Sh2 cells (n = 7).

p-PDH were increased with loss of HSulf-1, we further monitored the activities and levels of LDH, a key enzyme involved in conversion of pyruvate to lactate in order to maintain high glycolytic rate. HSulf-1 downregulated Sh1 and Sh2 clones showed a marked increase in LDHA expression (Figure 3A) and activity (Figure 3D). Moreover, we found that with the HSulf-1 re-expression, LDHA expression and activity were reduced in Cl7 cells (Figure 3A and 3D). Likewise, we found reduced LDHA level (Figure 3B) and activity (Figure 3E) in the HSulf-1 over expressing TOV21GCl compared to vector. Similar results were also observed in HSulf-1 KO MEF compared to MEF WT cells (Figure 3C and 3F).

We next investigated whether HSulf-1 deficiency reduced glucose's contribution into TCA cycle. To this end, we performed unbiased metabolic profiling of TCA metabolites using the Metabolon platform (Metabolon Inc, NC) in NTC, Sh1, Sh2 and Cl7 cells. Results showed a significant reduction of most of the TCA metabolites including citrate, fumarate, malate and succinate in cells with loss of HSulf-1 (Figure 3G). To further demonstrate that loss of HSulf-1 reduces TCA cycle fluxes in ovarian cancer cells, we performed 13-C GC-MS based isotope tracer analysis using labeled U-$^{13}C_6$ glucose to reveal the distribution of metabolites in this metabolic pathway. As seen in Figure 3H, M6 (6 carbon labeled) glucose is converted into M3 pyruvate and then M2 acetyl-CoA through pyruvate dehydrogenase. M2 acetyl-CoA, combining with unlabeled oxaloacetate (M0 OAA) derived from other nutrient sources, is then condensed into M2 citrate. Citrate is decarboxylated into α-ketoglutarate, and then into additional TCA cycle metabolites. The abundance of each isotopomer metabolite was used to illustrate the glucose contribution to TCA cycle fluxes in ovarian cancer cells. Figure 3H showed that complete loss of HSulf-1 resulted in decreased glucose contribution to the majority of TCA cycle metabolites (citrate, fumarate, malate,aspartate) (Figure S4). The M2 citrate level, directly reflecting glucose's entry flux into TCA cycle, decreased from 0.58nmole per million of control cells to around 0.3nmole per million for both Sh1 and Sh2 cells (Figure 3H). Similar trends were also observed with other metabolites including fumarate, malate, and aspartate. However, the ^{13}C-labeled metabolites levels of α-ketoglutarate, 2-hydroxyglutarate, and glutamate were unchanged. Collectively, these results suggest that HSulf-1 loss reduced the glucose contribution to TCA in mitochondria.

Loss of HSulf-1 is associated with reduced oxidative phosphorylation (OXPHOS) and impaired mitochondria

In order to investigate if the increased glycolytic flux and altered state of TCA cycle caused by the loss of HSulf-1 would have any impact on mitochondrial function, we measured the oxygen consumption rate (OCR). High resolution respirometry measurements in intact cells showed lower basal OCR in cells lacking HSulf-1 (Figure 4A). Sh1 and Sh2 cells showed reduction in OCR in all respiratory states compared to the controls (Figures 4B-4D). Moreover, these cells showed a lower coupled respiration rate compared to cells expressing HSulf-1, suggesting a regulatory role of HSulf-1 in mitochondrial ATP production (Figure 4D). Re-expression of HSulf-1 rescues the OCR to a level closer to NTC cells, suggesting that HSulf-1 might regulate mitochondrial oxidative phosphorylation. Moreover, Transmission Electron Microscopy (TEM) images clearly showed morphological alterations (Figure 4E) in mitochondria, reduced mitochondrial perimeter (Figure 4F), reduced area (Figure 4G) and less functional mitochondria as evaluated by mitotracker staining with loss of HSulf-1 in Sh1 (Figure 4H).

Conversely, enhanced expression of HSulf-1 in TOV21G Cll clearly showed higher OCR in all respirometry states compared to its vector (Figure 4I). The TOV21G Cll cells also recovered the morphological features (Figures 4J-4L) and functionality of mitochondria (as evidenced by mitotracker staining in TOV21G vector transfected compared to HSulf-1 transfected cells (Figure 4M). Consistent with these findings, HSulf-1 KO MEFs had lower OCR compared to WT MEF cells (Figure S5), suggesting a direct relationship between HSulf-1 loss and lower OXPHOS and mitochondrial alterations.

HSulf-1 deficiency altered glucose metabolism through c-Myc induction

Our gene microarray and ingenuity pathway analysis in NTC and Sh1 cells [6] demonstrated that the genes in Ras-Raf-MAPK/ERK pathway were expressed at a much higher levels in the Sh1 and-2 cells, suggesting a major involvement of Ras-Raf-MAPK/ERK pathway in the survival/ growth of cells in the absence of HSulf-1 (Figure 5A). Validation of microarray results with immunoblot analysis revealed a robust increase in ERK phosphorylation and c-Myc expression in Sh1 cells (Figure 5B). More importantly, HS-mimetic PG545, EGFR inhibitor lapatinib and MEK inhibitor U0126 attenuated ERK phosphorylation and c-Myc expression (Figure 5C), indicating an involvement of Raf-MAPK/ERK mediated c-Myc activation. Furthermore, c-Myc mRNA expression was 2.5 fold higher with enhanced cytoplasmic and nuclear localization of c-Myc in Sh1 cells compared to the NTC cells respectively (Figures 5D-5E). To determine if c-Myc could potentially play a role in this metabolic alteration, we used a specific c-Myc inhibitor (10058-F) and observed a dose dependent decrease in Glut 1, HKII and LDHA expression in Sh1 cells (Figure

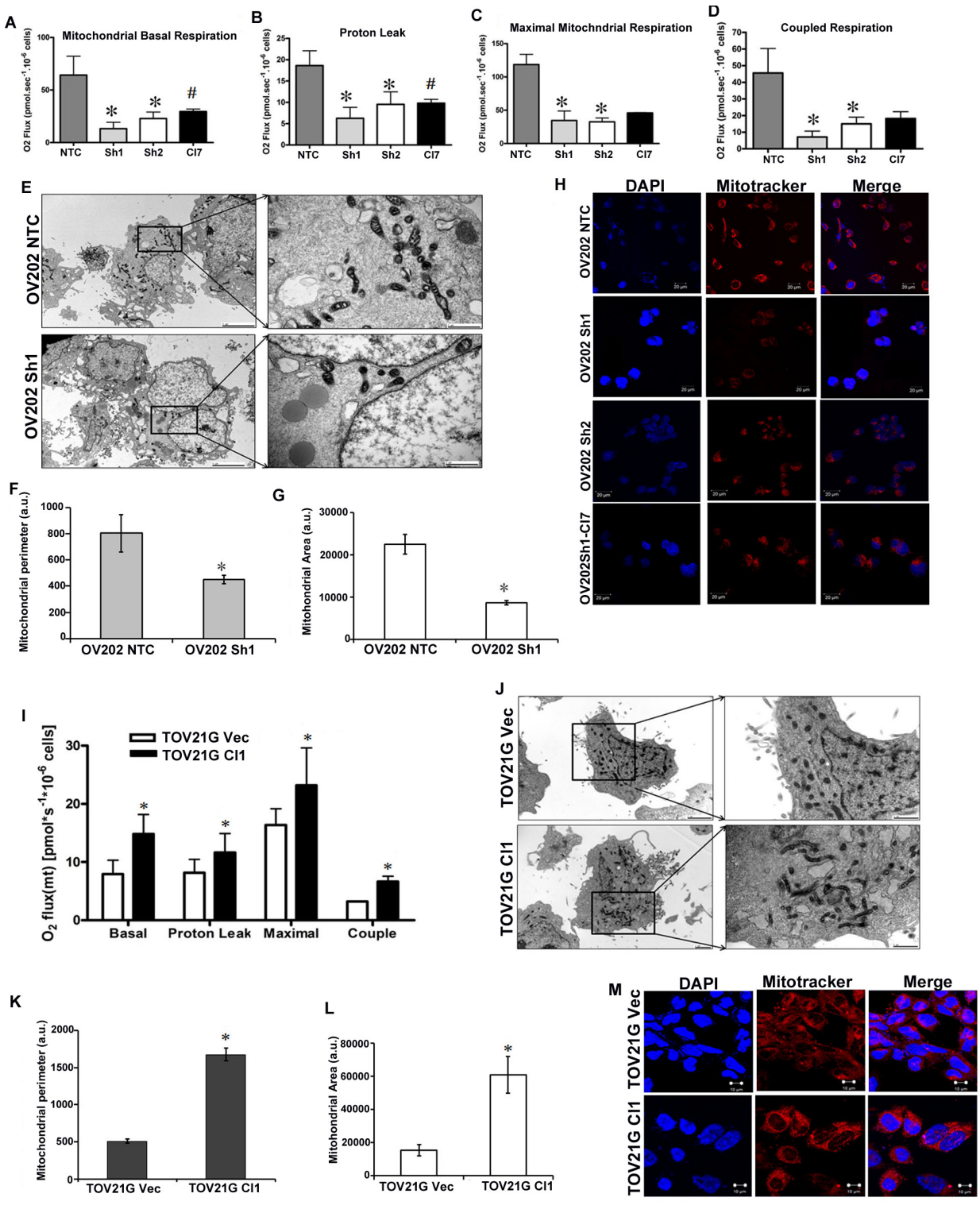

Figure 4: HSulf-1 is associated with reduced OXPHOS and impaired mitochondria. A. Basal oxygen consumption in OV202 clonal cells. Oligomycin, FCCP and Rotenone were added subsequently to measure leak **B.**, maximal **C.** and coupled respirations **D. E.** Cultured NTC and Sh1cells were photographed following TEM at 5000X and in inset 25000X magnification to show altered mitochondrial morphology. Mitochondrial perimeter **F.** and area **G.** were calculated using Image J software from TEM micrographs in 10 cells from three different micrographs, *$p < 0.05$. **H.** Mitotracker staining of OV202 clonal cells. **I.** Basal, leak, maximal and coupled respiration rates in TOV21G Vec and Cl1 cells. **J.** Electron micrographs of TOV21G Vec and Cl1 cells with 5000X and in inset 25000X magnification. Mitochondrial perimeter **K.** and area **L.** were calculated in TOV21G Vec and Cl using Image J software from TEM micrographs in 10 cells from three different micrographs, *$p < 0.05$. **M.** Mitotracker staining of TOV21G Vec and Cl cells.

5F, panel 2). However, Glut1 and HKII levels were downregulated only at the highest concentration of the c-Myc inhibitor (100μM) in the NTC cells with minimal changes in LDHA levels. To correlate whether HB-EGF mediated enhanced growth factor signaling in Sh1 cells results in higher c-Myc levels, we exogenously added HB-EGF and showed a time dependent increase of c-Myc expression along with augmented Glut 1, HKII and LDHA expression (Figure 5G). Pre-treatment of 10058-F reduced the HB-EGF mediated increment of Glut 1, HKII and LDHA levels (Figure 5H). These data suggests that loss of HSulf-1 can has a more pronounced effect in activating c-Myc through HB-EGF mediated ERK activation and subsequently reprograms the energy metabolism.

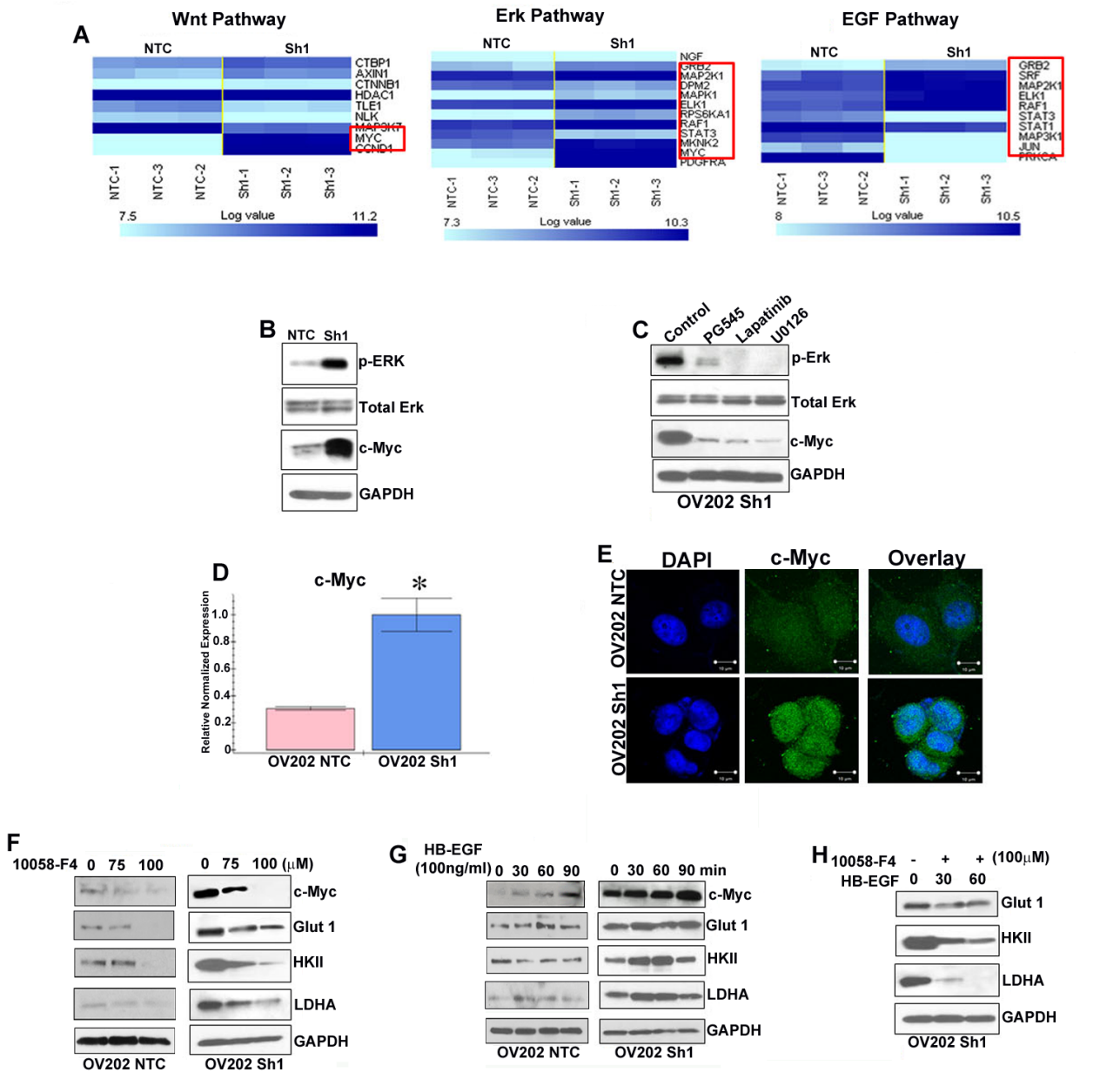

Figure 5: c-Myc is important for driving glycolysis in HSulf-1-deficient cells. A. Normalized unsupervised hierarchical clustering of Wnt, ERK and EGF pathway genes for NTC and Sh1, each class representing three biological replicates. **B.** Immunoblot analysis of p-ERK, ERK and c-Myc in NTC and Sh1. **C.** Cell lysate from 24 hr treatment with PG545 (20μM), Lapatinib (20nM) and U1026 (20μM) were immunoblotted against p-ERK, ERK and c-Myc. **D.** QRT-PCR analysis of c-Myc in NTC and Sh1 cells, $*P \leq 0.001$. **E.** NTC and Sh1 cells were immuno-stained with anti-c-Myc antibody (green) and mounted with DAPI and photographed using Zeiss LSM 510 confocal microscope. OV202NTC and Sh1 cells were treated with increasing concentration of c-Myc inhibitor for 24 hr and **F.** with HB-EGF for indicated time and immunoblotted **G.** for c-Myc, Glut 1, HKII and LDHA ($N = 2$). H. Sh1 cells were serum starved for 2 hr, treated with c-Myc inhibitor (10058-F4) for another 2 hr and then treated with HB-EGF for indicated time points. Protein lysates from each condition were probed against Glut 1, HKII and LDHA, where GAPDH served as loading control.

Tumor development and metabolic alteration by loss of HSulf-1 is attenuated by HS mimetic PG545

To better understand the role of the putative tumor suppressor HSulf-1 in HS-dependent growth factor signaling, and the subsequent metabolic reprogramming and pro-tumorigenicity, we treated Sh1 cells with PG545, which mimics the action of HSulf-1. PG545 treatment significantly reduced glucose uptake (Figures 6A-6B) and lactate production (Figure 6C) in these cells. Moreover, PG545 dose-dependently reduced the phosphorylation of ERK and the levels of Glut1, HKII, and LDHA more in NTC cells expressing HSulf-1 compared to Sh1 cells (Figures 6D and 6E respectively). Densitometric analysis of the fold change in the levels of cMyc, Glut1 and HKII in NTC and Sh1 cells is shown as bar graph following PG545 treatment in Figures 6F and 6G. We postulated that PG545 might attenuate glucose uptake in *vivo*, as PG545 treatment decreased c-Myc activation through ERK inhibition reduced glucose uptake and Glut 1 expression *in vitro*. ^{18}FDG-PET imaging in control and PG545 treated Sh1-xenografts showed a 50% reduction in ^{18}FDG uptake in PG545 treated mice (Figures 6H and 6I). These findings demonstrated that PG545 selectively suppresses glucose uptake *in vivo*.

In a parallel experiment, PG545 treatment markedly decreased the size and number of metastatic nodules compared to control mice (Shown as inset in Figure 6J). The mean excised tumor weight was reduced by 65.04% in PG545 treated mice compared to control (Figure 6J). Moreover, the abdominal circumference which reflects the tumor burden of the peritoneum was significantly less in the treated mice compared with untreated mice (Figure 6K). To test whether PG545 abrogated the HB-EGF mediated signaling and subsequently enhanced glycolysis, we determined the expression of the glycolytic enzymes, p-ERK and cMyc in the xenografts of control untreated and PG545 treated mice. Western blot analysis showed that PG545 significantly reduced the expression of p-ERK, c-Myc and the levels of Glut 1, HKII and LDHA in the tumor lysates (Figure 6L). Additionally, increase in cleaved PARP and cleaved capase3 in PG545 xenografts indicate that the reduction in the tumor growth could be the result of increased apoptosis in these cells (Figure 6M).

DISCUSSION

Increasing evidence suggest that the Warburg effect [25, 26] is common in cancer and is driven by oncogene addiction/tumor suppressor loss or mutations in the mitochondrial enzymes [27]. In this study, we report that HSulf-1 loss promotes glycolysis and impairs mitochondrial function leading to a significant reduction in OXPHOS. This phenotype is coupled to increased growth factor mediated ERK activation resulting in the upregulation of c-Myc activation. The frequent loss of HSulf-1 in OVCA may thus represent a genetic alteration promoting metabolic phenotype of OVCA.

Using HSulf-1 ShRNA downregulated OV202 cells and a clonal line of TOV21G with enhanced HSulf-1expression, we clearly showed modulation of the glycolytic pathway both *in vitro* and *in vivo*. Additionally, transient overexpression of HSulf-1 in prostate, lung and breast cancer cell lines reverses the glycolytic phenotype, suggesting a critical role of HSulf-1 in metabolic rearrangement in cancer. Glycolysis and mitochondrial respiration are tightly coupled processes. A key branch point in the glycolytic pathway is the production of pyruvate, which under anaerobic conditions is metabolized to lactate by LDH [28] and in normoxia by PDH to form acetyl-CoA [23]. The conversion of pyruvate to acetyl CoA by PDH is a crucial event which directs the energy flow from glycolysis to the TCA cycle [24]. Phosphorylation in the E1 complex of PDH by PDK inhibits its activity and energy flow to the mitochondria. In most cancers, LDHA is highly expressed and diverts the energy flow from mitochondria to from lactate. Indeed, our results demonstrated that silencing of HSulf-1 markedly enhanced LDHA level and activity in Sh1 and HSulf-1 KO MEF cells, whereas re-expression of HSulf-1 in Sh1 cells Cl7 resulted in the reduction of LDHA activity. Moreover, direct evidence from isotope tracer analysis confirmed less glucose entry into the TCA cycle. Together, these results demonstrate that HSulf-1 loss hindered the energy flow from glycolysis into TCA cycle.

Of note, it was originally hypothesized that these metabolic changes reflect a non-functional state of mitochondrial oxidative phosphorylation OXPHOS and that the high glycolytic rate in the tumors is due to impaired mitochondrial respiration [29]. Interestingly, our results showed that stable knockdown of HSulf-1 exhibited lower oxidative phosphorylation compared to NTC, while overexpression of HSulf-1 reversed this phenotype in TOV21G Cll cells. Because tumors arise through a Darwinian evolutionary process, the continuous absence of OXPHOS in tumor cells could dictate one or multiple reversible and/or irreversible adaptations that confer a growth advantage [30]. It is likely that the reduction of OXPHOS capacity of these tumor cell lines had been irreversibly diminished and could reflect on mitochondrial biogenesis and morphology as previously described [30]. Indeed, our results demonstrated that there is lower mitochondrial activity in HSulf-1-deficient cells which can be rescued by re-expression of HSulf-1. Interestingly, TEM analysis demonstrated a reduction in mitochondrial number and altered mitochondrial morphology (extended to round shape) in HSulf-1 deleted Sh1 cells. Alternatively, HSulf-1 overexpression in TOV21G cells resulted in a decrease in the mitochondrial activity and rescue of normal mitochondrial structure.

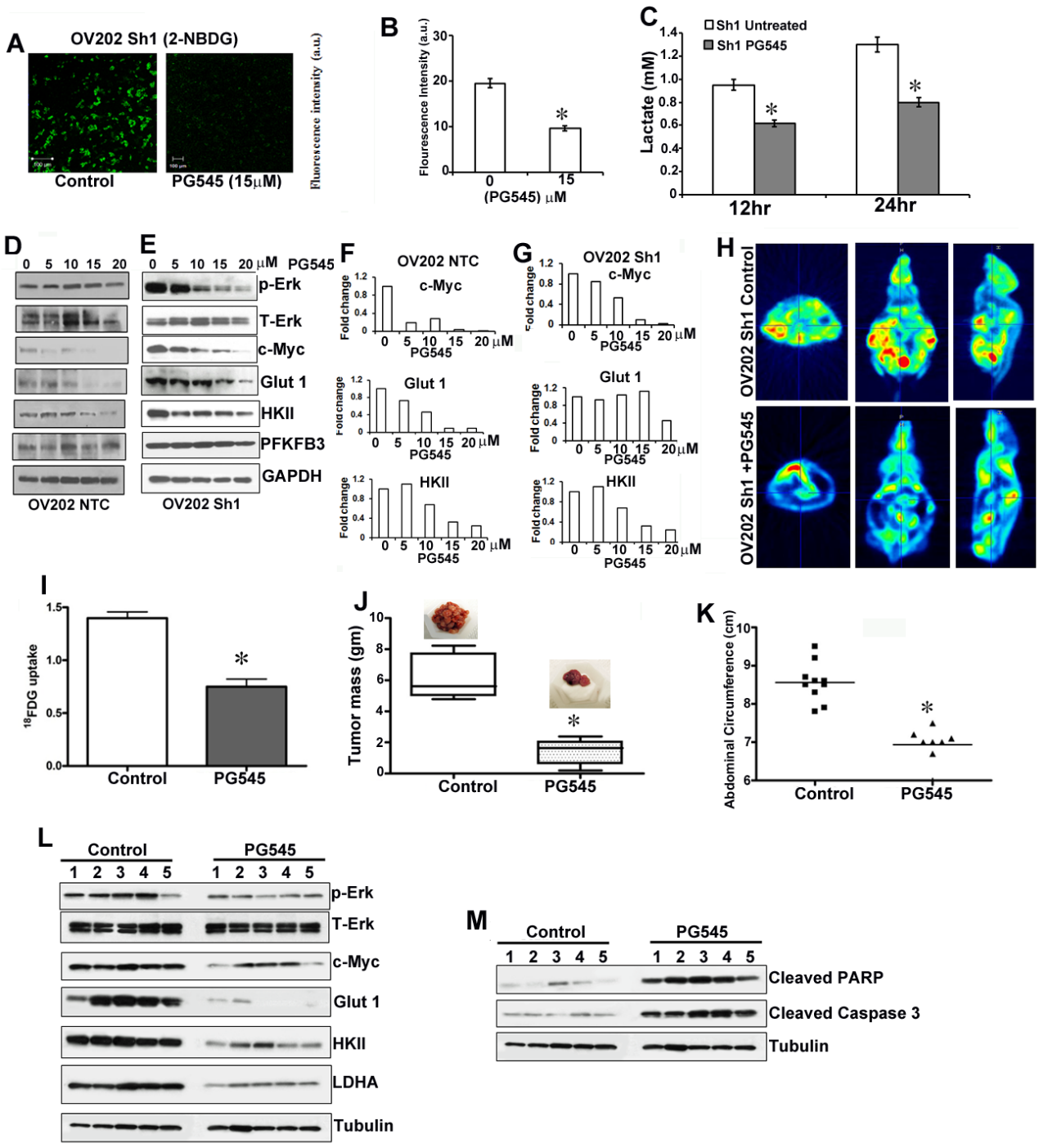

Figure 6: PG545 diminished HSulf-1-deficiency induced glycolysis and tumor growth. A. Glucose uptake in live Sh1cells after PG545 (15 μM) treatment for 1 hr. **B.** Fluorescent intensity of glucose uptake in control and PG545 treated Sh1 cells. **C.** Lactate secretion after 12 and 24 hr PG545 treatment in Sh1 cells. **D.** and **E.** Immunoblot analysis of OV202 NTC and Sh1 cells treated with PG545 (0-20μM) for 24 hr. **F.** and **G.** Augmented downregulation of c-Myc, Glut1 and HKII in OV202 NTC cells compared to Sh1 cells following PG545 treatment shown as fold change respectively. **H.** Micro-PET imaging of ^{18}FDG uptake in control and PG545 (20mg/kg, i.p.) treated mice. A representative image is provided in the transverse, coronal, and sagittal regions of interest in the tumor. I.^{18}FDG uptake intensities were calculated in at least 20 planes and analyzed using PMOD Software, $^{*}P \leq 0.01$. **G.** A separate experiment with randomized tumor-bearing mice ($n = 10$), were treated with water or PG545 (20mg/kg) twice a week and after 28 days mice were euthanized and imaged. **J.** Excised Tumor weight from control and PG545 treated mice, $^{*}P \leq 0.001$. **K.** Abdominal circumference from untreated and PG545 treated mice ($n = 10$) measured at the day of sacrifice.$^{*}P \leq 0.001$. **L.-M.** Tumor lysates from control ($n = 5$) and PG545 treatment ($n = 5$) were selected randomly and immunoblotted.

These results demonstrated a fine interplay between glycolysis and mitochondrial metabolism regulated by HSulf-1. Collectively, our findings clearly established a strong connection between loss of HSulf-1 and reprogramming of metabolism, by inducing glycolysis, disrupting the energy flow to mitochondria and affecting mitochondrial morphology and activity.

These metabolic changes appear to be strongly associated with HSulf-1-HB-EGF mediated signaling resulting in c-Myc activation. Studies suggests that the metabolically active pathways are regulated by an upstream cascade of signaling mechanisms involving growth factor receptor tyrosine kinases (RTK) and this involvement of RTK is implicated in glucose homeostasis [31]. Previous reports from our lab and others unequivocally established the role of HSulf-1in modulating heparin-binding growth factor signaling leading to enhanced ERK activation [6]. Consistent with these observations our microarray analysis and *in vitro* results showed activation of EGFR-Ras-Raf-MAPK axis which culminates in ERK-mediated c-Myc activation. c-Myc has been established as a master regulator of metabolism and directly regulates the glycolytic pathway by activating Glut 1, PFK, PKM2, LDHA and enolase [32]. Additionally, c-Myc has been found to regulate mitochondrial function, biogenesis and morphology [33]. Indeed, our results showed that HB-EGF stimulation resulted in a time-dependent induction of c-Myc both in NTC and Sh1 cells. However, HB-EGF treatment upregulated the glycolytic enzymes more in the Sh1 cells compared to the NTC cells. Importantly, c-Myc inhibition markedly reduced the basal and HB-EGF-induced Glut 1, HK-II and LDHA levels in Sh1 cells. These results provide a plausible explanation of how loss of HSulf-1 mediated enhanced HB-EGF-growth factor signaling can activate c-Myc and as a consequence, directly alter glucose metabolism. However, we noticed that HB-EGF enhanced the cMyc target genes at early time points and tapered at 90 mins, while sustaining c-Myc expression. This possibly could be due to two reasons. It has been reported that growth factor stimulation results in biphasic effects leading to sudden increase in the target gene expression followed by a tapering but sustained effect [34, 35]. Second, it is possible that c-myc acts in conjunction with other transcriptional complex factor in regulating these genes. Thus availability of all the factors is essential for expression of Glut 1, HKII and LDHA. Limited availability of other factors and/or shorter half- life of the factors involved may be a reason for decreased expression of target genes at later time points.

Metabolic targeting for cancer therapy is currently under investigation and small molecules specifically inhibiting key glycolytic steps have been evaluated as an anti-cancer approach. However, therapeutic agents that target glycolysis do not always provide satisfying outcomes in clinical trials [36]. We report here that PG545 attenuated glucose uptake and lactate production through the inhibition of p-ERK, c-Myc and the key glycolytic enzymes in *vitro* and *in vivo*. Moreover, PG545 decreased tumor growth possibly by inducing apoptosis as evidenced by increased cleaved Caspase 3 and PARP. More intriguing is the possibility that PG545,that mimics the action of HSulf-1 by competing for growth factor binding and thus inhibiting HB-EGF mediated signaling has additional effects *in vivo* by targeting the tumor microenvironment [6]. It is noteworthy that PG545 treatment of the NTC cells expressing HSulf-1 had a more pronounced effect in downregulating the expression of the Glut1, HKII and LDHA, thus supporting the role of HSulf-1 as a modulator of glycolysis. Our study, therefore, has important implications for the development of ovarian cancer therapies targeting the altered metabolism, where tumor suppressor HSulf-1 is lost.

MATERIALS AND METHODS

Materials

PG545 supplied by Progen Pharmaceuticals Ltd (Brisbane, Australia).Antibodies used: HSulf-1, PFKFB3 (Abcam, MA, USA), Glut1 (Santa Cruz Biotechnology, CA, USA), HKII, ALDOC, PGAM, PKM2, LDHA, PDH, PDK1, Tubulin, GAPDH (GeneTex, CA, USA),c-Myc, p-ERK, T-ERK (Cell signal technology, MA, USA). Secondary antibodies anti-HRP-Rabbit, anti-HRP-Mouse antibodies were from BD Pharmingen (CA, USA). ATP and LDH assay kits were from Biovision (CA, USA) and Sigma-Aldrich (MO, USA).

Cell lines and culture condition

H358 is a non-small cell lung carcinoma cell line derived from metastatic sites (http://www.phe culturecollections.org.uk/products/celllines/generalcell/ detail .jsp?refId=95111733&collection=ecacc_gc), highly metastatic prostate cancer cell line PC3 [37]and HSulf-1 deficient,MDA231, a triple negative breast cancer cell line [15] were cultured in 10% RPMI-1640 and DMEM respectively. HSulf-$1^{+/+}$ and HSulf-$1^{-/-}$ cells were isolated from HSulf-$1^{+/+}$ and HSulf-$1^{-/-}$ mice and immortalized as previously described [38]. MEFs were maintained in DMEM supplemented with 10% FBS and 650 µg/ml of G418. H358, PC3 and MDA231 are HSulf-1 deficient cells.

Transfection, plasmids and shRNA

Transient Transfection: pcDNA-HSulf-1 plasmid was transiently overexpressed in H358, PC3 and MDA231

cells using Lipofectamine Plus (Invitrogen, Grand Island, NY) according to the manufacturer's instruction.

Generation of HSulf-1 overexpression stable clones

Upon 60% confluency, HSulf-1 deficient ovarian clear cell cancer line TOV21G cells [10] were transfected with pcDNA3.1-WT-HSulf-1 using lipofectamine-LTX-plus. After 24hr of transfection, cells were selected on 100µg/ml G418 and individual clones were picked using propagated as HSulf-1 overexpressing TOV21G stable clones.

Generation of HSulf-1 downregulated Stable clone

OV202 stable clones OV202Sh1 and OV202Sh2 were generated as previously reported [16].

Rescue of HSulf-1 in Sh1 cells

As HSulf-1ShRNA targets the 3'UTR of HSulf-1 [16], HSulf-1 expression in Sh1 cells was rescued with CMV-driven WT-HSulf-1construct in OV202Sh1cells We used OV202Sh1-clone-7 as our rescue model and designated as Cl7 throughout the study. OV202 clones were cultured in minimal essential medium supplemented with 20% FBS with proper antibiotic selection.

Glucose uptake

Glucose uptake of the live cells was measured using 2-NBDG (Cayman Chemicals, Michigan, USA) according to manufacturer instruction. Fluorescent intensities were calculated using Image J software.

Immunoblot analysis

Immunoblot analysis was carried out as previously described [39].

ATP, LDH assay

Cellular ATP content and LDH activity were measured using kits from BioVision and calculated as per manufacturer's instruction.

Quantitative real time PCR

Quantitative real-time PCR was carried out with SYBR-Green PCR Master Mix (Applied Biosystems, NY, USA), using specific primers with GAPDH or 18S ribosomal subunit as an internal control as previously described [21].

Mitotracker staining and confocal microscopy

Cells ($5x10^4$/500µl) were seeded in a 4-well chamber slide, incubated overnight and stained with 100nM mitotracker red for 30 minutes. Cells were then washed, fixed and mounted with DAPI and analyzed under Zeiss LSM 510 confocal microscope. Intensity of red florescence was measured using Image J software.

Transmission electron microscopy

Cultured cells were washed and fixed in Trumps fixative containing 4% formaldehyde and 1% glutaraldehyde in a phosphate buffer pH ~7.3, post-fixed in 1.0% OsO4, dehydrated with ethanol gradation, and transitioned into propylene oxide for infiltration and embedding into spurr epoxy resin. Ultrathin sections were cut onto grids, stained with uranyl acetate and lead citrate, and examined with JEM-1400 (JEOL USA) transmission electron microscope and digitally photographed.

Microarray expression data analysis

OV202NTC, Sh1 and Sh2 cells in triplicates were profiled using Illumina Whole Genome DASL assay as previously described [21].

Liquid chromatography/Mass Spectrometry (LC/MS, LC/MS2) and Gas chromatography/Mass Spectrometry (GC/MS)

The samples destined for LC/MS, LC/MS2 and GC/MS analysis were prepared and analyzed as previously described [21].

Metabolic tracing using GC-MS

Metabolic extraction

At ~80% confluence, OV202 cells (NTC, Sh1, Sh2) were cultured with U-$^{13}C_6$ glucose, then extracted, derivatized and analyzed by GC/MS as previously described [40, 41].

Animal study

Both the animal experiments were performed with the approved protocol of Mayo Clinic Institutional Animal Care and Use Committee (IACUC).

FDG-PET imaging

Female athymic mice (5-6 weeks) were injected intraperitoneally (i.p.) with $5X10^6$ OV202 NTC (n = 5)

and OV202 Sh1 (n = 5) cells. After 2 weeks, mice were anesthetized by isoflurane and 500 µCi of ^{18}FDG was administered intravenously (i.v.) via the tail vein. After 45 minutes of ^{18}FDG injection, micro-PET imaging was acquired using Siemens Inveon PET/CT scanner (Siemens Medical Solutions, Molecular Imaging, TN, USA). Regions of interest in the tumor were quantified using the PMOD Biomedical Image Quantification and Kinetic Modeling Software (PMOD Technologies, Switzerland).

Tumor xenograft

Female athymic mice (5-6 weeks) were randomized in two groups (n = 10) and OV202 Sh1 cells (4X10^6) were injected i.p. PG545 treatment commenced 5 days after tumor inoculation at 20mg/kg, i.p., twice a week. Treatment continued for the next 4 weeks. However control mice were sacrificed during week 3 as the tumor burden exceeded 10% of their body weight. Mice were sacrificed according to standard IACUC procedure and the tumors and tissues were excised and preserved either in formalin or -80°C.

Statistical analysis

All the results were expressed as the mean ± S.D. data obtained from three separate experiments. All statistical analysis was evaluated using Graph pad Prism software (San Diego). Data were analyzed by the paired t test, and P values less than 0.05 or mentioned otherwise, was considered statistically significant.

ACKNOWLEDGMENTS

We would like to acknowledge the use of the microscopy core for confocal and transmission electron microscopy at the Mayo Clinic Rochester, MN. We sincerely acknowledge Geoffry L Curran, department of Neuroscience, Teresa D Decklever and Dianna L Glynn from department of Nuclear Medicine, Mayo clinic for their help and cooperation in FDG-PET imaging.

CONFLICTS OF INTEREST

The authors declare no conflict of interest.

GRANT SUPPORT

The work is supported in part by NIH -P50CA136393, CA106954 and Mayo Clinic CCaTS-UL1TR000135 (VS).

REFERENCES

1. De Luca A, Maiello MR, D'Alessio A, Pergameno M and Normanno N. The RAS/RAF/MEK/ERK and the PI3K/AKT signalling pathways: role in cancer pathogenesis and implications for therapeutic approaches. Expert Opin Ther Targets. 2012; 16 Suppl 2:S17-27.
2. Levine AJ and Puzio-Kuter AM. The control of the metabolic switch in cancers by oncogenes and tumor suppressor genes. Science. 2010; 330:1340-1344.
3. Jones RG and Thompson CB. Tumor suppressors and cell metabolism: a recipe for cancer growth. Genes Dev. 2009; 23:537-548.
4. Jastrebova N, Vanwildemeersch M, Lindahl U and Spillmann D. Heparan sulfate domain organization and sulfation modulate FGF-induced cell signaling. J Biol Chem. 2010; 285:26842-26851.
5. Robinson CJ, Mulloy B, Gallagher JT and Stringer SE. VEGF(165)-binding sites within heparan sulfate encompass two highly sulfated domains and can be liberated by K5 lyase. Journal of Biological Chemistry. 2006; 281:1731-1740.
6. Lai J, Chien J, Staub J, Avula R, Greene EL, Matthews TA, Smith DI, Kaufmann SH, Roberts LR and Shridhar V. Loss of HSulf-1 up-regulates heparin-binding growth factor signaling in cancer. J Biol Chem. 2003; 278:23107-23117.
7. Mummery RS and Rider CC. Characterization of the heparin-binding properties of IL-6. J Immunol. 2000; 165:5671-5679.
8. Pichert A, Samsonov SA, Theisgen S, Thomas L, Baumann L, Schiller J, Beck-Sickinger AG, Huster D and Pisabarro MT. Characterization of the interaction of interleukin-8 with hyaluronan, chondroitin sulfate, dermatan sulfate and their sulfated derivatives by spectroscopy and molecular modeling. Glycobiology. 2012; 22:134-145.
9. Esko JD and Lindahl U. Molecular diversity of heparan sulfate. J Clin Invest. 2001; 108:169-173.
10. Liu P, Khurana A, Rattan R, He X, Kalloger S, Dowdy S, Gilks B and Shridhar V. Regulation of HSulf-1 expression by variant hepatic nuclear factor 1 in ovarian cancer. Cancer Res. 2009; 69:4843-4850.
11. Lai JP, Chien J, Strome SE, Staub J, Montoya DP, Greene EL, Smith DI, Roberts LR and Shridhar V. HSulf-1 modulates HGF-mediated tumor cell invasion and signaling in head and neck squamous carcinoma. Oncogene. 2004; 23:1439-1447.
12. Khurana A, Beleford D, He X, Chien J and Shridhar V. Role of heparan sulfatases in ovarian and breast cancer. Am J Cancer Res. 2013; 3:34-45.
13. Narita K, Staub J, Chien J, Meyer K, Bauer M, Friedl A, Ramakrishnan S and Shridhar V. HSulf-1 inhibits angiogenesis and tumorigenesis *in vivo*. Cancer Res. 2006; 66:6025-6032.
14. Narita K, Chien J, Mullany SA, Staub J, Qian X, Lingle WL and Shridhar V. Loss of HSulf-1 expression enhances autocrine signaling mediated by amphiregulin in breast cancer. J Biol Chem. 2007; 282:14413-14420.
15. Khurana A, Liu P, Mellone P, Lorenzon L, Vincenzi B, Datta K, Yang B, Linhardt RJ, Lingle W, Chien J, Baldi A and Shridhar V. HSulf-1 modulates FGF2- and hypoxia-

mediated migration and invasion of breast cancer cells. Cancer Res. 2011; 71:2152-2161.

16. He X, Khurana A, Roy D, Kaufmann S and Shridhar V. Loss of HSulf-1 expression enhances tumorigenicity by inhibiting Bim expression in ovarian cancer. Int J Cancer. 2014; 135:1783-1789.
17. Liu L, Ding F, Chen J, Wang B and Liu Z. hSulf-1 inhibits cell proliferation and migration and promotes apoptosis by suppressing stat3 signaling in hepatocellular carcinoma. Oncol Lett. 2014; 7:963-969.
18. Xu G, Ji W, Su Y, Xu Y, Yan Y, Shen S, Li X, Sun B, Qian H, Chen L, Fu X, Wu M and Su C. Sulfatase 1 (hSulf-1) reverses basic fibroblast growth factor-stimulated signaling and inhibits growth of hepatocellular carcinoma in animal model. Oncotarget. 2014; 5:5029-5039.
19. Zhang H, Newman DR and Sannes PL. HSULF-1 inhibits ERK and AKT signaling and decreases cell viability *in vitro* in human lung epithelial cells. Respir Res. 2012; 13:69.
20. Ma HY, Zhang F, Li J, Mo ML, Chen Z, Liu L, Zhou HM and Sheng Q. HSulf-1 suppresses cell growth and down-regulates Hedgehog signaling in human gastric cancer cells. Oncol Lett. 2011; 2:1291-1295.
21. Roy D, Mondal S, Wang C, He X, Khurana A, Giri S, Hoffmann R, Jung DB, Kim SH, Chini EN, Periera JC, Folmes CD, Mariani A, Dowdy SC, Bakkum-Gamez JN, Riska SM, et al. Loss of HSulf-1 promotes altered lipid metabolism in ovarian cancer. Cancer Metab. 2014; 2:13.
22. Winterhoff B, Freyer L, Hammond E, Giri S, Mondal S, Roy D, Teoman A, Mullany SA, Hoffmann R, von Bismarck A, Chien J, Block MS, Millward M, Bampton D, Dredge K and Shridhar V. PG545 enhances anti-cancer activity of chemotherapy in ovarian models and increases surrogate biomarkers such as VEGF in preclinical and clinical plasma samples. Eur J Cancer. 2015; 51:879-892.
23. Sugden MC and Holness MJ. Recent advances in mechanisms regulating glucose oxidation at the level of the pyruvate dehydrogenase complex by PDKs. Am J Physiol Endocrinol Metab. 2003; 284:E855-862.
24. Wigfield SM, Winter SC, Giatromanolaki A, Taylor J, Koukourakis ML and Harris AL. PDK-1 regulates lactate production in hypoxia and is associated with poor prognosis in head and neck squamous cancer. Br J Cancer. 2008; 98:1975-1984.
25. Wu M, Neilson A, Swift AL, Moran R, Tamagnine J, Parslow D, Armistead S, Lemire K, Orrell J, Teich J, Chomicz S and Ferrick DA. Multiparameter metabolic analysis reveals a close link between attenuated mitochondrial bioenergetic function and enhanced glycolysis dependency in human tumor cells. Am J Physiol Cell Physiol. 2007; 292:C125-136.
26. Kroemer G and Pouyssegur J. Tumor cell metabolism: cancer's Achilles' heel. Cancer Cell. 2008; 13:472-482.
27. Vander Heiden MG, Cantley LC and Thompson CB. Understanding the Warburg effect: the metabolic requirements of cell proliferation. Science. 2009; 324:1029-1033.
28. Fantin VR, St-Pierre J and Leder P. Attenuation of LDH-A expression uncovers a link between glycolysis, mitochondrial physiology, and tumor maintenance. Cancer Cell. 2006; 9:425-434.
29. Zheng J. Energy metabolism of cancer: Glycolysis versus oxidative phosphorylation (Review). Oncol Lett. 2012; 4:1151-1157.
30. Capuano F, Guerrieri F and Papa S. Oxidative phosphorylation enzymes in normal and neoplastic cell growth. J Bioenerg Biomembr. 1997; 29:379-384.
31. Ward PS and Thompson CB. Signaling in control of cell growth and metabolism. Cold Spring Harb Perspect Biol. 2012; 4:a006783.
32. Miller DM, Thomas SD, Islam A, Muench D and Sedoris K. c-Myc and cancer metabolism. Clin Cancer Res. 2012; 18:5546-5553.
33. Kim J, Lee JH and Iyer VR. Global identification of Myc target genes reveals its direct role in mitochondrial biogenesis and its E-box usage *in vivo*. PLoS One. 2008; 3:e1798.
34. Uttamsingh S, Bao X, Nguyen KT, Bhanot M, Gong J, Chan JL, Liu F, Chu TT and Wang LH. Synergistic effect between EGF and TGF-beta1 in inducing oncogenic properties of intestinal epithelial cells. Oncogene. 2008; 27:2626-2634.
35. Zhang X, Meng J and Wang ZY. A switch role of Src in the biphasic EGF signaling of ER-negative breast cancer cells. PLoS One. 2012; 7:e41613.
36. Fan Y, Dickman KG and Zong WX. Akt and c-Myc differentially activate cellular metabolic programs and prime cells to bioenergetic inhibition. J Biol Chem. 2010; 285:7324-7333.
37. Tai S, Sun Y, Squires JM, Zhang H, Oh WK, Liang CZ and Huang J. PC3 is a cell line characteristic of prostatic small cell carcinoma. Prostate. 2011; 71:1668-1679.
38. Lamanna WC, Baldwin RJ, Padva M, Kalus I, Ten Dam G, van Kuppevelt TH, Gallagher JT, von Figura K, Dierks T and Merry CL. Heparan sulfate 6-O-endosulfatases: discrete *in vivo* activities and functional co-operativity. Biochem J. 2006; 400:63-73.
39. Mondal S, Mandal C, Sangwan R and Chandra S. Withanolide D induces apoptosis in leukemia by targeting the activation of neutral sphingomyelinase-ceramide cascade mediated by synergistic activation of c-Jun N-terminal kinase and p38 mitogen-activated protein kinase. Mol Cancer. 2010; 9:239.
40. Yang L, Moss T, Mangala LS, Marini J, Zhao H, Wahlig S, Armaiz-Pena G, Jiang D, Achreja A, Win J, Roopaimoole R, Rodriguez-Aguayo C, Mercado-Uribe I, Lopez-Berestein G, Liu J, Tsukamoto T, et al. Metabolic shifts toward glutamine regulate tumor growth, invasion and

bioenergetics in ovarian cancer. Mol Syst Biol. 2014; 10:728.

41. Nagrath D, Caneba C, Karedath T and Bellance N. Metabolomics for mitochondrial and cancer studies. Biochim Biophys Acta. 2011; 1807:650-663.

Loss of HSulf-1-The Missing Link between Autophagy and Lipid Droplets in Ovarian Cancer

Debarshi Roy[1], Susmita Mondal[1], Ashwani Khurana[1], Robert Hoffman[1], Xiaoping He[1], Eleftheria Kalogera[2], Thomas Dierks[3], Edward Hammond[4], Keith Dredge[4] and Viji Shridhar[1]

[1]Department of Experimental Pathology, Mayo Clinic College of Medicine, Rochester, MN, USA.,

[2]Division of Medical Oncology, Mayo Clinic College of Medicine, Rochester, MN, USA.,

[3]Department of Chemistry, Biochemistry I, Bielefeld University, Bielefeld, Germany

[4]Progen Pharmaceuticals Ltd., Brisbane, Queensland, Australia

Key words: Lipid droplet, Autophagy, HSulf-1, Ovarian cancer, Tumorigenesis

Address and Correspondence

Dr. Viji Shridhar

Department of experimental Pathology

Mayo Clinic College of Medicine

Rochester, MN 55905

Tel #-507-266-2775

Email: shridhar.vijayalakshmi@mayo.edu

Abstract

As defective autophagy and deranged metabolic pathways are frequently observed in cancer, simultaneous pharmacological targeting of these two pathways could provide a viable therapeutic option. These pathways have the ability to sense nutrient deprivation and thereby help to conserve and maintain the supply of cellular energy rich molecules. However, it is unknown how these pathways are regulated by limited availability of extracellular growth factors. Here we show that an endosulfatase, HSulf-1, a known tumor suppressor which attenuates heparan sulfate binding growth factor signaling also regulates the interplay between autophagy and lipid biogenesis. Silencing of HSulf-1 in ovarian cancer cell lines OV202 and TOV2223 resulted in suppressed autophagic flux, LC3B puncta and autophagosome formation and increased lipid droplet formation. In contrast HSulf-1 proficient cells exhibited significantly more autophagic vacuoles (AVs) and reduced number of lipid droplets (LDs). Increased accumulation of LDs in HSulf-1 depleted cells was associated with increased ERK mediated cPLA2^{S505} phosphorylation, a well-known marker for lipid biogenesis. Conversely, ectopic expression of HSulf-1 in SKOV3 cells reduced the number of LDs and increased the numbers of AVs compared to vector transfected controls. Furthermore, pharmacological (AACOCF3) and shRNA-mediated downregulation of cPLA2 resulted in reduced LDs confirming the role of cPLA2 in LD biogenesis and increased autophagy. Using mouse model of OV202 Sh1 derived xenograft, we show that AACOCF3 effectively attenuated tumor growth, LD biogenesis and reduced tumorigenesis *in vivo*. Collectively, these

results show a reciprocal regulation of autophagy and lipid biogenesis by HSulf-1 in ovarian cancer.

Introduction

Previous reports have shown that downregulation of HSulf-1 is common in ovarian cancer (OvCa) and regulates heparan sulfate binding growth factor signaling which subsequently promotes tumorigenesis.[1] We recently reported that loss of HSulf-1 promotes a "lipogenic phenotype" as evidenced by an increase in lipid related metabolites, fatty acid synthesis and beta-oxidation indicating an important role of HSulf-1 in metabolic regulation.[2]

Although adipocytes were described as the primary site for LD biogenesis, [3, 4] recent findings suggest lipid droplets as an important source of energy in cancer cells.[5-7] Enhanced LD biogenesis in cancer cells signifies its role in cell signaling, membrane trafficking and lipid metabolism, all associated with increased survival and growth of cancer cells.[8] LDs are considered as cellular hallmarks of many different diseases such as diabetes, atherosclerosis and cancer.[8-12] Though, the presence of LDs is associated with disease progression, the functional significance in promoting inflammation and tumorigenesis is not well understood. More importantly, the molecular alterations that promote LD accumulation in cancer cells have not been defined.

Primarily, LDs are storage organelles for neutral lipids and cholesterol esters.[13] Stress induced release of fatty acids from the stored LDs in adipocytes provide energy which subsequently promote tumor growth, metastasis and cell survival of OvCa.[14] Several of the LD associated proteins *SREBP1*, *PLINs, PLA2G4A*, *PLA2G3*, *ATGL*,

HSL, *MAGL*, *PPARγ* involved in LD biogenesis and release of fatty acids are upregulated upon HSulf-1 loss.[3, 15-20] Many of these genes are overexpressed in cancer cells and implicated as potential contributors towards tumorigenesis.[3, 21-24]

Autophagy is a lysosomal pathway by which long lived proteins and damaged organelles are degraded to provide energy to the cell and maintain cellular homeostasis.[25-27] Although it is generally accepted that LDs are substrates for lipases, Singh et al [28, 29] identified lipid droplets as substrates for macroautophagy and coined the term lipophagy to describe the engulfment of LDs by autophagosomes that ultimately fuse with lysosomes for the breakdown of LD components under stress conditions. Following this seminal finding, there are several reports on the regulation of LDs by autophagy.[30-32] However, the interplay and the molecular players involved in these two metabolic pathways are not known in the context of OvCa. In the present work, we identify HSulf-1, a major regulator of growth factor signaling as a missing link between autophagy and lipid droplets in OvCa acting through cPLA2α as one of the molecular pathways to promote LDs and inhibit autophagy.

Results

HSulf-1 loss promotes lipid droplet biogenesis and defective autophagy

We previously reported that stable genetic downregulation of HSulf-1 in OV202 cells achieved by two different shRNAs targeting HSulf-1 (OV202Sh1 and Sh2 cells) displayed increased LDs compared to non-targeted control transduced cells (NTC)[2]. We further confirmed these findings using OV202Sh1 to OV202Sh1 Clone C17 cells (generated by re-expression of CMV driven HSulf-1 construct in Sh1 cells.) HSulf-1

levels were verified in these clones by western blot analysis as shown in Fig 1A. Subsequently, lipid droplets were monitored by Bodipy staining in these cells. Rescue of HSulf-1 in OV202Sh1Cl7 cells reduced the number of LDs compared to OV202Sh1 and Sh2 cells (Fig.1B, Insets). Mean fluorescence intensity of Bodipy staining in these cells is shown in Fig.1C.

We further performed quantification of the changes in the LDs by Transmission Electron Microscopy (TEM). Data showed significantly higher numbers of LDs in OV202Sh1 and Sh2 cells compared to NTC cells (Figs. 1D and E). The increased lipid droplets indicate the nutrient rich or energy proficient state of the cells and therefore we hypothesized that cells will not activate catabolic process such as autophagy. Therefore, to verify, we determined the extent of autophagy via TEM analysis in these cells and observed that HSulf-1 depleted OV202Sh1 and Sh2 cells exhibit less autophagic vesicles (AV) when compared to OV202NTC cells. Also, rescue of HSulf-1 in Sh1Cl7 cells resulted in increased AV compared OV202Sh1 cells. To rule out the possibility of cell specific effects, downregulation of HSulf-1 in TOV2223 cells with ShRNA (Fig.1F) also showed increased numbers of LDs in TOV2223Sh1 cells compared to TOV2223NTC cells by both Bodipy staining (Fig.1G) and TEM analysis (Fig. 1H) indicating that these metabolic alterations were not unique to the OV202 cell line. Similarly, a high number of AVs was observed in both OV202NTC cells and TOV2223NTC cells as compared to corresponding HSulf-1 depleted cells. The quantification of LDs and AVs in TOV2223 cells is shown in Fig. 1I. Furthermore, HSulf-1 knockout (KO) mouse embryonic fibroblasts (MEFs) also displayed increased numbers of LDs compared to wild-type MEFs (Fig.IK). Similarly upon ectopic expression

of HSulf-1 in SKOV3 cells, there was a significant decrease in the numbers of LDs compared to vector transfected controls (Fig.S1). In contrast, vector transfected SKOV3 cells exhibited higher degree of AVs as quantified through TEM analysis, compared to HSulf-1 transfected SKOV3 cells (Figs S1B and D respectively). Quantification of LDs and AVs in 25 cells is shown in Fig.S1C.

cPLA2 is activated/phosphorylated in HSulf-1 depleted ovarian cancer cells

Since our initial observation indicated increased lipid droplet accumulation upon HSulf-1 depletion in ovarian cancer cells, we next wanted to determine the underlying mechanisms. LD often accumulates from anabolic process known as lipid biosynthesis. Previously we showed that lipid droplet associated proteins were upregulated in HSulf-1 depleted cells. Among them, one of the key proteins involved in lipid droplet formation is cPLA2α previously shown to be essential for LD biogenesis.[33] cPLA2α is activated and phosphorylation at Ser505 by p-ERK has been shown to be critical for cPLA2 mediated LD biogenesis.[34] Therefore, we first determined the activated/ phosphorylated levels of cPLA2α by Immunoblot analysis. Our data show that p-cPLA2^{ser505} was clearly increased in OV202Sh1 and to a lesser extent in OV202Sh2 cells (Fig. 2A). Re-expression of HSulf-1 also reduced the cPLA2 phosphorylation, indicating that phosphorylation was reversed by increasing levels of HSulf-1**.**

Pharmacological Inhibition of cPLA2 attenuates LD biogenesis in OV202Sh1 cells.

To further investigate the role of cPLA2 activation and lipid droplet accumulation/biosynthesis, we treated OV202Sh1 and OV2008 cells with a cPLA2 specific inhibitor, AACOCF3 (10 and 20μM). Western blot analysis show decreased

levels of p-cPLA2 in inhibitor treated cells (Figs.2B and C). Bodipy staining upon inhibition of cPLA2 activity with 10μM of AACOCF3 and MAFP (another cPLA2 inhibitor) in OV202Sh1 and -2 cells (Fig. 2D) showed almost complete inhibition of LD biogenesis in these cells compared to untreated control cells. Consistent with this data, TEM analysis of OV202Sh1 cells with AACCOF3 and MAFP also revealed significantly lower number of LDs (Fig.2E, with quantitation of LDs in 25 cellsshown next to the representative TEM images). Furthermore, transient downregulation of cPLA2 expression with two different ShRNA (ShcP-1 and ShcP-2) against cPLA2 (Fig. 2F) in OV202Sh1 cells resulted in the decrease of LDs as revealed by Bodipy staining (Fig. 2G). Similarly, stable downregulation of cPLA2 in OV2008 cells (Fig.2H) also resulted in reduced numbers of LDs (Fig.2I). To determine whether cPLA2 inhibitors were able to inhibit cPLA2 activity, we performed arachidonic acid (AA) release assay in OV202Sh1 and Sh2 cells. Cells treated with 10μM of AACOCF3 showed significant reduction of AA release indicating that activity of cPLA2 was inhibited (Figs. 2J and K).

Inhibition of growth factor mediated signaling reduced p-cPLA2 and LD biogenesis

cPLA2 is activated by phosphorylation at Ser residues 505, 515, and 727.[35] Within these sites, Ser-505 phosphorylation leads to increased catalytic activity, [36] which depends on MAPK, ERK and p38.[36-38] We previously showed that downregulation of HSulf-1 in OV202 cells results in increased ERK activity.[39] Conversely, re-expression of HSulf-1 in HSulf-1 deficient cells results in attenuation of growth factor mediated ERK activity.[40-42] To determine if inhibition of ERK activity will alter p-cPLA2 levels, OV202NTC, Sh1 and Sh2 cells were treated with 10μM U0126 (MEK inhibitor) for 24

hrs. As shown in figure 3A (Panels 2 and 4), treatment with U0126 resulted in the attenuation of p-ERK and p-cPLA2^{ser505} levels in OV202Sh1 and Sh2 cells compared to NTC cells. Bodipy staining of OV202 Sh1-and -Sh2 cells show figure 3B shows reduced LD accumulation as a result of U0126 mediated inactivation of ERK and p-cPLA2 (Fig.3B).

To further elucidate the role of growth factor signaling, we treated OV202Sh1 cells with PG545, a clinically-relevant HS mimetic that mimics the action of HSulf-1,[43] and evaluated the expression levels of total and p-cPLA2 (Fig 3C). PG545 functions as a HS mimetic and blocks heparan sulfate-mediated growth factor signaling (similar to HSulf-1), inhibits angiogenesis and carcinogenesis [44] including OvCa.[45] Our recent report indicated that PG545 effectively inhibited OV202Sh1 induced tumorigenesis and also modulated levels of glycolytic enzymes both *in vitro* and *in vivo*.[43] This is the first report to demonstrate that PG545 (20μM) treatment reduces the level of p-cPLA2, indicating its effect on the regulation of lipid metabolism. Consistent with this finding, PG545 treatment reduced the number of LDs in OV202Sh1 cells (Fig.3D). To evaluate the effect of PG545 on lipid metabolism *in vivo* we determined the level of p-cPLA2 in PG545 treated OV202Sh1 xenografts [43] by immunoblot analysis. As shown in Fig.3E, PG545 reduced the phosphorylation levels of p-cPLA2 in the treated xenografts compared to untreated controls. Collectively, these results clearly indicate that extracellular growth factor signaling is directly associated with LD biogenesis.

Defective autophagy is associated with loss of HSulf-1

Previous reports suggest that enhanced lipid metabolism may lead to autophagic impairment.[32, 46] To understand if HSulf-1 loss mediated lipogenic phenotype of OV202Sh1/Sh2 cells may be associated with an altered autophagic response, we analyzed the lipidated form of LC3BII levels by immunoblot analysis. As shown in figure 4A, while the OV202NTC and the Cl7 cells (rescue clone) with HSulf-1 expression expressed LC3BII, HSulf-1 deficient OV202Sh1 and -2 cells had negligible levels of LC3BII. Consistent with these findings, immunofluorescence (IFC) analysis also showed significantly less LC3B puncta and less acidic vesicles as evidenced by acridine orange staining in the Sh1 cells compared to NTC cells (Fig.4B, panels 2). We next analyzed the differences in autophagic flux in NTC and Sh1 cells. Cells were grown in the presence of EBSS medium (amino acid depleted medium) to induce autophagy for 24 hrs followed by 1 hr incubation with 100nM bafilomycin to inhibit autophagic degradation in the lysosomes. Immunoblot analysis showed no LC3BII at the basal level in the Sh1 cells (Fig. 4C, lane 1 in Sh1 cells). However, induction of autophagy by EBSS treatment induced the expression of LC3BII in the Sh1 cells as evidenced by immunoblot analysis (Fig. 4C) although, the level of LC3BII was much higher in the NTC cells exposed to EBSS (Fig.4C, lane 2 compared to Lane 2 in the Sh1 cells). Inhibition of autophagosome/lysosome fusion by bafilomycin treatment resulted in higher levels of LC3BII both in NTC and Sh1 cells, although it was more pronounced in the NTC cells (Lanes 3 in NTC and Sh1). Consistent with these results, Cyto-ID staining that detects autophagosomes and autolysosomes also indicated higher levels of autophagy in NTC cells compared to Sh1 cells (Fig. 4D, control compared to Fig.4E,control). Exposure of both OV202NTC and Sh1 cells to EBSS induced autophagy as evidenced by increased

Cyto-ID staining (Figs. 4D and E, panels 2 respectively), which was even more evident upon bafilomycin treatment (Figs.4D and E, panels 3 respectively), although it was more pronounced in the NTC cells. These data indicate that diminished autophagic flux in HSulf-1 depleted cells is associated with increased accumulation of lipid droplets.

Autophagy induction abrogates LD biogenesis in Sh1 cells

Previous reports clearly showed that inhibition of AV in rat hepatocytes resulted in increased accumulation of triglycerides in the form of LDs and that activation of autophagy decreased LD levels.[29] Based on these and other studies, we next examined the consequence of inducing autophagy in Sh1 cells on lipid droplets. EBSS treatment that induces autophagy in Sh1 cells resulted in the reduction of LDs accumulation (Fig.4F, lower left panel). Furthermore, inhibition of autophagy by bafilomycin rescued LDs signifying autophagy mediated lipophagy may be responsible for the reduction in LD levels in cells deficient in HSulf-1 (Fig.4F, lower right panel).

Previous reports by other groups[33, 47] and our data shown in figure 2D indicated that inhibiting p-cPLA2 activity with AACOCF3 abrogated LD biogenesis in Sh1 cells. Based on the notion that lipid accumulation beyond a certain physiological level impaired autophagic function [28], we surmised that AACOCF3 inhibition of p-cPLA2 activity resulting in the inhibition of LDs, may promote autophagy. IFC and immunoblot analysis of OV202Sh1 cells treated with AACOCF3 showed induction of autophagy by Cyto-ID staining (Fig.4G) and increase in LC3BII levels on immunoblot analysis (Fig.4I, top panel). Since it is also well established that increased growth factor signaling seems to be associated with increased lipogenesis[48-51], and our results showing PG545 treatment

decreases the number of LDs in these cells (Fig.3D), we determined the level of autophagy by Cyto-ID staining following PG545 treatment of OV202Sh1 cells. There was a dose dependent increase in the Cyto-ID staining following PG545 treatment (Fig.4H) and increase in LC3BII levels by immunoblot analysis (Fig.4J). Notably, similar to OV202NTC and Sh1 cells, HSulf-1 knockout (KO) MEFs showed negligible autophagy compared to wild-type (WT) MEFs (Fig.S2A, Panel 1). More importantly, EBSS treatment induced more autophagy which was even more pronounced upon bafilomycin treatment in the WT MEFs compared to HSulf-1 KO MEFs as evidenced by Cyto-ID staining (Fig.S2A, panels 2 and 3 respectively). Also, AACOCF3 and PG545 treatment of HSulf-1 KO MEFs resulted in the induction of autophagy and reduction of LDs in these cells (Fig.S2B).

Consistent with the notion that lipid accumulation beyond a certain physiological level impaired autophagic function, addition of exogenous lipids in the form of BSA conjugated palmitate in OV202NTC enhances LD accumulation in the cytoplasm (Fig.S3, top panel) and inhibits autophagy (Fig.S3, lower panel). Additionally, we have demonstrated greater LD accumulation in the ATG5 knockdown MEFs cells compared to the wild type MEFs, whereas ATG5 knockdown cells showed a lower level of Cyto-ID staining compared to the wild type cells (Fig S4).These results clearly show a relationship between induction of autophagy and abrogation of LDs.

Although increase in LC3BII is indicative of autophagic flux, a more reliable assay is the use of fluorescent tagged Cherry-GFP-LC3B construct to monitor autophagic flux [52, 53] following autophagy induction. As the GFP signal is pH sensitive and is quenched in the

lysosomes, autophagosomes light up as both red and green while autolysosmes are distinguished mostly by red signals (seen as orange to yellow in merged images) only. Following transient transfection (48 hrs) of Cherry-GFP-LC3B in OV202Sh1 cells, the cells were treated with 10μM of AACOCF3 and/or PG545. Induction of autophagy by these agents caused an increase in Cherry+/GFP+ signals (Fig.4K, panels 2 and 3) as well as Cherry+ signals (Panels 4 in the treated cells) compared to un-treated control cells (Panel1) clearly indicating the activation of autophagic flux.

AACOCF3 alone and in combination with carboplatin suppresses tumor growth, and inhibits lipid droplet biogenesis *in vivo*

To determine whether blocking cPLA2 activities via AACOCF3 confer any advantage in attenuating tumor growth in combination with chemotherapeutic agent such as carboplatin, we performed testing of these agents in vivo using a mouse model. The effect of AACOCF3 alone and in combination with carboplatin (CBP) on primary tumor growth was evaluated in OV202Sh1 cells bearing nude mice i.p. (intraperitoneally). $5X10^6$ Sh clones expressing luciferase cells in serum-free RPMI 1640 were injected intraperitoneally into female athymic nu/nu mice at 4 to 5 wk of age (National Cancer Institute-Frederick Animal Production Area (Frederick, MD). Once i.p implants were visible via non-invasive imaging (4 days after inoculation), mice were randomized (10 mice/group) and treated i.p. with the 10mg/kg body weight (b.w.) of cPLA2 inhibitor AACOCF3 (referred to as F3 in the figures) every other day till the end of the study, 51mg/kg b.w. carboplatin (CBP) every 5 days till the end of the study and a combination of CBP+F3 every 5 days, with vehicle treated group as control. Luciferase imaging of

the representative mice from four groups is shown in Fig.5A. Higher luciferase intensity in the control group and CBP group indicates increased tumor volume, progression and metastasis. Representative excised tumor from one of the mouse in each group is shown in Fig.5B. At necropsy, the measured tumor weight and circumference of mice in each group showed that the combination treatment was more effective at reducing cancer progression compared to all of the other groups (Figs.5C-D). There was no significant body weight loss in F3 or combination treated group compared to control group suggesting both F3 and CBP treatment were well tolerated without apparent toxicity to the animal (Fig.5E). More importantly, Bodipy staining of frozen sections of the xenografts clearly showed high levels of lipid droplets (Fig.5G) in the control and the CBP treated group and significantly less LDs in the F3 and combination treated group consistent with the *in vitro* data shown in figure 2D, top panel. In contrast, TUNEL staining showed increased TUNEL staining in the F3 and the combination treated groups compared to untreated control or CBP treated groups alone (Fig.5H) Anti-tumor effects of AACOCF3 monotherapy and combination with CBP correlated with significant reductions in tumor cell proliferation marker, Ki67 and phospho-cPLA2 as determined by IHC staining using the specific antibodies to these proteins (Figs. 5I and K).

Discussion:

Lipid droplet biogenesis is a mechanism by which cells store excess free fatty acids (FFA) in the form of triacylglycerides and cholesterylesters.[54] Under stress conditions, FFAs are released by lipolysis from the LDs and undergo beta oxidation in the mitochondria to provide energy to the dying cell.[3] During oncogenic transformation,

many cancer cells manifest a high rate of *de novo* lipid synthesis which results in the accumulation of cytoplasmic lipid droplets (LDs). [40, 48, 55] We recently reported that loss of HSulf-1 promotes a "lipogenic phenotype" by upregulating lipid related metabolites, fatty acid synthesis and beta-oxidation indicating an important role of HSulf-1 in the metabolic regulation.[2] In this study we have identified HSulf-1 as a molecular link – in regulating LDs accumulation by modulating autophagy. Using HSulf-1 ShRNA downregulated OV202 and TOV2223 ovarian cancer cells, we observed that HSulf-1 depleted cells accumulated LDs and exhibited diminished autophagic flux as evidenced by reduced autophagic vesicles (AVs). Autophagy maintains the cellular homeostasis by recycling cellular components, clearance of lipids and proteins [26]. Previous studies have shown that increased growth factor signaling may lead to defective autophagy [56] which is predominant in cells with loss of HSulf-1. Our data indicate that HSulf-1 expressing cells attenuate growth factor signaling and ERK-1/2 activation thereby limiting the direct activation of cPLA2, a key protein involved in lipid biogenesis. Limited growth promoting signaling and nutrient depletion are two positive regulators of autophagy. Our results show that by genetic depletion of HSulf-1, autophagic flux was significantly decreased and lipid droplets were significantly increased. Additional evidence indicates that autophagic clearance of lipid droplets maintains the cellular lipid homeostasis in a steady state; and impaired autophagy leads to accumulation of lipids in the form of LDs [28, 48, 57] which subsequently leads to growth and progression of the tumor. Consistent with these reports our results suggest that HSulf-1 loss leads to increased LD biogenesis, defective autophagic clearance of cytoplasmic LDs, thus leading to a lipogenic phenotype as we previously reported [2] providing favorable conditions for cell

growth and tumorigenesis. We previously reported that loss of HSulf-1 also promotes enhanced fatty acid oxidation in Sh1 and Sh2 cells compared to NTC cells. Our data also suggest that the free fatty acids (FFA) released by the action of lipases may be immediately converted to neutral lipids and stored in lipid droplets to be released under stress conditions. Additionally, we have also demonstrated that supplementation of BSA conjugated palmitic acid in the OV202 NTC cells promotes cytoplasmic LD accumulation but inhibits autophagy, which indicates an inverse association of LD biogenesis and autophagy.

This is the first report linking loss of HSulf-1 with increased cPLA2 activity that triggered LD biogenesis. Consistent with LD accumulation, OV202 Sh cells showed an increased AA release compared to NTC cells. Released AA is critical for inducing inflammatory responses in cancer cells though cyclooxygenase and lipoxygenase pathways.[58] Pharmacological inhibition of cPLA2 phosphorylation reduces AA release and LD biogenesis, suggesting that loss of HSulf-1 mediated LD biogenesis and AA release is dependent on cPLA2 activity.

Additionally, treatment with PG545, a HS mimetic that mimics the action of HSulf-1 in inhibiting heparan sulfate binding growth factor signaling [43] reduced the number of LDs, enhanced autophagy, reduced tumor growth [43] and reduced p-cPLA2 levels. Significantly, EBSS treatment promoted autophagy and reduction in LDs in HSulf-1KO MEFs suggesting the role of HSulf-1 in regulating these two interconnected metabolic pathways *in vivo*. Although a recent report by Shteingauz et al., [59] using heparanase-overexpressing (Hepa) U87 glioma cells showed that PG545 inhibited heparanase

induced autophagy, our results clearly shows PG545 as a promoter of autophagy in OvCa cells further affirming the role of role of autophagy as a promoter of cell death (and/or a survival mechanism) is context and cell type dependent phenomenon.

Our *in vivo* data using a specific cPLA2 inhibitor, AACOCF3 showed less tumor burden compared to the untreated control indicating that a higher level of cPLA2 itself can play a crucial role in ovarian tumorigenesis. Interestingly, AACOCF3 and carboplatin combination therapy was more effective to reduce tumor growth than carboplatin alone. This is a first report to show that HSulf-1 loss associated ovarian tumor formation is regulated by higher activity of cPLA2. More studies are required to test the synergistic effect, absorption and bioavailability of AACOCF3 alone versus the combination with carboplatin in the mouse model. Our findings indicate that cPLA2 inhibition is a potent therapeutic approach to synergize with conventional chemotherapies to reduce ovarian tumor growth.

Materials and Methods:

Cell culture

Human ovarian cancer cell line OV202 NTC, OV202 Sh1, OV202 Sh2 and OV202 Cl7 were grown in minimum essential medium alpha 1X (Cellgro, Cat# 15-012-CV) supplemented with 20% fetal bovine serum (Biowest, Cat # S1620) and 1% pen-strep. OV202 clones and NTC are grown in the presence of 1μg/ml puromycin as a selection marker for the HSulf-1 shRNA. Growth media for Cl7 cells are additionally

supplemented with 400μg/ml of G418 as a selection marker for overexpression plasmid of HSulf-1.

MEF (WT and HSulf-1 knock out) cells are obtained from Germany. They are grown in the DMEM 1X medium in the presence of 10% FBS and 1 % Pen strep with addition of 650 μg/ml of G418. OV2008 cells were grown in RPMI 1640 medium (Cellgro, Cat# 10-040-CV) supplemented with 10% fetal bovine serum and 1% pen-strep.

Inhibitors

AACOCF3, an inhibitor of phospho-cPLA2 (Cayman chemicals, Cat # 62120) was used to inhibit the cPLA2 activity and lipid droplet biogenesis. MEK inhibitor U0126 (Sigma-Aldrich, Cat #U120) was used to inhibit ERK activity. PG545, a heparanase inhibitor used to block the effect of extracellular growth factor signaling (Progen pharmaceuticals).

Cell proliferation

Cell proliferation was quantified by MTT assay (Promega, Cat #G4000) as previously described [60].

Generation of cPLA2 downregulated Stable clone

OV202 Sh1 cell line and OV2008 cells were transfected with Sh cPLA2 (ShCPLA2 1: TGATACAAATGTAGGGATATA and ShCPLA2 2: CCTTGTATTCTCACCCTGATT) using standard transfection protocol and reagents. Stable closes were further selected by puromycin. OV202 cells were cultured in 5% CO2-95% air humidified atmosphere at 37°C with minimal essential medium supplemented with 20% fetal bovine serum with

their specific antibiotic selection. All cell lines were tested using a PCR-based assay and found to be free of Mycoplasma contamination.

Western blot analysis

Western blot analysis was performed as described previously[8]. Whole cell lysates were analyzed with the following antibodies: HSulf-1 (Abcam, Cat # ab31960), phospho-cPLA2 (Sigma, Cat #SAB4503812), total-cPLA2 (SantaCruz, Cat #SC454), phospho-ERK (Cell Signaling, Cat #9106), total-ERK (Cell Signaling, Cat #9102), LC3B (Cell Signaling, Cat #3868), GAPDH (Cell Signaling, Cat #3683), β-actin (Gene Tex, Cat # GTX629630) and β-tubulin (GeneTex, Cat #GTX109639).

Detection of autophagic vesicles by Cyto-ID staining

OV202 NTC and Sh1 cells were seeded in the 4-well tissue culture chambered slides and treated with indicated concentrations of AACOCF3 or starved with EBSS in the presence or absence of bafilomycin. Then, autophagic vesicles were detected with a Cyto-ID autophagy detection kit (Enzo Life Sciences, Cat #ENZ-51031). Images were captured using a Zeiss LSM 510 microscope.

Detection of acidic vesicular organelles using Acridine orange staining

OV202 NTC and Sh1 cells were seeded in 4-well tissue culture chambered slides and grown overnight. Next day cells were stained with acridine orange (1μg/ml; Molecular Probes, Cat #A1301) in a serum free medium for 15 minutes at 37^{o} C. Acridine orange was removed and images were captured in Zeiss LSM microscope. Red fluorescence indicates the acidic vesicles as described earlier[61].

Transmission Electron microscopy

Cultured cells were washed twice with PBS and then fixed in Trumps fixative containing 4% formaldehyde and 1% glutaraldehyde in a phosphate buffer pH ~7.3, post-fixed in 1.0% OsO4, dehydrated with ethanol gradation, and transitioned into propylene oxide for infiltration and embedding into spurr epoxy resin. Ultrathin sections were cut onto grids, stained with uranyl acetate and lead citrate, and examined with aJEM-1400 (JEOL USA) transmission electron microscope, and digitally photographed. Morphologically we assessed the cytoplasmic lipid droplets and autophagosomes and the numbers were counted. A total of 25 cells per sample were analyzed.

Bodipy staining

Cells (50,000) were seeded on a coverslip in a 24-well plate and were grown for 24 hrs in the presence of complete growth medium. Cells were washed and fixed in 4% paraformaldehyde for ten minutes at room temperature before staining with 1µg/ml Bodipy (493/503; Sigma, Cat #790389) in PBS for ten minutes at room temperature. Coverslips were washed with PBS and mounted in a slide with Prolong Gold Antifade Reagent (Invitrogen, Cat #P36935). Bodipy stained cells were examined under Zeiss-LSM 510 fluorescence microscope.

Immunoflouroscence

Cells were grown on coverslips overnight, and then fixed with 100% methanol followed by blocking with 1% BSA in PBS. After blocking, the cells were incubated with respective primary antibodies at room temperature for 1 hr, then washed three times with 1X PBS and then incubated in dark with alexa fluor goat anti-rabbit (488 nm)

or/with alexa fluor rabbit anti-mouse (593 nm) in 1% BSA in PBS. Coverslips were washed three times before mounting with Prolong Gold Antifade reagent (Invitrogen). Stained samples were visualized using a Zeiss-LSM 510 fluorescence microscope.

Arachidonic acid release assay

Arachidonic acid (AA) release was evaluated in OV202 NTC, Sh1, Sh2, Cl7 cells and OV2008 vector and clones. In a 6-well plate $0.5x10^6$ cells were plated and grown overnight in complete media. On the next day, growth medium was removed and the cells were incubated with ^{3}H-AA under serum free medium for 24 hrs. The media was removed and cells were washed three times with 1X PBS and complete growth medium was added with or without AACOCF3 (10μM) for another 24 hrs. Aliquots of growth medium from the cells were measured for radioactivity at the end of treatment. Radioactivity is showed as counts per minute (cpm/ml).

Nude mouse tumor model

$5x10^6$ OV202 Sh1 cells expressing luciferase were injected intraperitoneally (i.p) to the nude mice. 4 days following i.p inoculation the mice were treated with (10mg/kg) AACOCF3 every 3rd day until the end of study, or carboplatin (51mg/kg) in every 5th day for 4 cycles, or combination of carboplatin (51 mg/kg) and AACOCF3 (10mg/kg) every 5th day for 4 cycles. All the animals were sacrificed by the 28th day of the experiment. Mayo clinic animal care and use committee approved all procedures.

***In vivo* bioluminescence measurements**

Weekly bioluminescent reporter imaging was performed to monitor the seeding of OV202Sh1-luc cells, using the Xenogen IVIS 200 System (Caliper life sciences) as previously described[45].

Immunohistochemistry: Immunohistochemical (IHC) staining was done on tumors from control, F3, CBP and F3+CBP treated mice. Paraffin embedded tissue sections from the tumors were stained for Ki67 and phospho-cPLA2. The standard IHC procedure was performed at the Pathology Research Core (Mayo Clinic, Rochester, MN) as previously described[45].

TUNEL Staining: The terminal dUPT nick end-labeling (TUNEL) assay of frozen tissue sections of tumors from control, F3, CBP and F3+CBP treated mice were performed using ApopTag Fluorescein Direct In Situ Apoptosis Detection Kit (Millipore, Cat # S7110) according to the manufacturer's instructions. Green fluorescence indicates TUNEL staining and red fluorescence indicates propidium iodide (PI) staining.

Statistical analyses

All results were expressed as the mean ± S.D. data obtained from three separate experiments. All statistical analysis was evaluated using Graph pad Prism software (San Diego, CA). Data were analyzed by the paired t test, and P values less than 0.05 or mentioned otherwise, was considered statistically significant.

Acknowledgements

We would like to thank Dr. Eleftheria Kalogera for the critical reading of the manuscript. We acknowledge the receipt of TOV2223 from Dr. Barbara Vanderhyden, Ottawa

Hospital Research Institute, Ottawa, Canada. We would like to acknowledge the use of the Pathology Research Core, microscopy core for confocal and transmission electron microscopy and the flow cytometry facility at the Mayo Clinic Rochester, MN.

Disclosure of potential conflicts of interest

There is no conflict of interest to disclose.

Grant Support

The work is supported in part by the grants from the National Institutes of Health CA106954, Department of Defense Ovarian Cancer Research Program Award W81XWH-13-1-0119 OC120250 and the Mayo Clinic (VS).

References

1. He X, Khurana A, Roy D, Kaufmann S, Shridhar V. Loss of HSulf-1 expression enhances tumorigenicity by inhibiting Bim expression in ovarian cancer. Int J Cancer 2014; 135:1783-9.
2. Roy D, Mondal S, Wang C, He X, Khurana A, Giri S, et al. Loss of HSulf-1 promotes altered lipid metabolism in ovarian cancer. Cancer Metab 2014; 2:13.
3. Takahashi Y, Shinoda A, Furuya N, Harada E, Arimura N, Ichi I, et al. Perilipin-mediated lipid droplet formation in adipocytes promotes sterol regulatory element-binding protein-1 processing and triacylglyceride accumulation. PLoS One 2013; 8:e64605.
4. Heid H, Rickelt S, Zimbelmann R, Winter S, Schumacher H, Dorflinger Y, et al. On the formation of lipid droplets in human adipocytes: the organization of the perilipin-vimentin cortex. PLoS One 2014; 9:e90386.
5. Cabodevilla AG, Sanchez-Caballero L, Nintou E, Boiadjieva VG, Picatoste F, Gubern A, et al. Cell survival during complete nutrient deprivation depends on lipid droplet-fueled beta-oxidation of fatty acids. J Biol Chem 2013; 288:27777-88.
6. Lettieri Barbato D, Aquilano K, Baldelli S, Cannata SM, Bernardini S, Rotilio G, et al. Proline oxidase-adipose triglyceride lipase pathway restrains adipose cell death and tissue inflammation. Cell death and differentiation 2014; 21:113-23.
7. Zirath H, Frenzel A, Oliynyk G, Segerstrom L, Westermark UK, Larsson K, et al. MYC inhibition induces metabolic changes leading to accumulation of lipid droplets in tumor cells. Proceedings of the National Academy of Sciences of the United States of America 2013; 110:10258-63.

8. Bozza PT, Viola JP. Lipid droplets in inflammation and cancer. Prostaglandins Leukot Essent Fatty Acids 2010; 82:243-50.
9. Lang PD, Insull W, Jr. Lipid droplets in atherosclerotic fatty streaks of human aorta. J Clin Invest 1970; 49:1479-88.
10. Greenberg AS, Coleman RA, Kraemer FB, McManaman JL, Obin MS, Puri V, et al. The role of lipid droplets in metabolic disease in rodents and humans. J Clin Invest 2011; 121:2102-10.
11. Zhang X, Zhang K. Endoplasmic Reticulum Stress-Associated Lipid Droplet Formation and Type II Diabetes. Biochem Res Int 2012; 2012:247275.
12. Bostrom P, Rutberg M, Ericsson J, Holmdahl P, Andersson L, Frohman MA, et al. Cytosolic lipid droplets increase in size by microtubule-dependent complex formation. Arterioscler Thromb Vasc Biol 2005; 25:1945-51.
13. Krahmer N, Guo Y, Farese RV, Jr., Walther TC. SnapShot: Lipid Droplets. Cell 2009; 139:1024- e1.
14. Nieman KM, Kenny HA, Penicka CV, Ladanyi A, Buell-Gutbrod R, Zillhardt MR, et al. Adipocytes promote ovarian cancer metastasis and provide energy for rapid tumor growth. Nat Med 2011; 17:1498-503.
15. Pol A, Gross SP, Parton RG. Review: biogenesis of the multifunctional lipid droplet: lipids, proteins, and sites. J Cell Biol 2014; 204:635-46.
16. Kraemer FB, Shen WJ. Hormone-sensitive lipase: control of intracellular tri-(di-)acylglycerol and cholesteryl ester hydrolysis. J Lipid Res 2002; 43:1585-94.
17. Brasaemle DL. Thematic review series: adipocyte biology. The perilipin family of structural lipid droplet proteins: stabilization of lipid droplets and control of lipolysis. J Lipid Res 2007; 48:2547-59.
18. Skinner JR, Shew TM, Schwartz DM, Tzekov A, Lepus CM, Abumrad NA, et al. Diacylglycerol enrichment of endoplasmic reticulum or lipid droplets recruits perilipin 3/TIP47 during lipid storage and mobilization. J Biol Chem 2009; 284:30941-8.
19. Subramanian V, Rothenberg A, Gomez C, Cohen AW, Garcia A, Bhattacharyya S, et al. Perilipin A mediates the reversible binding of CGI-58 to lipid droplets in 3T3-L1 adipocytes. J Biol Chem 2004; 279:42062-71.
20. Labar G, Wouters J, Lambert DM. A review on the monoacylglycerol lipase: at the interface between fat and endocannabinoid signalling. Curr Med Chem 2010; 17:2588-607.
21. Nomura DK, Long JZ, Niessen S, Hoover HS, Ng SW, Cravatt BF. Monoacylglycerol lipase regulates a fatty acid network that promotes cancer pathogenesis. Cell 2010; 140:49-61.
22. Patel MI, Kurek C, Dong Q. The arachidonic acid pathway and its role in prostate cancer development and progression. J Urol 2008; 179:1668-75.
23. Straub BK, Herpel E, Singer S, Zimbelmann R, Breuhahn K, Macher-Goeppinger S, et al. Lipid droplet-associated PAT-proteins show frequent and differential expression in neoplastic steatogenesis. Mod Pathol 2010; 23:480-92.
24. Wang X, Sun Y, Wong J, Conklin DS. PPARgamma maintains ERBB2-positive breast cancer stem cells. Oncogene 2013; 32:5512-21.
25. Galluzzi L, Pietrocola F, Bravo-San Pedro JM, Amaravadi RK, Baehrecke EH, Cecconi F, et al. Autophagy in malignant transformation and cancer progression. Embo J 2015; 34:856-80.
26. Glick D, Barth S, Macleod KF. Autophagy: cellular and molecular mechanisms. J Pathol 2010; 221:3-12.

27. Roberts EA, Deretic V. Autophagic proteolysis of long-lived proteins in nonliver cells. Methods Mol Biol 2008; 445:111-7.
28. Singh R, Cuervo AM. Lipophagy: connecting autophagy and lipid metabolism. Int J Cell Biol 2012; 2012:282041.
29. Singh R, Kaushik S, Wang Y, Xiang Y, Novak I, Komatsu M, et al. Autophagy regulates lipid metabolism. Nature 2009; 458:1131-5.
30. Kaushik S, Cuervo AM. Degradation of lipid droplet-associated proteins by chaperone-mediated autophagy facilitates lipolysis. Nat Cell Biol 2015; 17:759-70.
31. Schweiger M, Zechner R. Breaking the Barrier-Chaperone-Mediated Autophagy of Perilipins Regulates the Lipolytic Degradation of Fat. Cell Metab 2015; 22:60-1.
32. Dall'Armi C, Devereaux KA, Di Paolo G. The role of lipids in the control of autophagy. Curr Biol 2013; 23:R33-45.
33. Gubern A, Casas J, Barcelo-Torns M, Barneda D, de la Rosa X, Masgrau R, et al. Group IVA phospholipase A2 is necessary for the biogenesis of lipid droplets. J Biol Chem 2008; 283:27369-82.
34. Kwon JH, Lee JH, Kim KS, Chung YW, Kim IY. Regulation of cytosolic phospholipase A2 phosphorylation by proteolytic cleavage of annexin A1 in activated mast cells. J Immunol 2012; 188:5665-73.
35. Ghosh M, Tucker DE, Burchett SA, Leslie CC. Properties of the Group IV phospholipase A2 family. Prog Lipid Res 2006; 45:487-510.
36. Pavicevic Z, Leslie CC, Malik KU. cPLA2 phosphorylation at serine-515 and serine-505 is required for arachidonic acid release in vascular smooth muscle cells. J Lipid Res 2008; 49:724-37.
37. Guijas C, Perez-Chacon G, Astudillo AM, Rubio JM, Gil-de-Gomez L, Balboa MA, et al. Simultaneous activation of p38 and JNK by arachidonic acid stimulates the cytosolic phospholipase A2-dependent synthesis of lipid droplets in human monocytes. J Lipid Res 2012; 53:2343-54.
38. de Souza PL, Castillo M, Myers CE. Enhancement of paclitaxel activity against hormone-refractory prostate cancer cells in vitro and in vivo by quinacrine. Br J Cancer 1997; 75:1593-600.
39. Artesi M, Kroonen J, Bredel M, Nguyen-Khac M, Deprez M, Schoysman L, et al. Connexin 30 expression inhibits growth of human malignant gliomas but protects them against radiation therapy. Neuro Oncol 2014.
40. Lai J, Chien J, Staub J, Avula R, Greene EL, Matthews TA, et al. Loss of HSulf-1 up-regulates heparin-binding growth factor signaling in cancer. J Biol Chem 2003; 278:23107-17.
41. Lai JP, Chien J, Strome SE, Staub J, Montoya DP, Greene EL, et al. HSulf-1 modulates HGF-mediated tumor cell invasion and signaling in head and neck squamous carcinoma. Oncogene 2004; 23:1439-47.
42. Staub J, Chien J, Pan Y, Qian X, Narita K, Aletti G, et al. Epigenetic silencing of HSulf-1 in ovarian cancer:implications in chemoresistance. Oncogene 2007; 26:4969-78.
43. Mondal S, roy D, Camacho-Pereira J, Khurana A, Chini E, Baddour J, et al. HSulf-1 deficiency dictates a metabolic reprograming of glycolysis and TCA cycle in ovarian cancer. Oncotarget (IN PRESS) 2015.
44. Hammond E, Brandt R, Dredge K. PG545, a heparan sulfate mimetic, reduces heparanase expression in vivo, blocks spontaneous metastases and enhances overall survival in the 4T1 breast carcinoma model. PLoS One 2012; 7:e52175.

45. Winterhoff B, Freyer L, Hammond E, Giri S, Mondal S, Roy D, et al. PG545 enhances anti-cancer activity of chemotherapy in ovarian models and increases surrogate biomarkers such as VEGF in preclinical and clinical plasma samples. Eur J Cancer 2015; 51:879-92.
46. Tamboli IY, Hampel H, Tien NT, Tolksdorf K, Breiden B, Mathews PM, et al. Sphingolipid storage affects autophagic metabolism of the amyloid precursor protein and promotes Abeta generation. J Neurosci 2011; 31:1837-49.
47. Gubern A, Barcelo-Torns M, Casas J, Barneda D, Masgrau R, Picatoste F, et al. Lipid droplet biogenesis induced by stress involves triacylglycerol synthesis that depends on group VIA phospholipase A2. J Biol Chem 2009; 284:5697-708.
48. Baenke F, Peck B, Miess H, Schulze A. Hooked on fat: the role of lipid synthesis in cancer metabolism and tumour development. Dis Model Mech 2013; 6:1353-63.
49. Berwick DC, Hers I, Heesom KJ, Moule SK, Tavare JM. The identification of ATP-citrate lyase as a protein kinase B (Akt) substrate in primary adipocytes. J Biol Chem 2002; 277:33895-900.
50. Hardie DG. AMP-activated/SNF1 protein kinases: conserved guardians of cellular energy. Nat Rev Mol Cell Biol 2007; 8:774-85.
51. Porstmann T, Griffiths B, Chung YL, Delpuech O, Griffiths JR, Downward J, et al. PKB/Akt induces transcription of enzymes involved in cholesterol and fatty acid biosynthesis via activation of SREBP. Oncogene 2005; 24:6465-81.
52. Farkas T, Hoyer-Hansen M, Jaattela M. Identification of novel autophagy regulators by a luciferase-based assay for the kinetics of autophagic flux. Autophagy 2009; 5:1018-25.
53. Klionsky DJ, Abeliovich H, Agostinis P, Agrawal DK, Aliev G, Askew DS, et al. Guidelines for the use and interpretation of assays for monitoring autophagy in higher eukaryotes. Autophagy 2008; 4:151-75.
54. Hsieh K, Lee YK, Londos C, Raaka BM, Dalen KT, Kimmel AR. Perilipin family members preferentially sequester to either triacylglycerol-specific or cholesteryl-ester-specific intracellular lipid storage droplets. J Cell Sci 2012; 125:4067-76.
55. Nieva C, Marro M, Santana-Codina N, Rao S, Petrov D, Sierra A. The lipid phenotype of breast cancer cells characterized by Raman microspectroscopy: towards a stratification of malignancy. PLoS One 2012; 7:e46456.
56. Lum JJ, Bauer DE, Kong M, Harris MH, Li C, Lindsten T, et al. Growth factor regulation of autophagy and cell survival in the absence of apoptosis. Cell 2005; 120:237-48.
57. Zhou J, Farah BL, Sinha RA, Wu Y, Singh BK, Bay BH, et al. Epigallocatechin-3-gallate (EGCG), a green tea polyphenol, stimulates hepatic autophagy and lipid clearance. PLoS One 2014; 9:e87161.
58. Funk CD. Prostaglandins and leukotrienes: advances in eicosanoid biology. Science 2001; 294:1871-5.
59. Shteingauz A, Boyango I, Naroditsky I, Hammond E, Gruber M, Doweck I, et al. Heparanase Enhances Tumor Growth and Chemoresistance by Promoting Autophagy. Cancer research 2015; 75:3946-57.
60. Integrated genomic analyses of ovarian carcinoma. Nature 2011; 474:609-15.
61. Tong Y, Liu YY, You LS, Qian WB. Perifosine induces protective autophagy and upregulation of ATG5 in human chronic myelogenous leukemia cells in vitro. Acta Pharmacol Sin 2012; 33:542-50.

Figure Legends

Figure1: HSulf-1 loss promotes lipid droplet biogenesis and defective autophagy in OV202, TOV2223 and in HSulf-1 knockout mouse embryonic fibroblast cells

A. Protein expression of HSulf-1 was assessed by western blot in OV202 clones (NTC, Sh1, Sh2 and Cl7 cells). Actin was probed as a loading control. **B**. OV202-NTC, Sh1, Sh2 and Cl7 cells were labeled with Bodipy 493/503 (green) and DAPI (Blue) to determine the cytoplasmic lipid droplets (LD) and nuclei respectively. **C.** Mean fluorescence of Bodipy in NTC, Sh1, Sh2 and Cl7 is measured using Carl Zeiss Zen (2009) software and the data is plotted as a bar diagram. **D.** Representative trans-electron microscopic (TEM) images of NTC, Sh1, Sh2 and Cl7 cells are shown; cytoplasmic LDs are marked with green arrows, whereas red arrows indicate autophagic vesicles (AV). **E.** LDs and AVs quantified in NTC, Sh1 and Sh2 cells (total 25 cells counted in each category) demonstrated in bar graph. **F.** Protein expression of HSulf-1 in TOV2223 NTC and Sh1 cells is detected by immunoblot analysis; β-actin is probed as a loading control. **G**. Bodipy staining performed in TOV2223 NTC and Sh1 cells to detect LDs. **H**. Representative TEM images of TOV2223 NTC and Sh1 cells were shown. **I.** AVs and LDs in TOV2223 cells are quantified **J.** Protein expression of HSulf-1 in Mouse Embryonic Fibroblast (MEF) wild type (WT) and HSulf-1 knock out (Sulf-1 $^{-/-}$) cells is detected by western blotting. β-Tubulin has been used as a loading control. **K**. MEF cells were labeled with Bodipy 493/503 (green) to determine the cytoplasmic lipid droplets (LD).

Figure 2: Inhibition of cPLA2 attenuates LD biogenesis in OV202Sh1 cells.

A. Immunoblot analysis shows phospho-cPLA2 and total-cPLA2 levels in OV202 NTC, Sh1, Sh2 and Cl7 cells. **B.** & **C**. Immunoblot analysis shows phospho-cPLA2 and total-cPLA2 levels in OV202 Sh1 and OV2008 cells after treatment with 10μM and 20μM of cPLA2 inhibitor, AACOCF3. **D.** Sh1 and SH2 cells were treated with either 10μM AACOCF3 or MAFP for 24 hrs followed by Bodipy (493/503) staining to show the LDs. **E.** Representative TEM images of OV202 Sh1 cells untreated and treated with 10μM AACOCF3 and MAFP for 24 hrs. LDs are marked with green arrows, whereas red arrows indicate autophagic vesicles (AV). LDs are quantified from 25 cells from untreated and treated cells from TEM images and demonstrated in a bar diagram. **F.** & **H**. Total cPLA2 expression was transiently downregulated with two different ShRNAs targeting the open reading frame of cPLA2 in OV202Sh1 and OV2008 cells. Immunoblot analysis shows total cPLA2 expression in non-targeted control transduced (NTC), ShcP-1 and ShcP-2 cells. **G. & I.** Bodipy staining of LDs in OV202 Sh1 and OV2008 cells after transiently transfecting them with either empty vector or sh-cPLA2. **J.** Arachidonic acid (AA) release is evaluated in OV202 NTC, Sh1, Sh2 and Cl7 cells treated or untreated with 10μM AACOCF3. Cells were incubated with H^3-AA under serum starved condition for 24 hrs. Fresh medium was added to the cells after washing and aliquots of growth medium were measured for radioactivity after 24 hrs. Radioactivity is shown as counts per minute (cpm)/ml. **K.** AA release is evaluated in OV202 Sh1 and Cl7 cells.

Figure 3: Inhibition of growth factor mediated signaling reduced p-cPLA2 and LD biogenesis

A. OV202 NTC, Sh1 and Sh2 cells were treated with 20μm of U0126, an MEK inhibitor for 24 hrs followed by western blot analysis to detect the protein expressions of phospho-ERK, total-ERK, phospho-cPLA2 and total-cPLA2. **B.** Bodipy staining for LDs in OV202Sh1 and Sh2 cells after treatment with 20 μM U0126. **C.** Immunoblot analysis of phospho-cPLA2 and total-cPLA2 in OV202Sh1 cell is shown after treatment with 10 and 20 μM PG545. **D**. Bodipy staining of LDs in OV202 Sh1 cells after treating with 10 and 20μm of PG545. **E**. Immunoblot analysis of phospho-cPLA2 and total-cPLA2 in lysates from untreated and PG545 treated OV202Sh1 Xenografts.

Figure 4: Dysfunctional autophagy is associated with loss of HSulf-1 and activation of cPLA2.

A. Immunoblot analysis with anti-LC3B antibody in OV202NTC, Sh1, Sh2 and Sh1Cl7 cells. **B.** Immunoflourescence analysis of OV202 NTC and Sh1 cells with anti-LC3B antibody (green, Top panels), Acridine orange (Red, Lower panels) and DAPI (blue).

C. Immunoblot analysis of LC3BI and II in OV202NTC and Sh1 cells treated with EBSS with or without bafilomycin A1 (100nm) for 1 hour with GAPDH as loading control.

Cyto-ID staining of **D.** OV202NTC **E.** OV202 Sh1 cells in control, EBSS and EBSS+Baf treated cells. Cells were grown in either regular media or EBSS to induce autophagy. **F.** Bodipy staining of LDs in OV202Sh1 cells treated with EBSS with or without bafilomycin A1 (100nm) for 1 hour. Cells grown in complete media is used as controls (-EBSS). Immunoflourescence analysis of Cyto-ID staining of OV202Sh1 cells treated with 10 and 20μM **G.** AACOCF3 and **H.** PG545 showing increase in autophagy. Immunoblot analysis of increase in LC3BII levels in OV202Sh1 cells treated with increasing concentrations of **I.** AACOCF3 and **J.** PG545. **K.** Autophagic flux in AACOCF3 and

PG545 treated OV202Sh1 cells following transient expression of Cherry-GFP-LC3B (48 hrs). The cells were treated for 24 hrs. Confocal microscopy analysis shows changes in the autolysosome formation. Green (GFP), and red fluorescence (Cherry) signals and the merged images show orange signals in the autolysosomes in the treated cells. Representative pictures from two independent experiments are shown.

Figure 5: AACOCF3 alone and in combination with carboplatin suppresses tumor growth, and inhibits lipid droplet biogenesis *in vivo*

A. Randomized OV202Sh1 tumor-bearing mice (n=10), were treated with water or AACOCF3 (F3) (10mg/kg), or carboplatin (CBP) (51mg/kg) or with a combination of AACOCF3 and CBP for 4 weeks and after 28 days mice were euthanized. Representative images of the mice prior to sacrifice from control, F3 treated, CBP treated and CBP+F3 combination treatment groups using IVIS luminescence imaging system series 2000. Color bar shows photon intensity. **B.** Representative images of excised tumors from OV202 Sh1 xenografts. **C**. Excised tumor weights from control, F3, CBP and CBP+F3 combination treatment groups. **D**. Abdominal circumference from different groups of mice measured on the day of sacrifice. **E.** Total body weight of untreated control and treated with F3, CBP, CBP+F3. **F.** Immunoblot analysis of LC3BI/II in lysates from untreated, F3, CBP and F3+CBP treated Xenografts with GAPDH as loading control. **G.** Tumor xenografts were stained with Bodipy to detect lipid droplets; DAPI was used to stain the nuclei. **H.** Representative images of TUNEL staining of frozen section of xenografts from different treatment groups and untreated control. Green fluorescence indicates TUNEL and red fluorescence indicates propidium iodide (PI) staining. **I.** Representative images of immunohistochemical staining of Ki67,

J. Bar graph showing the Ki67 proliferation index (*p=<0.05 and **p=<0.01). Proliferation index (PI) of Ki-67 staining was measured using ImmunoRatio, from public domain image analysis software. **K.** phospho-cPLA2 in FFPE sections of treated and untreated xenografts.

Supplementary figure legends

Fig S1

A. Protein expression of HSulf-1 was determined by western blot in SKVO3 vector and cl7 cells. GAPDH was probed as loading control **B.** Representative electron micrograph images of SKOV3 vector and cl7 cells are shown; LDs and AVs are indicated by green and red arrows respectively. **C.** Quantification of LDs and AVs from electron micrograph images are determined in SKOV3 vector and cl7 cells and are demonstrated in a bar diagram. **D.** SKOV3 vector and cl7 cells were labeled with Bodipy 493/503 (green) and DAPI (blue) to determine the cytoplasmic LDs and nuclei respectively.

Fig S2

A. Mouse Embryonic Fibroblast (MEF) wild type (WT) and HSulf-1 knock out (Sulf-1 $^{-/-}$) cells were either grown in complete media (CM) or starved with EBSS in the presence and absence of bafilomycin A1 followed by Cyto-ID staining to demonstrate the autophagic vesicles. **B.** MEFs were treated with 10μm of AACOCF3 and PG545 respectively, and then stained with either Bodipy or Cyto-ID to detect LDs and AVs.

Fig S3

OV202NTC cells were treated with 25 and 50μM of BSA conjugated sodium palmitate for 24 hrs. After treatment, cells were labeled with Bodipy and Cyto-ID to detect lipid droplets and autophagic vesicles respectively.

Fig S4

Wild type (WT) and ATG 5 knockdown mouse embryonic fibroblast (MEF) cells were stained with Bodipy and/or Cyto-ID to identify lipid droplets and autophagic vesicles.

Figure 1

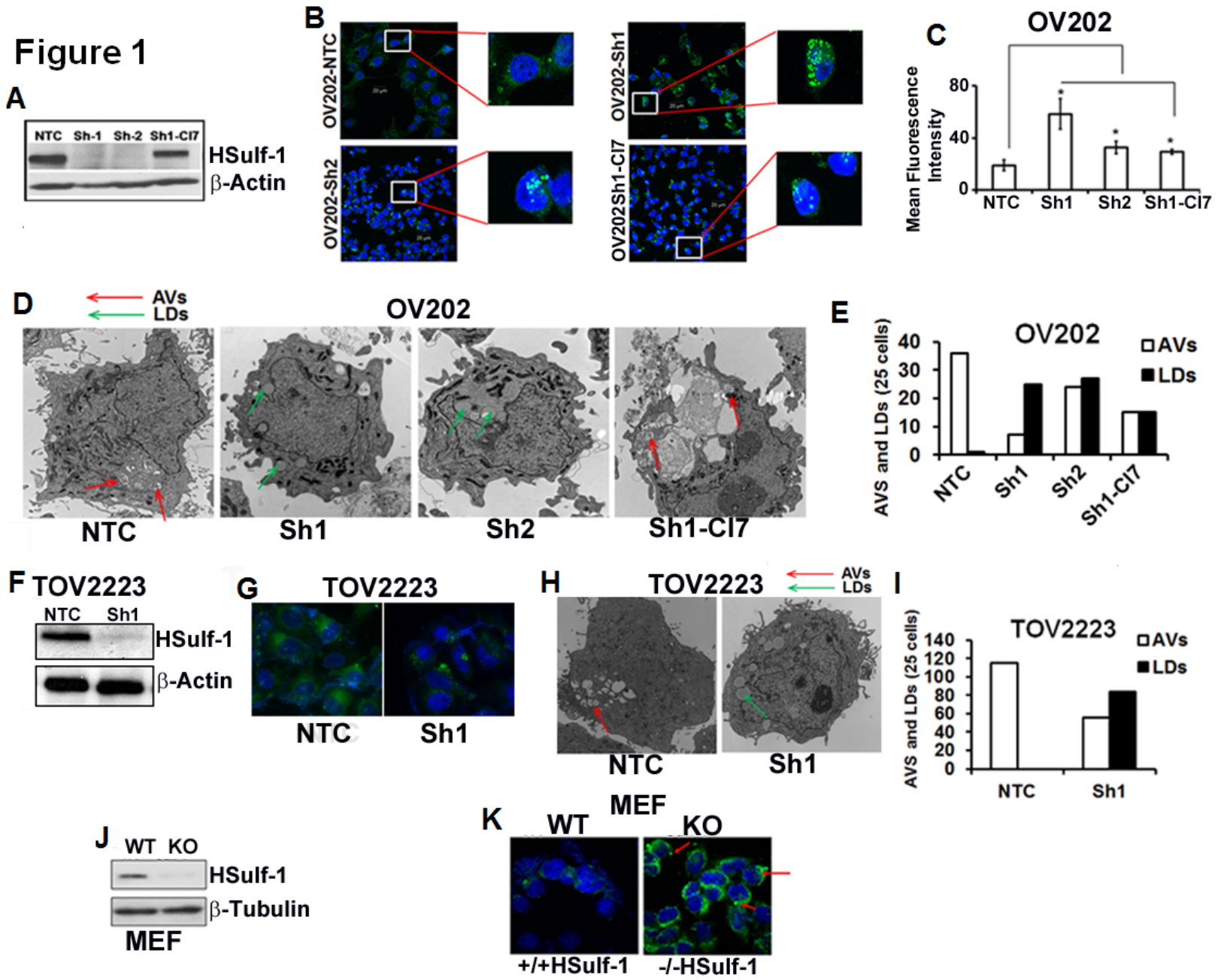
A
NTC
Sh-1
Sh-2
Sh1-Cl7
HSulf-1
β-Actin
B
OV202-NTC
OV202-Sh1
OV202-Sh2
OV202Sh1-Cl7
C
OV202
Mean Fluorescence Intensity
80
40
0
NTC
Sh1
Sh2
Sh1-Cl7
D
AVs
LDs
OV202
NTC
Sh1
Sh2
Sh1-Cl7
E
OV202
AVs
LDs
AVS and LDs (25 cells)
40
30
20
10
0
NTC
Sh1
Sh2
Sh1-Cl7
F
TOV2223
NTC
Sh1
HSulf-1
β-Actin
G
TOV2223
NTC
Sh1
H
TOV2223
AVs
LDs
NTC
Sh1
I
TOV2223
AVs
LDs
AVS and LDs (25 cells)
140
120
100
80
60
40
20
0
NTC
Sh1
J
WT
KO
HSulf-1
β-Tubulin
MEF
K
MEF
WT
KO
+/+HSulf-1
-/-HSulf-1

Figure 2

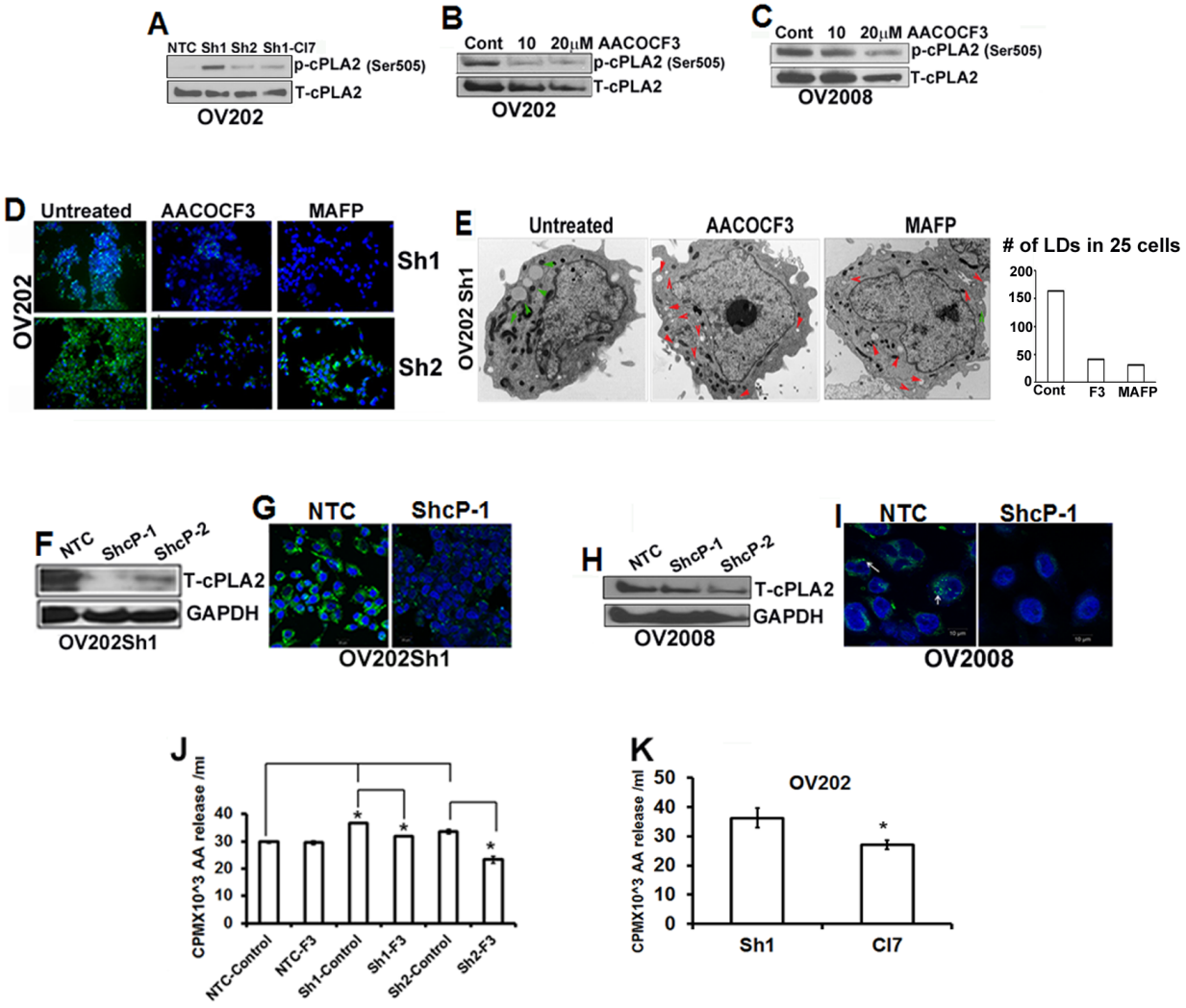
A
NTC Sh1 Sh2 Sh1-Cl7
p-cPLA2 (Ser505)
T-cPLA2
OV202
B
Cont 10 20μM AACOCF3
p-cPLA2 (Ser505)
T-cPLA2
OV202
C
Cont 10 20μM AACOCF3
p-cPLA2 (Ser505)
T-cPLA2
OV2008
D
Untreated
AACOCF3
MAFP
OV202
Sh1
Sh2
E
Untreated
AACOCF3
MAFP
OV202 Sh1
# of LDs in 25 cells
200
150
100
50
0
Cont
F3
MAFP
F
NTC
ShcP-1
ShcP-2
T-cPLA2
GAPDH
OV202Sh1
G
NTC
ShcP-1
OV202Sh1
H
NTC
ShcP-1
ShcP-2
T-cPLA2
GAPDH
OV2008
I
NTC
ShcP-1
OV2008
J
CPMX10^3 AA release /ml
40
30
20
10
0
NTC-Control
NTC-F3
Sh1-Control
Sh1-F3
Sh2-Control
Sh2-F3
K
OV202
CPMX10^3 AA release /ml
50
40
30
20
10
0
Sh1
Cl7

Figure 3

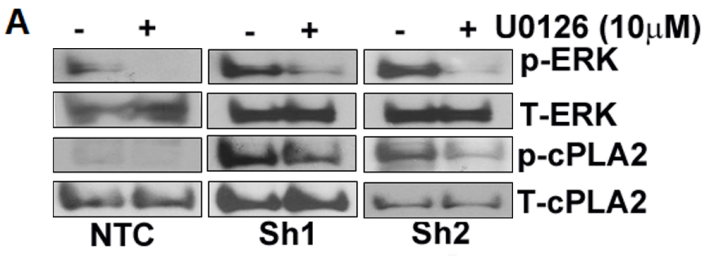
A
- + - + - + U0126 (10μM)
p-ERK
T-ERK
p-cPLA2
T-cPLA2
NTC
Sh1
Sh2

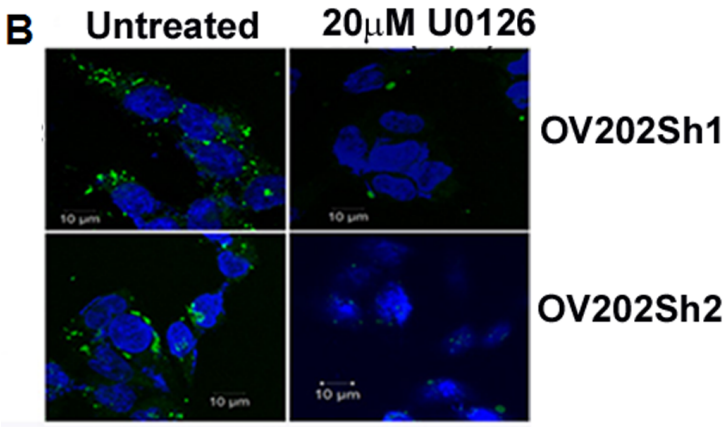
B
Untreated
20μM U0126
OV202Sh1
OV202Sh2

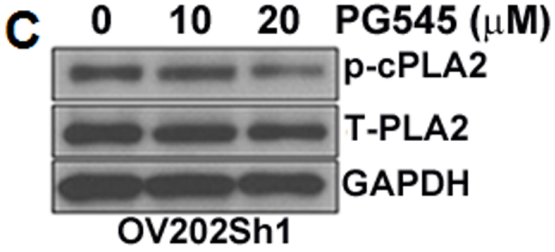
C
0 10 20 PG545 (μM)
p-cPLA2
T-PLA2
GAPDH
OV202Sh1

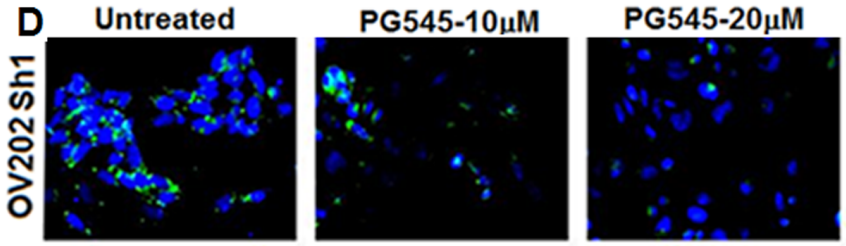
D
Untreated
PG545-10μM
PG545-20μM
OV202 Sh1

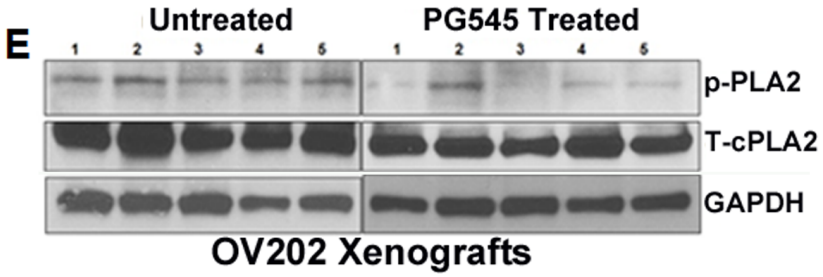
E
Untreated
PG545 Treated
1 2 3 4 5 1 2 3 4 5
p-PLA2
T-cPLA2
GAPDH
OV202 Xenografts

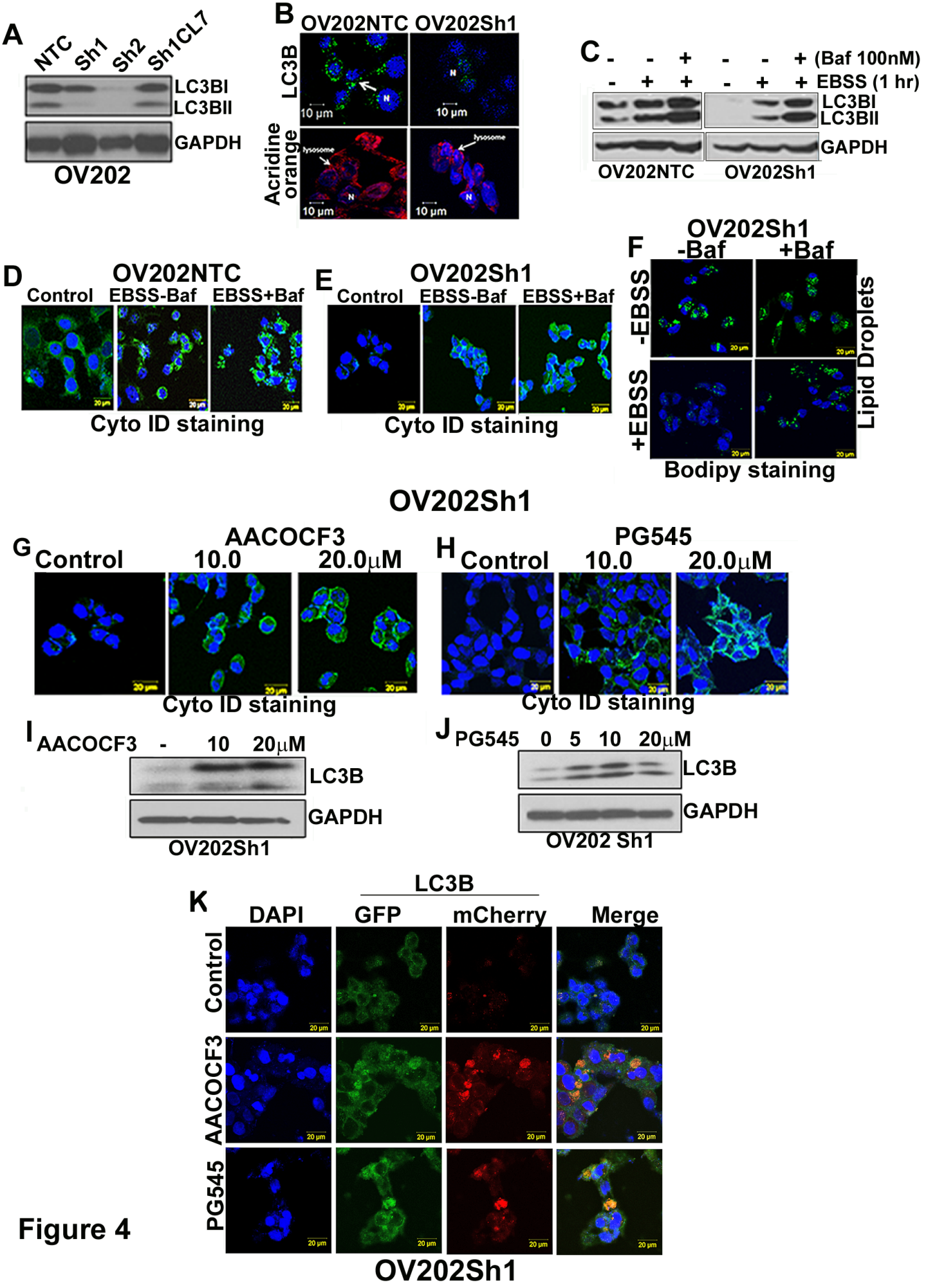
A
NTC
Sh1
Sh2
Sh1CL7
LC3BI
LC3BII
GAPDH
OV202
B
OV202NTC
OV202Sh1
LC3B
Acridine orange
10 μm
N
lysosome
C
- - + - - + (Baf 100nM)
- + + - + + EBSS (1 hr)
LC3BI
LC3BII
GAPDH
OV202NTC
OV202Sh1
D
OV202NTC
Control
EBSS-Baf
EBSS+Baf
Cyto ID staining
E
OV202Sh1
Control
EBSS-Baf
EBSS+Baf
Cyto ID staining
F
OV202Sh1
-Baf
+Baf
-EBSS
+EBSS
Lipid Droplets
Bodipy staining
OV202Sh1
G
AACOCF3
Control
10.0
20.0μM
Cyto ID staining
H
PG545
Control
10.0
20.0μM
Cyto ID staining
I
AACOCF3 - 10 20μM
LC3B
GAPDH
OV202Sh1
J
PG545 0 5 10 20μM
LC3B
GAPDH
OV202 Sh1
K
LC3B
DAPI
GFP
mCherry
Merge
Control
AACOCF3
PG545
20 μm
OV202Sh1

Figure 4

Figure 5

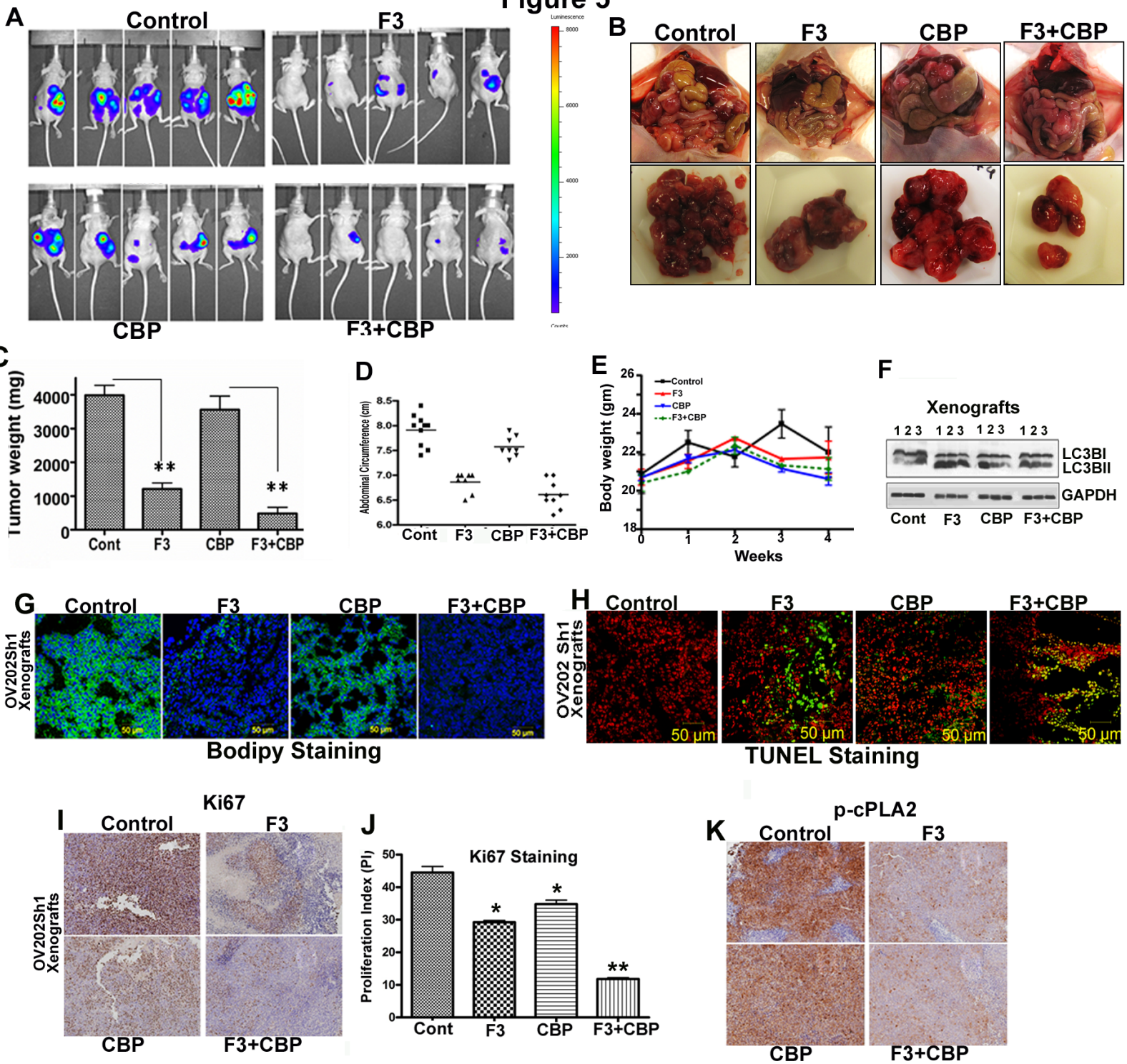
A
Control
F3
CBP
F3+CBP
Luminescence
8000
6000
4000
2000
B
Control
F3
CBP
F3+CBP
C
Tumor weight (mg)
4000
3000
2000
1000
0
**
**
Cont
F3
CBP
F3+CBP
D
Abdominal Circumference (cm)
8.5
8.0
7.5
7.0
6.5
6.0
Cont
F3
CBP
F3+CBP
E
Body weight (gm)
26
24
22
20
18
Control
F3
CBP
F3+CBP
0
1
2
3
4
Weeks
F
Xenografts
1 2 3
1 2 3
1 2 3
1 2 3
LC3BI
LC3BII
GAPDH
Cont
F3
CBP
F3+CBP
G
Control
F3
CBP
F3+CBP
OV202Sh1 Xenografts
50 µm
Bodipy Staining
H
Control
F3
CBP
F3+CBP
OV202 Sh1 Xenografts
50 µm
TUNEL Staining
I
Ki67
Control
F3
OV202Sh1 Xenografts
CBP
F3+CBP
J
Ki67 Staining
Proliferation Index (PI)
50
40
30
20
10
0
*
*
**
Cont
F3
CBP
F3+CBP
K
p-cPLA2
Control
F3
CBP
F3+CBP